METHODS FOR DETECTION AND

IDENTIFICATION OF PATHOGENIC BACTERIA

By

DAVID WESLEY GOAD

Bachelor of Science in Animal Science
Kansas State University
Manhattan, Kansas
1986

Master of Science in Animal Science
Kansas State University
Manhattan, Kansas
1990

Submitted to the Faculty of the
Graduate College of the
Oklahoma State University
in partial fulfillment of
the requirements for
the Degree of
DOCTOR OF PHILOSOPHY
July, 2008

METHODS FOR DETECTION AND

IDENTIFICATION OF PATHOGENIC BACTERIA

Dissertation Approved:

Jerry R. Malayer

Dissertation Adviser

Cyril R. Clarke

Jean M. Clarke

Rebecca J. Morton

Charles G. MacAllister

A. Gordon Emslie

Dean of the Graduate College

TABLE OF CONTENTS

Chapter Page

LIST OF FIGURES

CHAPTER I

INTRODUCTION

The advent of the polymerase chain reaction (PCR) to amplify and detect low-abundance nucleic acid targets has been a tremendous asset to bacterial detection and identification, and PCR assays are commonly used in diagnostic assays. Armed with little more than knowledge of the nucleic acid sequence of a particular pathogen an assay can quickly be designed to detect the organism. DNA sequencing technology had developed at a tremendous rate, and sequencing of entire genomes is now fairly routine. However, in the case of poorly characterized or newly emerging and often threatening pathogens, genomic information may be lacking. In other situations pathogenicity may arise in an organism which previously had been of little threat to health. There is a need for a fairly rapid method to effectively compare genomes and identify potential disease markers, and to be able to detect emerging pathogens efficiently.

Although a number of advancements in rapid, portable PCR-based detection systems have been made, it remains primarily a laboratory testing tool. Rapid, sensitive point-of-care diagnostics which can be used at the bedside or in a

physician's office are in high demand. In addition, sometimes it is desirable to detect protein rather than nucleic acid targets, especially when the phenotypic trait is closely linked to pathogenicity of an organism. Traditional immunoassays remain a highly effective tool for identification of protein targets, particularly when coupled with sensitive assay methods such as fluorometry. However, detection which relies on traditional fluorescent immunoassay methods is a multi-step process which is time- and labor-intensive, typically requiring multiple antibodies for maximum sensitivity. As a result these tests are normally performed in a diagnostic laboratory environment and are not easily performed as a point-of-care diagnostic. Coupling sensitive fluorescent protein detection with assay portability has been a challenge.

Ideally the best system to effectively detect and identify bacterial pathogens should be highly sensitive, fast, easily performed with a minimum of training, and unencumbered by the need for additional reagents. Rapid, label-free detection methods are of great interest in medical diagnostics, biodefense and food safety.

The work described in this dissertation strives to address all the aforementioned points, tied together under the common theme of detection and identification of pathogenic bacteria:

1. Suppression subtractive hybridization is employed to identify genetic markers unique to *Clostridium piliforme*, an essentially uncharacterized pathogen of great importance in animal health, and to laboratory animals

in particular, with the goal of identifying markers tied to production of cytotoxic factors.

2. Development of a rapid, amplified fluorescent assay to detect low-affinity penicillin binding protein, PBP2a, the protein responsible for the antibiotic-resistant phenotype associated with methicillin-resistant *Staphylococcus aureus*, a serious human and animal pathogen.
3. Development of a label-free optical method using microring resonator technology to detect whole *Salmonella* Typhimurium and *Escherichia coli* O157:H7 bacterial cells. These are both major foodborne disease pathogens, and demonstrate applicability of the assay to a multiplex detection platform.

CHAPTER II

REVIEW OF LITERATURE

Clostridium piliforme and Tyzzer's Disease

Clostridium piliforme was originally identified by Tyzzer (1917) as the causative organism involved in fatal necrotic hepatitis in rodents. It is a large (30-40 µm) rod-shaped, motile, spore-forming organism, existing in the vegetative state as an obligate intracellular pathogen in infected host cells. Originally named *Bacillus piliformis*, the organism has been reclassified as a *Clostridium* species based on phylogenetic grouping from 16S ribosomal RNA (rRNA) sequence analysis (Duncan et al., 1993). *C. piliforme* is the causative agent of Tyzzer's disease, an often fatal enterohepatic disease which affects a wide range of animal species. The organism is difficult to culture owing to its obligate intracellular nature, and is propagated *in vitro* in host cell or egg cultures, or *in vivo* in laboratory rodent hosts. Isolates have been obtained from natural infections, and individual isolates differ substantially in host toxicity and host range.

Tyzzer's Disease

Tyzzer's disease occurs most often in rodent species as well as rabbits and hares, and it is a significant laboratory animal disease. After rodents, the next most common occurrence of the disease is in horses, and in both mice and horses clinical symptoms of the disease are usually associated with young animals, from birth to weanling stage (Harrington, 1975; Whitwell, 1976; Harrington, 1976; Turk et al., 1981; Fosgate et al., 2002). The disease has also been reported in cattle (Webb et al., 1987), deer (Brooks et al., 2006), dogs (Boschert et al., 1988; Young et al., 1995), coyotes (Marler et al., 1976), snow leopards (Schmidt et al., 1984), muskrats (Chalmers et al., 1977), grey foxes (Stanley et al., 1978), red panda (Langan et al., 2000), raccoon (Wojcinski et al., 1986), and marsupials (Canfield et al., 1991). The disease has also been reported in avian species (Raymond et al., 2001; Saunders et al., 1993), and isolated occurrences in humans (Smith et al., 1996) and tamarins (Sasseville et al., 2007) have also been reported.

There appear to be 2 forms of the disease: An acute, often fatal clinical form and a latent subacute form associated with asymptomatic carriers of the *C. piliforme* pathogen. In the acute form of the disease clinical symptoms may include lethargy, edema and diarrhea, although onset of the disease is rapid with death usually occurring within 24 hours, and frequently animals are found dead with no other clinical indicators. The disease is characterized by pronounced hepatomegaly, multifocal lesions of hepatic necrosis, and acute hepatitis, and

cytological examination of infected tissue reveals the presence of intracellular *C. piliforme* bacteria, often arranged in bundles within host cells (Fujiwara et al., 1978; Ganaway et al., 1971; Franklin et al., 1993). In the subacute form there are no clinical signs and animals appear healthy. In laboratory animals, stress or immunocompromization may trigger transition to the fatal acute form (van Andel et al., 1997; van Andel et al., 1998). In adult animals the organism may establish itself as part of the normal gut flora, and transmission of the disease may occur as a result of fecal-oral transmission of spores to susceptible individuals (Motzel and Riley, 1992). After spore ingestion the exact method of hepatic colonization is unknown. However, based on histological evidence there appears to be initial infection within the small and large intestine and cecum, with dissemination to the liver (Ganaway, 1971). Franklin et al. (1993) presented an *in vitro* model of invasion which suggests that phagocytic processes are involved, and direct cell-to-cell spreading of the organism is a key factor, since *C. piliforme* infectivity diminishes rapidly following release from infected cells.

There is considerable variability among *C. piliforme* isolates with regard to infectivity, preferred hosts and cytotoxic activity. Experimental inoculation of different animal species with isolates derived from naturally occurring hamster (H2), rat (R1) and mouse (M1) infections resulted in no infection in rats or mice using any of the isolates tested, while hamsters succumbed to the disease following inoculation with the H2 isolate. However, in rats and mice infected with R1 and M1 cultures, respectively, there was a significant immune response

(Franklin et al., 1994). Serological surveys of horses in 4 Midwestern states using isolate-specific monoclonal immunoassays indicated that of 162 samples tested, 37 had a significant immunoresponse to equine isolate while 23 tested were seropositive for antibodies to a rat isolate, implying multiple strains were capable of infecting horses (Hook et al., 1995). Differences in antigenicity (Boivin et al., 1993) and expressed protein profiles (Riley et al., 1990) in various isolates has been demonstrated, and may play a major role in infectivity and host range. Notable differences in cytotoxicity of various isolates have also been reported (Riley et al., 1992). Culture filtrates of seven isolates were added to mouse or rat cell cultures and toxigenic effects were observed. Of the seven filtrates tested, four demonstrated cytotoxic effects when added to cell cultures (rabbit, guinea pig, gerbil and hamster), although cytotoxicity tended to be dependent upon cell line. Isolates which had no cytotoxicity included mouse, rat and horse. Testing of size-fractionated filtrates suggested the factor(s) responsible for increased cytotoxicity were proteins or protein complexes with molecular weight greater then 100 kDa. It was postulated that production of cytotoxic factors was in part responsible for the increased incidence of acute Tyzzer's disease associated with cytotoxin-producing isolates.

Detection of *C. piliforme*

Early diagnoses of Tyzzer's disease relied on post-mortem examination of affected tissues, and microscopic visualization of lesion-associated *C. piliforme* served as positive confirmation of the disease. Motzel and Riley (1991)

developed an enzyme-linked immunosorbent assay (ELISA) for detection of serum antibodies to *C. piliforme*, and a screening and diagnosis tool based on immunoassay was described by Hansen et al. (1994). Isolate-specific competitive immunoassays have also been developed (Boivin et al., 1994). Goto and Itoh (1994) described a polymerase chain reaction (PCR) test to detect the presence of *C. piliforme* rDNA by amplification of specific sequences associated with *C.piliforme* 16S rRNA in heart and liver samples from infected animals. PCR-based disease confirmation in horses has also been reported (Borchers et al., 2006). Furukawa et al. (2002) demonstrated successful amplification of *C. piliforme* 16S targets from spiked fecal samples. Additional amplification studies using 23S and 16S ribosomal targets have allowed a small degree of isolate-specific detection (Feldman et al., 2006). Immunoassay is still regarded as a fundamental screening tool for the presence of *C. piliforme*, with confirmatory testing using PCR or microscopic examination (Otto and Franklin, 2006). However, commercial services for screening fecal samples for presence of the organism by 16S ribosomal analysis are available (www.zoologix.com). To date the organism is poorly characterized genetically, and no practical isolate-specific DNA tests have been reported.

Methicillin-Resistant *Staphylococcus aureus*

Importance In Human Health

Methicillin-resistant *Staphylococcus aureus* (MRSA) represents a serious, worldwide health threat. In 2005 in the U.S. alone, invasive MRSA infections were estimated to be 94,360, with 18,650 deaths associated with MRSA (Klevins et al., 2007). The threat continues to increase. According to the Centers for Disease Control (CDC) the number of staphylococcal infections attributable to MRSA were only 2% in 1974, rising to 22% in 1995 and 63% in 2004 (Centers for Disease Control and Prevention (October 17, 2007), "MRSA: Methicillin-resistant *Staphylococcus aureus* in Healthcare Settings"). The majority of infections are associated with healthcare settings, particularly nosocomial infections involving hospital- (or health care-) associated MRSA (HA-MRSA), although the number of community-associated MRSA (CA-MRSA) is rising rapidly. Proper choice of antibiotic therapy is of great importance, as increased use of antibiotics is implicated as a causative factor in promotion of resistance. Moreover, inappropriate use of antibiotics appears to drive increased pathogenicity at molecular and cellular levels, promoting emergence of new resistant strains. These changes include activation or modification of quorum sensing, altered production of staphylococcal toxins, changes associated with induction of bacterial SOS responses, and changes in ability of bacteria to adhere to and colonize host tissues (Dancer, 2008).

Methicillin was developed as a penicillinase-resistant antibiotic in 1959, and by 1961, the first MRSA strain was isolated in the United Kingdom (Jevons, 1961). Resistance to the drug is provided by a low-affinity penicillin binding protein (PBP2a or PBP2') which is capable of continued cell wall synthesis in the presence of methicillin and oxacillin, effectively replacing the function of proteins with higher binding affinity found in methicillin-sensitive *S. aureus* (MSSA) which are inactivated by irreversible binding of the antibiotic (Giesbrecht et al., 1998). The PBP2a protein is a product of the *mecA* gene, which is part of a larger mobile genetic element called the staphylococcal cassette chromosome *mec* (SCC*mec*).

HA-MRSA, CA-MRSA and SCC*mec*

There are five main types of SCC*mec* (I-V). SCC*mec* types I, IV and V are responsible only for resistance to ß-lactam antibiotics, while types II and III drive multidrug resistance. Resistance to drugs other than ß-lactams is conferred by additional integrated plasmids or transposons, and includes resistance to kanamycin, tobramycin, bleomycin, penicillins, heavy metals, macrolides, lincosamides and streptogramins (Duerenberg et al., 2007). HA-MRSA is associated with SCC*mec* types I, II and III. Multidrug resistance is not commonly associated with CA-MRSA strains, which predominantly carry the SCC*mec* types IV and V, in addition to a potent pore-forming exotoxin, the Panton-Valentine leukotoxin (PVL) (de Lencastre et al., 2007; Duerenberg et al., 2007). PVL is not carried on SCC*mec*, but instead is the product of a phage-encoded genetic

element. The toxin is associated with necrotizing pneumonia, skin and soft tissue infections and necrotizing fasciitis (Boyle-Vavra and Daum, 2007; Lina et al., 1999). There is evidence to indicate that CA-MRSA is derived from CA-MSSA which acquired a mobile SCC*mec* methicillin resistance element rather than a PVL-containing variant of HA-MRSA (Feng et al., 2008; Boyle-Vavra and Daum, 2007). However, clear distinctions between HA-MRSA and CA-MRSA are becoming more difficult to establish, as more HA-MRSA infection is becoming spread throughout the community as result of delayed infection after leaving the hospital setting. Definitions of MRSA infections have therefore been revised to reflect healthcare-associated infection with either community onset or hospital onset (appearing >48 hours after admission) subgroups, and community-associated MRSA (Klevins et al., 2007).

mecA Gene

The *mecA* gene codes for the PBP2a protein, the phenotypic determinant of methicillin resistance, and is carried on the SCC*mec* element along with genes for regulators of protein expression from the *mecA* locus, *mecI* and *mecR1*. MecR1 is a ß-lactam-sensing transmembrane receptor/transducer element, while MecI acts as a repressor of PBP2a expression from *mecA*. Binding of inducer to the receptor triggers activation of an intracellular protease domain which cleaves the repressor and activates expression from *mecA* and *mecR1-mecI*. MecI shares considerable homology to BlaI, the repressor associated with production of staphylococcal penicillinase, and both proteins can function as repressors for

the *mecA* and *blaZ* genes (Lewis and Dyke, 2000). However, MecR1 and BlaR1 are specific for their cognate repressors and cannot act interchangeably (McKinney et al., 2001). Methicillin and oxacillin are poorly sensed by the MecR1 transducer, and induction is slow in the presence of these antibiotics. Thus, strains which carry the *mecA* gene may appear phenotypically susceptible. However, under antibiotic pressure inactivation or deletion of *mecI* or promoter mutations occur which results in constitutive expression of PBP2a and the fully resistant phenotype (Rohrer et al., 2003; Berger-Bachi and Rohrer, 2002; Hiramatsu et al,.1996).

PBP2a Protein

Cell wall synthesis in *S. aureus* requires transpeptidation to achieve a high degree of peptidoglycan crosslinking, an activity provided by 4 membrane-anchored proteins, termed penicillin binding proteins 1-4 (PBP1-PBP4) (Chambers, 1997). These proteins are deactivated by irreversible binding of ß-lactams via acyl-enzyme-antibiotic complex formation within the active site of the transpeptidase domain, resulting in inhibition of cell wall synthesis and termination of cell growth and division (Giesbrecht et al., 1998). The *mecA* gene codes for a 76 kDa membrane-associated penicillin binding protein, PBP2a, with low affinity for ß-lactam antibiotics, and in the presence of these agents remains capable of transpeptidase activity (Hartman and Tomasz, 1984). A combination of decreased acylation rate and low affinity with regard to pre-acylation complexes is responsible for the decreased affinity which allows the enzyme to

maintain function (Fuda et al., 2004). However, transpeptidase activity is primarily confined to forming muropeptide dimers when all other PBPs are deactivated by antibiotic binding (deJonge and Tomasz, 1993). Nonetheless, sufficient activity remains to facilitate growth in the presence of methicillin or oxacillin and yield the fully resistant MRSA phenotype. Structurally, the PBP2a protein contains an N-terminal hydrophobic membrane-spanning domain with an adjacent region believed to be a transglycosylase domain, with a C-terminal transpeptidase domain. Interestingly, the transglycosylase domain appears to have little functional activity, as PBP2a has been shown to be dependent on transglycosylation activity provided by the it's high-affinity PBP2 counterpart (Pinho et al., 2001).

The transmembrane domain imparts considerable hydrophobicity to the PBP2a protein, and water-soluble forms of the protein have been created by deletion of the N-terminal anchoring sequence (Fuda et al., 2004; Wu et al., 1992). These recombinant forms appear to be functionally similar to the native proteins, and have been used for kinetic antibody binding studies and to study the mechanism of antibiotic resistance in PBP2a (Fuda et al., 2004).

Detection of MRSA

Traditional testing for antibiotic-resistant bacteria has utilized growth inhibition assays such as agar disc diffusion or broth microdilution. However, these methods are time-consuming and labor-intensive, sometimes requiring days

before confirmation of MRSA infection. Additional complications are introduced due to heterogeneous expression of PBP2a in mixed bacterial populations in clinical samples, resulting in a wide range of observed minimum inhibitory concentrations (MIC) values (Chambers, 1997; Sabath et al., 1972). Additional challenges are presented by borderline resistant cultures (BORSA), which can be classified into 2 groups – those which have the *mecA* gene in a very small resistant subpopulation, which can grow at high drug concentrations, and those which lack *mecA* and low-level resistance is due to overexpression of ß-lactamase or other factors (Chambers, 1997). In each of these cases it may be necessary to induce high-level expression by culture in the presence of antibiotic to make accurate determination of MRSA, although reversion to a heterogeneous phenotype is common upon additional culture in antibiotic-free medium. In addition, heteroresistant cultures tend to grow more slowly, and culture at reduced temperatures is recommended to ensure accurate identification, and screening by plating on oxacillin-containing medium at lower incubation temperatures is recommended.

Disc diffusion susceptibility testing using cefatoxin has proven to be much better than oxacillin (reviewed by Appelbaum, 2007) and this method, as well as selective growth on oxacillin-containing medium, are recommended as growth-based screening methods for MRSA by the Clinical and Laboratory Standards Institute (CLSI; formerly the National Committee for Clinical Laboratory Standards). New growth-based methods based on chromogenic detection have

also been developed (for review see Malhotra-Kumar et al., 2008) which allow simultaneous determination of antibiotic resistance (primarily by inclusion of antibiotic in test medium) and positive identification of *S. aureus* by production of insoluble colored products, giving rise to colonies with distinct colors which are easily distinguishable. There are a variety of commercially-available products of this type, and some are capable of producing results within 24 hours. Recently Brown et al. (2005) published suggested guidelines for laboratory diagnosis and susceptibility testing of MRSA. The publication includes an expanded list of testing methodology and procedures, as well as growth characteristics associated with a variety of screening media.

In the case of clinical presentation of the disease, application of effective antibiotic therapy is extremely time-sensitive and cannot be delayed while awaiting laboratory results. In these cases treatment is often started immediately, sometimes using “last line of defense” drugs like vancomycin, while awaiting laboratory results. However, inappropriate use of these antibiotics fosters undesirable development of resistance to these drugs and emergence of resistant strains, which may pose a much larger health threat (Dancer, 2008). Therefore, rapid tests to accurately identify MRSA are highly desirable. In addition, the potential to deploy these tests in a hospital admission protocol, to allow screening of infected individuals so that proper isolation precautions can be taken, is very appealing.

There are several recent reviews pertaining to development and current status of rapid diagnostics for bacterial infections (Tenover, 2007; Barken et al., 2007) , and in particular rapid detection of MRSA (Malhotra-Kumar et al., 2008; Carroll, 2008). Virtually all of these tests utilize the power of the polymerase chain reaction (PCR) to amplify target nucleic acid sequences to enable fast, accurate detection with a minimum of culture time, particularly when modern rapid blood culture systems are used. The tests are typically performed using real-time PCR equipment which allows integrated detection of products via fluorescent signal generation. Some assays amplify and detect the *mecA* gene individually or in multiplex with other *S. aureus* targets, including the *lukS-lucF* genes encoding PVL associated with CA-MRSA. One notable exception, which has received FDA approval, is the IDI-MRSA (a.k.a, GeneOhm MRSA, BD Biosciences) which targets an amplicon spanning the terminal end of SCC*mec* and includes a portion of the adjacent *S. aureus*-specific *orfX* gene, allowing simultaneous identification of *S. aureus* and presence of SCC*mec*. The system has been proven effective for detection of MRSA from a variety of clinical samples including direct detection from nasal, perineum and throat swabs. Another FDA-approved assay using similar technology, the GeneXpert MRSA assay (Cepheid), is capable of generating results within 75 minutes with a minimum of sample preparation and technical expertise required (Malhotra-Kumar et al., 2008). A new highly multiplexed fluorescent assay system has also been developed:The Staphplex system (Genaco Biomedical Products) is capable of performing simultaneous

PCR on 17 targets with characterization of individual products based on Luminex® multicolor fluorescent bead technology (Malhotra-Kumar et al., 2008).

All of the aforementioned rapid assays target genetic elements for identification of MRSA. However, the true determinant of the MRSA phenotype is the expression of PBP2a protein, and some strains which carry SCC*mec* may lack expression of PBP2a (see above), and are phenotypically MSSA. Testing of these strains using genomic assays would yield a false positive result, although an argument could be made that these strains are "poised" to jump toward the MRSA phenotype. Rapid assay development for protein detection has been limited because protein targets cannot be amplified as is routinely done with genetic targets. The standard method currently used for detection of PBP2a, and the method approved by CLSI, involves the agglutination of antibody-functionalized latex beads (Nakatomi and Sugiyama, 1998). Several of these assays are available commercially (e.g., MASTALEX-MRSA™ (Mast Group); Staphaurex Plus (Oxoid, LTD.); MRSA Latex Test (Denka Seiken)), and utilize monoclonal antibody to PBP2a attached to latex beads. Cells are lysed and mixed with beads, and if MRSA are present, visible agglutination occurs. The process requires a large number of cells from a colony grown on a plate, to work effectively. Although the test is fairly rapid, on the order of several minutes, the preparation time (culture growth) precludes the use of these products as true rapid assays. However, the latex agglutination assay is considered a gold standard for testing MRSA based on PBP2a expression.

Foodborne Enteric Pathogens: *Salmonella* and *Escherichia coli* O157:H7

Organism Significance

In the U.S. each year it is estimated that 76 million people are affected by food- and water-borne illnesses, resulting in 325,000 hospitalizations and 5,000 deaths (Mead et al., 1999). Of the bacterial organisms associated with foodborne illness, the most prevalent are enterohemorrhagic *E. coli*, particularly serovar O157:H7, and *Salmonella enterica* serotypes including serotype Typhimurium (old nomenclature *S. typhimurium*). According to the World Health Organization, between 200 million and 3 billion cases of intestinal disease are associated with non-typhoidal *Salmonella* infections each year, with an estimated 3 million deaths (World Health Organization, 2005). Both *Salmonella* and *E. coli* are considered major foodborne pathogens and, in addition to medical costs associated with *Salmonella* and *E. coli* infections there is a large burden on food producers as well. *E. coli* O157:H7 is now considered a food adulterant, and products containing *E. coli* O157:H7 are considered unfit for consumption. Recent outbreaks of foodborne illness associated with *E. coli* include a multi-state incident in 2006 involving fresh spinach, that resulted in 199 reported cases with 16% developing hemolytic-uremic syndrome (HUS), and 3 confirmed deaths. A more recent outbreak in 2007 involving contaminated beef patties resulted in the recall of 21.7 million pounds of suspect product, ultimately forcing the supplier out of business (Nugen and Baeumner, 2008). Most recently (June, 2008) a

widespread outbreak of *Salmonella* associated with tainted tomatoes has resulted in 756 people infected across 34 states and the District of Columbia (CDC, 2008).

The possibility of using these organisms as terrorist weapons to poison food distribution chains or water reservoirs has been recognized (Sobel et al., 2002a; Sobel et al., 2002b). Centralized processing and delivery facilities that prepare and ship food items to different parts of the country and beyond are especially vulnerable to such attacks. *Salmonella* Typhimurium is one of the few organisms in recent history that has been employed for deliberate contamination of food. An incident of intentional *Salmonella* Typhimurium contamination of salad bars in Oregon (1984) resulted in 751 people developing salmonellosis (Torok et al., 1997). In addition, *E. coli* O157:H7 has been identified as one of the most likely Category B organisms posing a bioterrorist threat (US Dept. Health Hum. Serv. et al., 2006).

E. coli O157:H7

E. coli infections result from the consumption of contaminated food, mainly undercooked meat, unpasteurized milk or juice, and fresh vegetables (Goldman, 2006). Infection can also be acquired by contact with contaminated water and can be spread from person to person. The organism is a common inhabitant of the ruminant digestive tract, and ruminants are considered a large natural reservoir for the bacteria (Gyles, 2007). *E. coli* associated with disease is

classified into broad groups based on their mode of pathogenesis: Enterotoxigenic *E. coli* (ETEC), enteropathogenic *E. coli* (EPEC), enteroinvasive *E. coli* (EIEC), and enterohemorrhagic *E. coli* (EHEC), also called Shiga toxin-producing *E. coli* (STEC). The hallmark of STEC is the production of the Shiga toxin Stx (consisting of 2 subgroups, Stx1 and Stx2). Of the EHEC serotypes O157:H7 is one of the most virulent, with infectious human dose believed to be less than 100 bacteria (Deisingh and Thompson, 2004).

Early clinical symptoms are abdominal cramping and watery diarrhea, later turning to bloody diarrhea. In severe cases patients can suffer hemolytic-uremic syndrome (HUS) as a result of bacterial production of Stx toxin in the colon. Stx acts in the kidney by damaging renal cells and occluding microvasculature resulting in renal inflammation and possibly fatal acute renal failure (Kaper et al, 2004). Typical treatment of E. coli O157:H7 infection is primarily supportive, and antibiotic therapy is not recommended due to the potential to induce HUS (Karch et al., 2005). Confirmatory diagnosis relies primarily on culture of the organism from stool samples, sometimes supported by immunoassays such as latex agglutination.

Salmonella

The genus *Salmonella* is comprised of 2 major species containing over 2500 different serovars. Some *S. enterica* serovars are associated with typhoid (S. Typhi), while most serovars cause enterocolitis and diarrhea in humans (Coburn

et al., 2007). Symptoms associated with Salmonella-induced enterocolitis are similar to those found in EHEC infections, namely abdominal cramps and diarrhea which may become bloody. Unlike EHEC, *Salmonella* infectious dose is much higher (greater than 50,000 bacteria), and onset of symptoms is usually more rapid and may involve fever. Also unlike EHEC, *Salmonella* is an intracellular pathogen which survives in intracellular vacuoles following phagocytosis, and the organism has developed a wide range of virulence factors to enhance host colonization (Coburn et al., 2007). Laboratory confirmation of *Salmonella* infection is primarily by culture of stool samples on selective medium.

In contrast to clinical testing, the needs for testing food products are more demanding, requiring high sensitivity to accurately detect *E. coli* and *Salmonella*. Methods for detection of *E. coli* O157:H7 have been reviewed by Deisingh and Thompson (2004a), and include conventional culture methods on selective medium, sometimes with a pre-enrichment step such as immunomagnetic collection to enhance sensitivity. Immunological detection methods such as ELISA or immunofluorescence are also used, but maximum sensitivity is usually attained using PCR methodology, including real-time PCR. However, these methods are laborious and time-consuming, and there is great interest in the development of biosensors to allow rapid detection of foodborne pathogens. Sensor platforms developed for food applications also have the potential to be employed for clinical diagnosis applications. Of particular interest are rapid,

label-free assays which require minimum effort, no additional reagents and which can achieve the desired result in a much shorter time period.

Non-Optical Label-Free Biosensor Platforms

Electrochemical Methods

Electrochemical detection methods rely on the interaction of analyte with electrodes in an assay cell. Sensing of biomolecules may use a variety of electrical measurement techniques including voltammetry, conductivity, capacitance, potentiometry and impedance, and the reader is directed toward recent comprehensive reviews describing the principles and methods of electrochemical biosensing for proteins, amino acids and peptides (Lambrianou et al., 2008; Herzog and Arrigan, 2007; Yu et al., 2006) and DNA (Lucarelli et al., 2008; Odenthal and Gooding, 2007). Electrochemical methods have also been used for detection of pathogenic bacteria, and electrochemical impedance methods are routinely used to monitor growth of cells in culture (impedance microbiology, for review see Yang and Bashir, 2008). Of particular interest is the use of electrical impedance for the development of sensors to specifically detect food pathogens. These devices use electrical impedance spectroscopy (EIS) to detect binding of cells to electrodes functionalized with antibodies to specific bacteria. Binding of bacteria results in increased impedance between electrodes in an electrical cell due to the insulating properties of bacterial cell membranes, which effectively blocks electrode surfaces. Presence of bacteria is determined by a change in current or change in electrical impedance measured as a function of interrogating frequency (Yang and Bashir, 2008; Maalouf et al., 2007). Label-free detection is realized by use of interdigitating electrodes with small electrical

gaps (~15 um), and has been used to detect the presence of viable *Salmonella typhimurium* and *E. coli* O157:H7, with a limit of detection of ~10^6 CFU/ml (Yang, 2008; Yang et al., 2004).

Surface Acoustic Wave (SAW) Sensors

Principle of operation, types of SAW sensors, and the sensors' use in biological sensing applications has been recently reviewed (Cooper and Singleton, 2007; Gronewold, 2007). SAW devices utilize piezoelectric materials such as quartz to generate an acoustic wave (SAW) which propagates down the length of the sensor. SAW sensors have multiple layers, the composition and thickness depending upon the type of wave form desired (e.g., Love wave sensors). In all cases, the acoustic wave, which is typically produced by electrical excitation of the piezoelectric material, is carried in a guide layer on the surface of the piezoelectric substrate and has a defined velocity and amplitude. Interaction with the surface (such as during a binding event) affects the velocity/amplitude of the acoustic wave. SAW sensors have been used for a wide range of biosensing applications including protein interactions, DNA hybridization, kinetic binding assays and whole cell and bacterial detection. Branch and Brozik (2004) demonstrated the utility of specially-designed Love wave sensors by immobilized antibody-mediated binding of *Bacillus* spores. Recently, Moll et al. (2007) described the use of a Love wave device for detection of *E. coli* with a detection limit of ~10^6 bacteria/ml. However, successful detection was dependent upon binding of *E. coli* through a 2-antibody "sandwich" strategy.

Quartz crystal microbalances (QCMs) are another type of acoustic wave sensor. In comparison to Love wave-type sensors, QCMs are generally bulk wave sensors, where the wave is propagated throughout the substrate. For a detailed examination of bulk wave sensor design and materials used to create them, as well as the use of these devices in biosensing applications, the reader is referred to the comprehensive review of Cooper and Singleton (2007). These types of sensors have been also been used for a wide range of biosensing applications including detection of proteins and nucleic acids, whole cell detection, etc.(see Cooper and Singleton, 2007; Gronewold, 2007; Deisingh and Thompson, 2004b; Cooper, 2003). As acoustic mass transducers, they are attractive for detection of whole bacterial cells and have been used for sensitive detection of *Salmonella* (Huang and Cooper, 2006; Olsen et al., 2003; Pathirana et al., 2000) and *E. coli* (Huang and Cooper, 2006; Serra et al., 2008; Wang et al., 2008; Berkenpas et al., 2006) with effective linear bacterial detection range from 10^2-10^8 CFU/ml.

Microcantilever/Cantilever Devices

Cantilever-type devices have been recently reviewed by Waggoner and Craighead (2007). They function primarily as bound mass sensors, and the principles of operation are derived from their atomic force microscopy (AFM) origin. They are classified as micro- or nanoelectromechanical systems (MEMS or NEMS, respectively), and can be operated in static or resonance mode. Similar to SAW devices, they take the general form of a sensing region

connected to a support by means of a flexible beam structure, and are fabricated from single or multiple layers of materials in sizes ranging from hundreds of nanometers to millimeters (as in the case of cantilever devices). An example of a microcantilever device is shown in Figure 3. In the static mode, binding of mass to the sensor surface induces a deflection in the beam which is measured optically or electronically. In resonance mode, cantilever devices may be excited by simple thermal energy, via electrical input or by coupling to piezoelectric materials, and changes in resonant state as a function of increasing bound mass can be determined optically or electronically (Waggoner and Craighead, 2007; Hansen and Thundat, 2005).

Deflection-based sensors have been used as label-free biosensors to detect protein binding, DNA hybridization and binding of whole bacterial cells or spores to the sensor surface (Waggoner and Craighead, 2007). *Bacillus* endospores were detected in liquid at a concentration of 5×10^7 spores/ml (Dhayal et al., 2006). Using microcantilevers functionalized with antibodies to *Salmonella*, Weeks et al. (2003) claimed detection sensitivity as low as 25 bacterial cells bound to the sensor surface. Detection of *E. coli* O157:H7 was also demonstrated using an antibody-functionalized, deflection mode sensor, although substantially higher detection limits (1×10^6 CFU/ml) were reported (Zhang and Ji, 2004). However, in most cases deflection measurements must be performed in air using a dried, normalized sensor surface, and real-time detection using

these devices is generally not feasible (Waggoner and Craighead, 2007; Dhayal et al., 2006; Yu et al., 2006; Hansen and Thundat, 2005).

In comparison to deflection-based devices, resonance-mode microcantilever designs have seen wider use in biosensing applications, and in some cases a device can be employed in both modes (Waggoner and Craighead, 2007; Hansen and Thundat, 2005). For resonance mode devices, mass sensitivity is a function of quality factor, or *Q*, which is defined as:

$$Q = f_0 \Delta f_{fwhm}^{-1},$$

where f_0 is the resonant frequency and Δf_{fwhm} is the full-width at half maximum of the resonance peak. Thus, narrow and well defined peaks will have higher *Q* values associated with them, and very small shifts in resonant frequencies can be discriminated (Waggoner and Craighead, 2007). By decreasing sensor mass and increasing *Q* factors, extremely high sensitivity to bound mass can be achieved, to the attogram (Ekinci et al., 2004; Ilic et al., 2004) or even zeptogram (Yang et al., 2006) level.

Binding and detection of *E. coli* O157:H7 cells to a resonance device was demonstrated by Ilic et al. (2000). Unfortunately, utility of these devices for detection in liquid samples, particularly in real-time, has been limited due to damping forces of liquid medium on the cantilever surface. However, recent work using millimeter-sized cantilevers and devices fabricated from new composites have demonstrated the ability to detect *Salmonella* (Zhu et al.,

2007a; Zhu et al., 2007b) and *E. coli* O157:H7cells (Campbell and Mutharasan, 2007; Campbell et al., 2007; Campbell and Mutharasan, 2005a; Campbell and Mutharasan, 2005b; Maraldo and Mutharasan, 2007) in liquid, with detection limits of 500 cells/ml for *Salmonella* (Zhu et al., 2007b) and 700 cells/ml for *E. coli* (Campbell and Mutharasan, 2005b).

Optical Label-Free Biosensor Platforms

Surface Plasmon Resonance (SPR)

Surface plasmon resonance is an optical method for determining interactions (binding events) occurring at a sensor surface, wherein changes in bound mass are manifested as changes in refractive index (RI). The principle of SPR and the relationship to biosensing applications has been presented in several reviews (Ricci et al., 2007; Cooper, 2003; Homola, 2003; Homola, 1999). A basic overview of SPR is presented to allow understanding of how SPR biosensors function and for comparison to other optical biosensing methods. SPR is based on the transfer of light energy (photons) to electrons in a metal film. When polarized light passes through a prism or grating and strikes a thin metal film (gold for example) which is bordered by a dielectric layer, oscillations in free electrons, or surface plasmons, are generated in the metal layer and are propagated parallel to the dielectric layer. The result is generation of an electromagnetic field, or evanescent wave, with maximum charge density at the metal-dielectric interface, and which decays exponentially with distance from the metal surface to a maximum decay length of about 200 nm from the metal layer. SPR is extremely sensitive to changes in refractive index associated with the dielectric layer and within the evanescent field caused by adsorption or desorption of molecules from the surface. The refractive index is detected by monitoring the angle of light reflected from the back of the thin metal film. When photon and plasmon energies are equal there is coupling into the dielectric layer,

which is detected as a dip or “shadow” at a specific angle of reflection. SPR is sensitive to any mass within the evanescent field, whether bound or unbound, and for this reason assays are typically performed under constant flow conditions so that only specific binding events are detected. When refractive index changes as a result of surface binding events the angle shifts slightly, and the resulting shift in SPR dip can be plotted as a function of time (a sensorgram) (Figure 4) (Yu et al., 2006; Cooper, 2003; Homola, 2003).

SPR has been utilized for a wide range of biosensing applications from small molecules such as drugs and metabolites to larger targets including proteins, toxins, antibodies and whole cells (for examples see Homola, 2008; Ricci et al., 2007; Homola, 2003). Typically, immobilization of antibodies on the sensor surface confers target specificity, and localized mass increases as a result of ligand binding drive refractive index changes. Of particular interest is the detection of whole bacterial cells, particularly those associated with foodborne illness. Although SPR is a relatively new method, a number of experimental reports associated with foodborne or enteric pathogen detection have been published. Detection of *E. coli* O157:H7 from culture dilutions was demonstrated using a direct assay involving binding of whole cells to immobilized anti-*E. coli* antibodies, with a detection limit of 10^6 CFU/ml. Addition of secondary antibody in a sandwich assay decreased the limit of detection to 10^4 CFU/ml (Subramanian et al., 2006). Waswa et al. (2006) spiked skim milk samples with varying concentrations of *E. coli* and *Salmonella* and, using a direct binding

assay, reported sensitivities of 25 and 23 CFU/ml for *E. coli* and *Salmonella*, respectively, with a total assay time of less than 1 hour. Previously, Bokken et al. (2003) had demonstrated high selectivity to specific *Salmonella* serovars using an SPR immunoassay, with minimum detection limit of 1.7×10^3 CFU/ml for *Salmonella* in a mixed bacterial assay sample. Self-assembled protein G-antibody layers on gold surfaces have been shown as highly effective methods of functionalizing sensor surfaces for detection of *Salmonella* in direct binding assays, with effective detection range of 10^2-10^7 CFU/ml (Oh et al., 2004a) or 10^2-10^9 CFU/ml (Oh et al., 2004b). Recently, similar detection limits were reported for *Listeria monocytogenes*, *Campylobacter jejuni*, *Salmonella* Typhimurium and *E. coli* species from mixed cultures using low-level (8-channel SPR) multiplexing for simultaneous detection of all 4 targets (Taylor et al., 2006).

Microring Resonators

Description and Principle of Operation. Microring resonators are micron-scale optical devices which have seen wide use in communication circuits as optical switches, wavelength filters and frequency converters (Ibrahim et al., 2003; Little et al., 1997). Several design formats for microring resonators have been reported (Ibrahim et al, 2003; Chu et al., 1999; Yanagase et al., 2002; Little et al., 2004), with the general form being ring-shaped waveguide structures optically coupled to one or more linear waveguides, patterned on a planar surface (Little et al., 2000). Recently they have shown utility as transducing elements for biosensor applications, functioning as evanescent field, refractive index sensors

similar to surface plasmon resonance described previously. However, unlike SPR, excitation of a metal surface to generate an evanescent field is not utilized. Rather, in microring resonators light is coupled into a ring structure made of high refractive-index material via waveguides closely positioned to the resonator so as to allow coupling between the waveguide (light "bus") and the ring structure (Figure 5). The devices rely on total internal reflectance to guide light within the ring structure, taking advantage of a phenomenon called whispering gallery mode (WGM). In WGM devices, light is coupled into a circular light path and establishes a resonance mode, travelling continuously around the path until it is absorbed or scattered, resulting in exceptionally long path lengths (Ramachandran et al., 2008; Sun et al., 2008; Yalcin et al., 2006). .WGM devices have been evaluated for utility in biosensing applications (Zhu et al., 2006; White et al., 2005; Vollmer et al., 2003; Vollmer et al., 2002). Similar optical resonance patterns have been demonstrated in other devices including microcylinders and microdiscs (Smotrova et al., 2006; Deng et al., 2004; Zeng et al., 1999).

Microring resonators employ narrow light paths such that light which is channeled through the resonator structure is tightly constrained, and an evanescent field surrounding the optical structure is generated as a result of optical boundary conditions defined by the microring structure (Ramachandran et al., 2008; Sun et al., 2008). Conceptually, the effect could be considered similar to light "leakage" from the optical waveguide. The evanescent field effect is used for optically coupling ring structures to input and output waveguides as well as for optical

sensing (Figure 5). Microring resonators make use of high refractive index (RI) materials (refractive indices greater than 1.4), and optical sensing is achieved by functionalizing the microring surface such that specific molecular binding events result in an increase in bound mass within the evanescent field, in turn causing a change in refractive index in these areas of the structure (Ramachandran et al., 2008; Sun et al., 2008; Yalcin et al., 2006; Ksendzov and Lin, 2005). When coupled with WGM, the functionalized surface can be interrogated many times as light travels through the ring structure. Optical resonance in the microring is attained when the condition in the following equation is satisfied,

$$2\pi R\eta = \lambda m$$

where R is the radius of the microring, η is the effective refractive index (RI) of the microring, λ is the wavelength, and m is any integer. The product of the ring circumference $(2\pi R)$ and effective RI (η) is termed the optical path length (OPL).

Light entering the microring structure via the input waveguide of a specific wavelength (defined by the status of the ring structure – see equation above) continuously builds in phase resulting in an amplified evanescent field extending 100-300 nm beyond the outer surface of the microring. A small amount of light is coupled to the output waveguide and the resonant wavelength is analyzed. Changes in the evanescent field (e.g., binding events on the resonator surface) alter the local refractive index and, in turn, the resonance properties of the structure, with the end result being a shift in the wavelength of resonant light coupled to the output waveguide. The shift in output wavelength is measured by

continuously analyzing the optical spectrum of output light (Ramachandran et al., 2008). The high RI of ring resonator materials imparts high *Q* values, on the order of 10^4, which allows generation of resonance peaks which are very narrow and sharp. The *Q* value correlates with resolution and, in turn, sensitivity, as wavelength shifts in sharper peaks are easier to detect (within the limits of the detection device).

Biosensing Applications. Optical microring resonators have been used in proof-of-concept studies to demonstrate detection of specific protein-protein interactions at the resonator surface. Label-free detection of an avidin- or streptavidin-biotin interaction has been demonstrated on simple microring resonator structures using only silica or polymer as structural material (Chao et al., 2006; Yalcin et al., 2006; Ksendzov and Lin, 2005). Immunobinding on more complex slot-waveguide structures was demonstrated with bovine serum albumin (BSA) with an anti-BSA antibody coupled to the sensing surface and label-free detection of antigen-antibody binding (Barrios et al., 2008). The slot-waveguide resonator is similar to the simple resonator but is fabricated to include a vertical slot on the ring structure (Barrios et al., 2007). Recently the utility of microring resonators for a wider range of biosensing applications has been shown (Ramachandran et al., 2008). These studies demonstrated detection of DNA hybridization, quantitative antibody analysis and binding of whole *E. coli* O157:H7 to the resonator surface. Whole cell bacterial detection limits reported were on the order of 10^5 CFU/ml.

Figure 1. Effect of ß-lactam antibiotics on penicillin binding proteins and cell wall synthesis. Transpeptidase-mediated cell wall crosslinking continues in PBP2a (PBP2') (green), while other penicillin binding proteins (red) are deactivated by binding of antibiotic to enzyme active site. Figure from Hiramatsu, 2001.

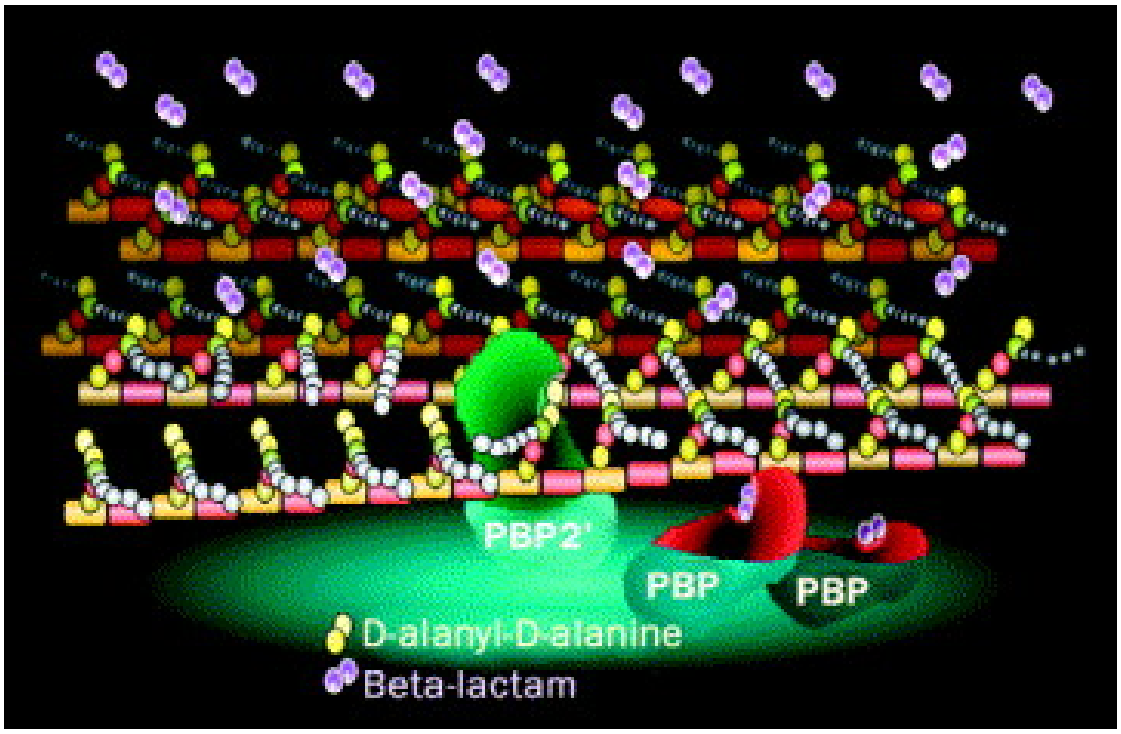
PBP2'
PBP
PBP
D-alanyl-D-alanine
Beta-lactam

Figure 2. Schematic diagram of different types of SCC*mec*. *mec*: resistance to methicillin/oxacillin; *ccr*: site of cassette excision; pUB110: aminoglycoside resistance; Tn*554*: transposon encoding erythromycin and streptomycin resistance; ΨTn*554*: cadmium resistance. Figure from Martins and Cunha, 2007.

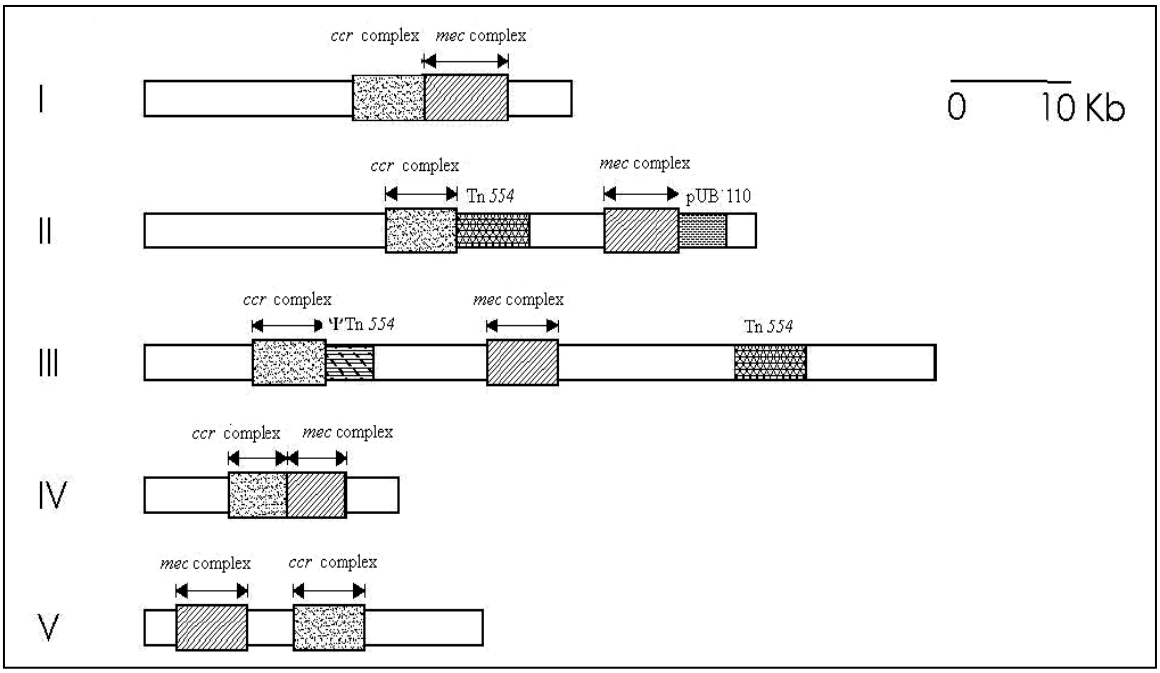
ccr complex
mec complex
I
0
10 Kb
ccr complex
mec complex
Tn 554
pUB 110
II
ccr complex
mec complex
ΨTn 554
Tn 554
III
ccr complex
mec complex
IV
mec complex
ccr complex
V

Figure 3. Examples of microcantilever devices. Top: An 8-cantilever array used for vapor sensing used as a deflection-type sensor. Bottom: A cantilever device with a single *E. coli* cell bound near the tip. Bar equals 5 µm. From Waggoner and Craighead, 2007.

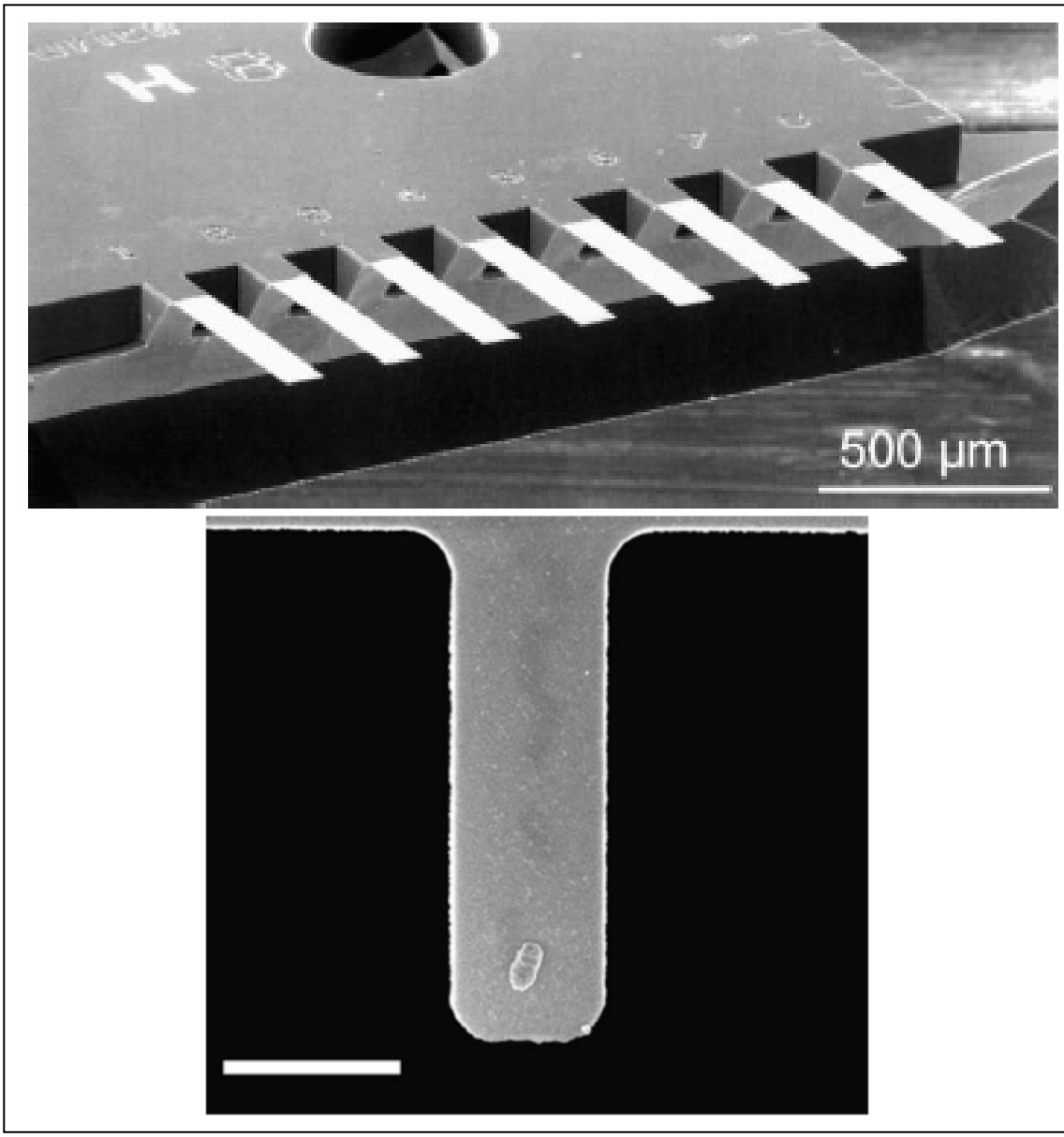
500 µm

Figure 4. Diagram of typical set-up for a surface plasmon resonance (SPR) biosensor. Polarized light is directed through a prism to a layer of gold film to excite surface plasmons. Reflected light is directed to an optical detection unit such as a diode array. Bound mass on the sensor surface changes the angle of reflected light which is displayed on the sensorgram. Figure from Cooper, 2003.

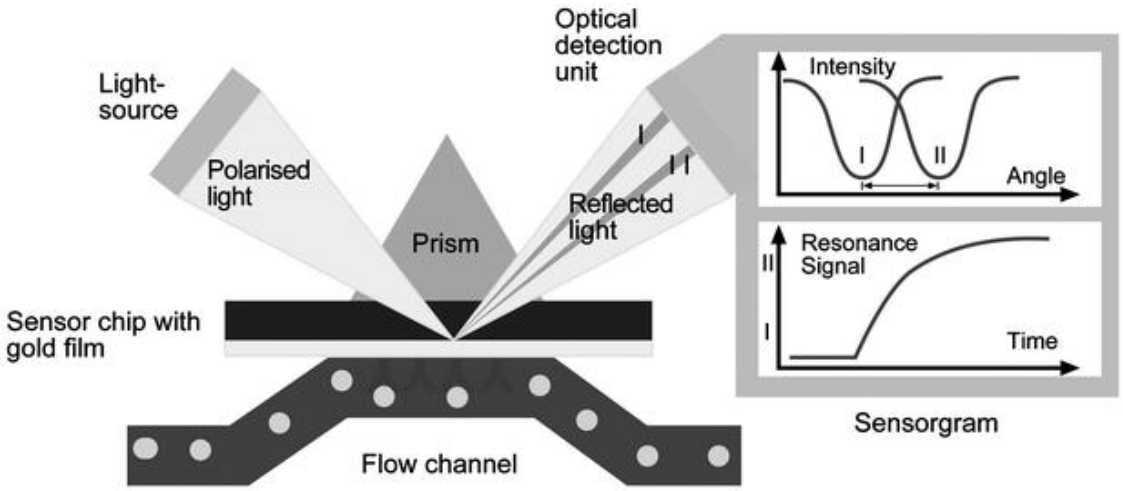
Optical
detection
unit
Light-
source
Polarised
light
Prism
Reflected
light
I
I I
Intensity
I
II
Angle
Resonance
Signal
II
I
Time
Sensor chip with
gold film
Flow channel
Sensorgram

Figure 5. Schematic of microring resonator. (a) Arrows indicate the direction of light flow. Resonant light from the input waveguide couples into the microring structure and circulates several times before a fraction escapes into the output waveguide. (b) Cross-section of a vertically-coupled microring resonator.

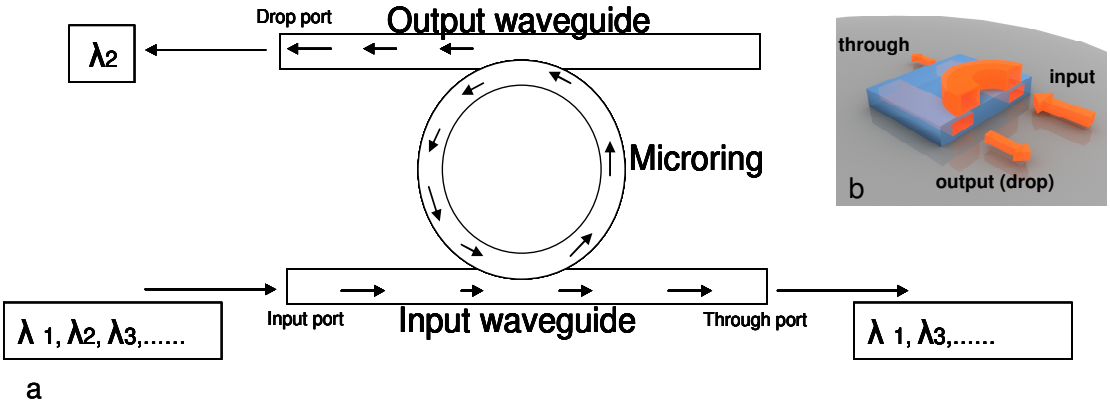
Drop port
Output waveguide
λ2
Microring
λ 1, λ2, λ3,.....
Input port
Input waveguide
Through port
λ 1, λ3,.....
a
through
input
output (drop)
b

CHAPTER III

Use of Suppression Subtractive Hybridization to Identify Unique Markers for *Clostridium piliforme* isolate H1

Introduction

Tyzzer's disease is a fatal, necrotic hepatitis caused by the obligate intracellular pathogen *Clostridium piliforme*. The organism is capable of infecting multiple species and is most commonly observed in laboratory animals and horses. Bacteria within the species are identified by the host from which they were originally isolated during naturally occurring infections. Previous reports have indicated there are differences in cytotoxic activity associated with different isolates when grown *in vitro* on different host cell monolayers, and that there is some heterogeneity in protein expression between isolates. The isolate from hamster (H1) has been show to have higher cytotoxicity *in vitro* and is more capable of causing fatal infection *in vivo* across several species, and production of cytotoxic factors was suggested as a factor in increased pathogenicity. The organism is difficult to maintain in culture, requiring host cells for intracellular propagation. As a result, the organism is poorly characterized genetically, and

the only means of identifying presence of the organism by PCR is the use of 16S ribosomal markers as amplification targets.

Suppression subtractive hybridization (SSH) was originally developed as a means of isolating unique coding sequences from eukaryotic organisms (Daitchenko et al., 1996), and has become a common procedure in differential eukaryotic expression assays (Kültz et al., 2007; Sternberg and Gepstein, 2007; Røsok and Sioud, 2007). The procedure originally described involves ligation of different linkers containing internal PCR priming sites to 2 separate pools ("tester" pools) of total cDNA from the organism from which isolation of differentially expressed sequences is desired (Figure 1). Hybridization to excess "driver" cDNA from a comparative sample is used to subtract fragments having high homology between the 2 tester pools and the driver sample. Multiple hybridization steps coupled with downstream amplification results in a pool of cDNA which is present in the tester samples but not in the driver samples. The procedure has been successfully applied to bacterial genomic studies to examine differences between genomic DNA pools (Huang et al., 2007; Winstanley, 2002), and has been developed into a commercial bacterial genomic analysis kit (PCR-Select™ Bacterial Genome Subtraction Kit, Clontech).

The goal of this study was to identify genomic sequences in *C. piliforme* cytotoxic isolate H1 which were not present in the non-toxic isolate R1 originating from a natural rat infection, and to associate these sequences with possible cytotoxin

production by the H1 isolate. Results from this study could serve as a foundation for future work to isolate and clone genetic elements associated with cytotoxin production, and for isolation and characterization of H1-associated pathogenicity factors.

Materials and Methods

Culture of *C. piliforme*

C. piliforme isolates R1 and H1 were a generous gift provided by Lela Riley (University of Missouri). Bacterial isolates were cultured on buffalo rat liver cells (BRL 3A; ATCC CRL 1442) as previously described (Riley et al., 1990). Intracellular growth of bacteria in confluent host cell monolayers was monitored via inverted microscope, and when cultures were infected at high density, usually 24-48 hr. post-inoculation, cells were scraped from cell culture flasks and frozen in culture medium containing 10% dimethyl sulfoxide in liquid nitrogen for later use. Assay cultures were initiated by application of 1 ml thawed inoculum to BRL 3A cells at ~70-80% confluence in multiple 75 cm^2 tissue culture flasks. Infected cell cultures were washed with fresh culture medium after 12 hours and grown until intracellular infection was well established.

DNA Isolation

C. piliforme DNA was isolated by scraping active cell cultures into a small volume of phosphate-buffered saline (PBS, pH 7.4) and host cells were lysed by

repetitive aspiration through a 1 ml micropipette tip. Intact host cells and large debris were precipitated by centrifugation (300 x g, 20 min.). Supernatant was collected and bacterial cells were recovered by high-speed centrifugation (10,000 x g, 5 min.). Excess host cell nucleic acids were removed by resuspending bacterial cells in PBS and repeating the centrifugation, with the wash procedure repeated 2 times. Bacterial cells were lysed by incubation in SET buffer (25% wt/vol sucrose, 50mM Tris-HCl, 50mM EDTA) containing 1 mg/ml lysozyme (Sigma Chemical Co.) at 37C for 1 hr., followed by addition of sodium dodecyl sulfate (SDS) to a final concentration of 1% (wt/vol) and proteinase K (Promega) at final concentration of 1 mg/ml. Samples were incubated at 55C for 2 hr. with occasional inversion, followed by addition of one-third volume sodium chloride and one volume chloroform. Contaminants were removed by centrifugation (4500 x g, 15 min.). Supernatant was recovered and further purified by phenol-chloroform extraction and ethanol precipitation. BRL 3A DNA was purified by standard phenol-chloroform isolation. Bacterial and host cell DNA was analyzed by agarose gel electrophoresis to verify presence and purity of high molecular weight DNA following extraction

Restriction Digestion of DNA

In order to generate fragments of suitable length for SSH (<2000 bp) high molecular weight DNA was subjected to restriction digests with a mixture of frequently-cutting enzymes with 4 bp recognition sites. Combinations of *Msp*I, *Hae*III, *Hin*fI and *Sau*3A I enzymes (Promega) were used in an initial assay to

determine which combinations would result in desired fragmentation of DNA to be used in the SSH procedure. Final restriction digestion utilized a combination of all enzymes as follows: 10 µg DNA, 12.5 µl universal reaction buffer and 12.5 U of each enzyme in a total reaction volume of 125 µl at 37C for 13 hr. Following digestion samples were blunt-ended by addition of 10 U T4 DNA polymerase, 200 µM each of dATP, dCTP, dGTP and dTTP in a total reaction volume of 187.5 µl with incubation at 37C for 1 hr., followed by addition of 12.5 U Klenow DNA polymerase and incubation at 37C for an additional hr. Reaction products were purified by phenol-chloroform extraction and ethanol precipitation and resuspended in water at a final concentration of 300 ng/µl.

Preparation of Tester (H1) DNA

Preparation of H1 DNA to be used as tester followed the general procedure of Diatchenko et al. (1996). Blunt-ended *C. piliforme* H1 tester DNA was diluted 1:5 in distilled water and used in 2 separate adapter ligation reactions. One reaction used 2 µl diluted tester (120 ng), 2 µl adapter 1 (10 µM), 0.5 U T4 DNA ligase, 1 µl rATP, 1 µl ligase buffer and 6 µl distilled water. The other reaction was identical with the exception of substitution of adapter 2 for adapter 1. Samples were incubated at 16C for 16 hr., and then ligase was inactivated by addition of 1 µl 0.2 M EDTA and heated at 70C for 5 min. Sequences for adapters and PCR primers were as follows:

Adapter 1:

```
5′-GTAATACGACTCACTATAGGGCTCGAGCGGCCGCCCGGGCAGGT-3′
                                        3′-CCCGTCCA-5′
```

Adapter 2:

```
5′-TGTAGCGTGAAGACGACAGAAAGGGCGTGGTGCGGAGGGCGGT-3′
                                  3′-GCCTCCCGCCA-5′
```

Primer 1: 5′-GTAATACGACTCACTATAGGGC-3′

Primer 2: 5′-TGTAGCGTGAAGACGACAGAA-3′

Primer N1: 5′-TCGAGCGGCCGCCCGGGCAGGT-3′

Primer N2: 5′-AGGGCGTGGTGCGGAGGGCGGT-3′

SSH Hybridization Procedure

The hybridization procedure followed that of Diatchenko et al. (1996) with the exception that both *C. piliforme* R1 DNA and rat liver cell (bacterial culture host) DNA served as driver. Thus, simultaneous subtraction of DNA fragments shared by both *C. piliforme* isolates and contaminating host cell DNA fragments was possible. Two µl each of R1 and rat cell driver were added to 2 tubes containing 2 µl of either adapter 1- or adapter 2-ligated H1 tester. Samples were mixed and ethanol precipitated (15,000 x g, 20 min., 4C) and resuspended in 1.5 µl hybridization buffer (50 mM HEPES, pH 8.3/0.5 M NaCl/0.02 mM EDTA, pH 8.0/10% (wt/vol) PEG 8000). Individual tester samples were denatured at 98C for 1.5 min., and then held at 68C for 10 hr for the first hybridization step. Individual tester samples were then combined with the addition of 1.5 µl of heat-denatured driver (1.5 µg each of R1 and rat DNA in hybridization buffer). Pooled sample was hybridized an additional 10 hr at 68C, then diluted in 200 µl dilution buffer (20 mM HEPES, pH 8.3/50 mM NaCl/0.2 mM EDTA) and heated at 72C for 7 min.

PCR Amplification of Hybridization Products

PCR amplification of hybridization products was performed as described by Diatchenko et al. (1996) with minor modifications. An initial PCR reaction to amplify hybridization products was followed by a nested PCR reaction to further purify and amplify H1 unique sequences. The first PCR reaction used 1 µl of diluted, subtracted DNA from the previous step, 1 µl each of 5 µM stock of primers P1 and P2, 1 µl dNTP stock (10 mM dATP, dCTP, dGTP and dTTP), 2.5 µl AmpliTaq® PCR buffer (Applied Biosystems), 1 µl AmpliTaq® DNA polymerase, and 1µl $MgCl_2$ (1.5 mM) in a 25 µl total reaction volume. For both initial and nested reactions a parallel reaction using double the concentration of $MgCl_2$ was performed to determine if elevated $MgCl_2$ was beneficial to yield of final product. The nested reaction was the same as the initial reaction, with the exception of substitution of primers PN1 and PN2 for P1 and P2, respectively. These nested primers anneal to binding sites incorporated into the adapter sequences ligated to H1 tester DNA immediately internal to the initial primer (P1 and P2) binding sites. For the nested reaction 1 µl of a 10-fold dilution of the initial reaction product served as template. All reactions used a common temperature cycling protocol: 75C for 7 min.; 30 cycles at (91C for 30 sec.; 68C for 30 sec.; 72C for 2.5 min.); with a final extension at 68C for 7 min. Following nested PCR a sample of each reaction product was subjected to agarose gel electrophoresis. Best product yield and product size diversity was obtained with elevated $MgCl_2$ level in the PCR reaction, and these products were used for all downstream cloning procedures.

Cloning and Analysis of PCR Products

The TOPO-TA cloning system (Invitrogen) employing the PCR4-TOPO sequencing vector was used for cloning of PCR products. Four µl of nested PCR product was used in the ligation reaction according to manufacturer protocols. Ligation product was transformed into TOP10 One Shot cells using manufacturer-recommended chemical transfection protocols. Transformants were screened on Luria-Bertani agar plates containing IPTG and X-Gal for blue-white colony selection. White colonies representing clones with SSH product insert were picked and maintained for DNA sequencing. Plasmid DNA was isolated from overnight cultures of insert-positive clones using the Wizard® Miniprep kit (Promega) according to manufacturer protocols. Purified plasmid DNA was submitted to the Oklahoma State University Core Facility DNA sequencing service, with sequencing primers consisting of T7 sequencing primer. Resulting DNA sequences were used for computerized BLAST homology search (http://blast.ncbi.nlm.nih.gov) after trimming vector remnants from query sequences. The “nr” database was used as were the default nBLAST algorithm settings.

Results and Discussion

Subtractive Hybridization

DNA cleavage by multiple restriction enzymes was quite efficient, with nearly all fragments below 1.5 kb. Smaller fragment size was considered more desirable to maximize removal of rat host cell DNA by increasing overall hybridization efficiency. A higher concentration of smaller fragments is expected to promote faster hybridization kinetics, particularly among highly complementary sequences, while smaller fragment size helps prevent loss of shorter unique tester sequences which may be embedded in longer sequences having overall comparatively higher complementarity to driver. Post-hybridization nested PCR reactions run on agarose gels in parallel with original digested tester indicated a mixed PCR product size range similar to original digested H1 DNA (Figure 2).

A total of 69 distinct colonies were picked from culture plates, cultured and plasmid DNA submitted for DNA sequencing. Following BLAST analysis the majority yielded rat DNA sequences representing insert originating from rat liver cell DNA used as driver (19/69 colonies picked), or mouse sequences, which are expected to be highly homologous to rat driver cell genomic sequences (9/69 colonies picked). These colonies were discarded, as were those having inserts matching human DNA sequences (12/69 clones). Despite screening of colonies for plasmid insert using α-complementation culture conditions, 12 colony clones had no insert present by DNA sequencing analysis. DNA sequences are

presented in the appendix alongside computer output of the BLAST search results.

Generally, if sequences showed one or two medium- to low-strength matches (E value ~1 x 10^{-6} or greater) to human or mouse, and much lower homology to any other mammalian sequence, then the sequence was retained for further analysis. The E value or “expect value” is a parameter that describes the number of hits one can "expect" to see by chance. The E value decreases exponentially as the total score of the match increases. However, with shorter query sequences (such as many of the ones reported in the appendix) even a match over a relatively short stretch will give higher E values than may occur with a longer query sequence, since the query length is a component of the E value calculation. For this analysis, if true matches to human, mouse or rat sequences occurred, it would be expected that similar matches in the genomic sequences of other species which are at least somewhat genetically similar, or possibly that multiple strong matches in the same sequence, would be seen. In addition, there is always the possibility that some GenBank submissions are incorrect when added to the database, so indiscriminately discarding medium-strength matches could remove possibly useful sequences from the candidate list. Using this strategy is more conservative, and potentially useful sequences are not discarded.

Cloned PCR product A1 is a good example (see appendix). This sequence (122 bp) had one medium-strength match to human ceramide kinase-like protein (E=1e-04), and much lower matches to everything else. The remaining matches were mostly to plant sequences as well as some mammalian sequences, but the E value was sufficiently high to suggest this candidate should not be discarded and could possibly be used as template to generate primers to test for isolate H1-specific PCR amplification. In the case of shorter sequences, it is generally not feasible to design primers to amplify the entire fragment as a single amplicon because the likelihood of finding compatible primer pairs within such a short sequence is low. Rather, in these cases the strategy is to synthesize a single primer to be used for sequencing of genomic DNA and, taking data from primer extension to generate PCR primer pairs from the extended sequence for testing H1 isolate-specific DNA amplification.

PCR product A2 yielded matches to mouse sequences, but with very high E values (low match probability). However, after 2 rounds of sequencing the query sequence still had over 10% unresolved bases and was not a suitable initiating sequence for primer walking exercises. Remaining sequences, with the exception of K5 and K7, had complete or nearly complete sequence data with very few unidentified bases.

Seven clones had a good match to bacterial sequences, of which 5 had *Clostridium* species within the top matches (A3, D2, E6, E1 and K4). Two

products had extremely strong matches to *Rhodobacter* species, while 3 showed homology mainly to plant sequences. While it is possible some similarity exists between *Rhodobacter* and *C. piliforme*, matches to plants may be representative of an artifact either introduced as a contaminant during sequencing or during the selection and cloning process. However, these sequences and corresponding database match data are presented in the appendix for the sake of completeness of data. Remaining clones for the most part were cryptic with few acceptable matches reported, and may represent new, novel sequences and merit further investigation.

Clone A3 was of particular interest because it had a significant match to a *Clostridium* species (*Clostridium phytofermentans*) and because it had sequence of sufficient length and composition to permit use as a target amplicon. Primers were custom synthesized:

Forward: 5'-AATCATAAATCTCTTGACTATATATCAACAAATG -3'

Reverse: 5'-GCGTCTGTAAACTTTCCATAGCTTT-3'

Genomic DNA from isolates H1 and R1 were subjected to PCR using the same parameters as described for nested PCR reactions. Agarose gel electrophoresis indicated a band corresponding to the expected product size (106 bp) was present in both samples. These results suggest clone A3 sequence may represent a *C. piliforme*-specific marker but is not specific for isolate H1.

Unfortunately, a failure of the cryogenic storage system resulted in loss of all *C. piliforme* stocks and additional testing using the remaining candidate clone sequences was not possible. Nonetheless, the results obtained from clone A3 analysis indicate isolation of a potentially useful marker for specific amplification of *C. piliforme* for use in diagnostic PCR assays. Additional testing against closely related *Clostridia* and other species is indicated.

Conclusions

The results of the present study suggest the utility of suppression subtractive hybridization as a tool to identify unique genomic makers in an essentially uncharacterized obligate intracellular bacterial pathogen. Although results of the experiment did not yield isolate-specific marker sequences, it did result in new sequences with the potential to serve as *C. piliforme*-specific markers, and as diagnostic tools to indicate the presence of Tyzzer's disease. Additional sequences were identified which may correspond to genomic sequences in isolate H1 which code for toxins or other pathogenicity factors, although these were not tested. Future experiments can take advantage of these results by using sequences identified in this study as starting points for synthesis of sequencing primers to facilitate expansion of genomic sequence information by primer extension of H1 genomic DNA. Expanded sequence information can then be used to identify and characterize coding sequence for possible cytotoxins or

other cytotoxic factors, and for assembly of target amplicons for H1- or *C. piliforme*-specific genetic PCR markers. Here we have presented a method which allows identification of potentially useful markers in a largely uncharacterized intracellular pathogen even in the presence of contaminating host cell DNA. The possibility of extending this methodology to other unknown organisms, particularly uncharacterized emerging pathogens, gives SSH high utility as a genomic analysis tool.

Figure 1. Overview of suppression subtractive hybridization (SSH) procedure. Fragmented genomic DNA from the sample from which one wishes to subtract, is split into 2 tester pools and different linkers are ligated to ends of fragments in each pool. Two rounds of subtractive hybridization/PCR against a fraction having common elements to be subtracted (driver), results in isolation and amplification of sequences in tester populations which are not present in the driver population. In the experiments described, H1 isolate DNA was tester and R1 isolate and rat genomic DNA served as driver. Figure taken from the Clontech PCRSelect^{TM} Bacterial Genome Subtraction kit User Manual (BD Biosciences Clontech).

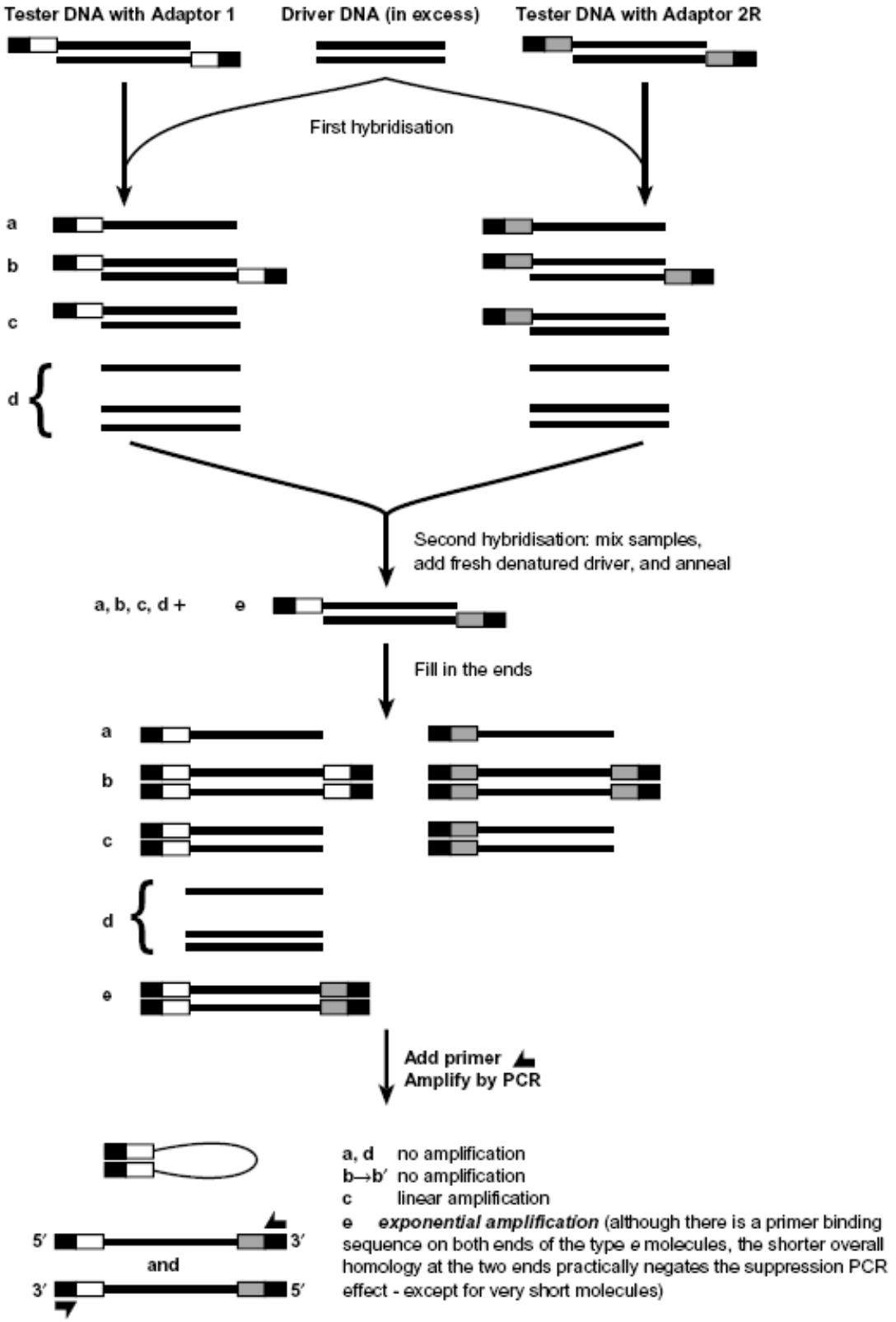
Tester DNA with Adaptor 1
Driver DNA (in excess)
Tester DNA with Adaptor 2R
First hybridisation
a
b
c
d
Second hybridisation: mix samples,
add fresh denatured driver, and anneal
a, b, c, d +
e
Fill in the ends
a
b
c
d
e
Add primer
Amplify by PCR
5′
3′
and
3′
5′
a, d no amplification
b→b′ no amplification
c linear amplification
e exponential amplification (although there is a primer binding sequence on both ends of the type e molecules, the shorter overall homology at the two ends practically negates the suppression PCR effect - except for very short molecules)

Figure 2. Results of nested PCR reactions of SSH product prior to cloning. A small size distribution is visible indicated by the smeared band. Most product was in the range of 50-150 bp. Lane identification: M, molecular weight marker; A, nested PCR from SSH procedure; B, restriction digested H1 genomic DNA used in SSH procedure.

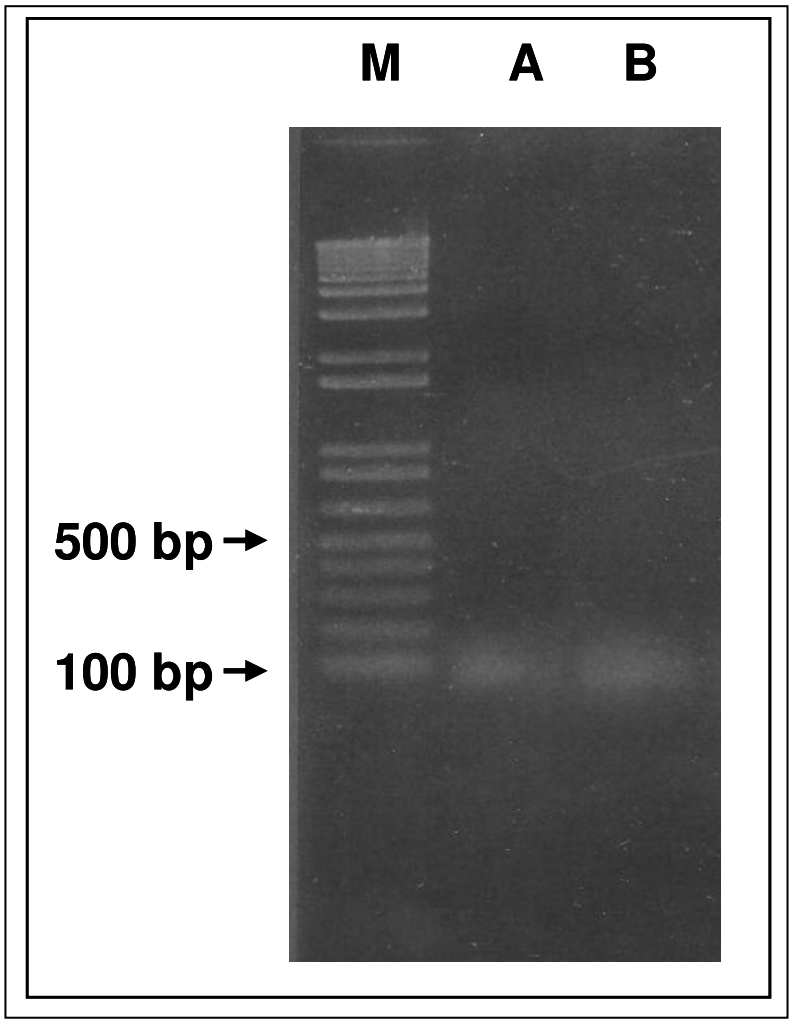
M
A
B
500 bp
100 bp

CHAPTER IV

Development of an Amplified Fluorescent Antigen Displacement Assay For Detection of Methicillin-Resistant *Staphylococcus aureus*

Introduction

The goal of the described research was to develop a detection component for a highly sensitive, rapid, specific, and low-cost method for diagnosis of infections by methicillin-resistant *Staphylococcus aureus*. The availability of a system capable of identifying antimicrobial-resistant bacteria will promote immediate and effective therapeutic intervention and will minimize the spread of antimicrobial resistance. Such a sensor must be able to detect indicators of resistance. For example, resistance indicators for methicillin-resistant *S. aureus* (MRSA) have been thoroughly researched and include the *mecA* gene and low-affinity penicillin binding protein 2a (PBP2a). This work was undertaken to develop a sensor that will identify MRSA by detecting the PBP2a protein.

Current assay strategies for detection of protein in clinical samples rely on antibody recognition of the protein target followed by some transduction event to

give a readable signal and detection of the presence of the protein and, in turn, detection of the organism from which it came. Current microplate-based immunological assays can be very sensitive, particularly when coupled with fluorescent detection strategies. However, these methods tend to be slow and labor-intensive and in many cases prone to error. In the case of MRSA, the standard course of action when infection is a possibility, is confinement and treatment with potent antibiotics until a positive identification can be made after culturing the organism in the laboratory, often days later. The aggressive antibiotic therapies include “last line of defense” drugs such as vancomycin. Unnecessary use of antibiotics is likely to hasten development of resistance to those drugs. Therefore, it is highly desirable to have an assay that is rapid, sensitive and has the potential to be used at the bedside or within a physician’s office.

Amplifying fluorescent polymers are a new generation of tunable poly(phenylene ethynylene) (PPE) polymers that amplify the fluorescence response of each captured analyte molecule, thus attaining very high sensitivity (Figure 1). These materials were developed by Professor Timothy Swager (MIT) (Swager, 1998; McQuade et al., 2000), and have been utilized in several sensor-based applications. When the polymer is excited by light, photon energy in the form of excitons migrates rapidly along the conjugated polymer chain, and to some extent between chains. Interaction with certain molecules (quenchers and fluorescence resonance energy transfer (FRET) acceptors) at any point along the

polymer chain can generate a collective response in the entire chain, visible as a decrease in fluorescence ("turn off" event) or increase in fluorescence, respectively. In comparison to standard fluorescence interactions involving unimolecular fluorophore-quencher interactions, AFP-based systems have intrinsic amplifying capability by converting one quencher molecule interaction into multiple quenching events (Figure 2). For biological agent detection, these PPE-based signal amplifying polymers have been modified and can be used in a number of different formats, including aqueous dispersions of nanoparticles, thin films (slide or capillary), membranes, fiber-optic probe constructs, and 96-well plates.

The goal of the present study was to develop a rapid, sensitive assay to detect the protein which imparts the methicillin-resistant phenotype to MRSA. The strategy was to couple the intrinsic fluorescent amplification potential of amplifying fluorescent polymer (AFP) with a simple immunological step involving displacement of a quencher-labeled peptide from an immobilized antibody, followed by flow of labeled peptide *in vitro* to an AFP-coated surface. The presence of an amplified fluorescence quenching event would be the indicator for presence of the protein in the sample, and hence presence of MRSA.

Materials and Methods

Determining Peptide Antigens

Protein sequence representing PBP2a protein of *S. aureus* methicillin-resistant strain R27 was retrieved from PubMed protein database search (Accession X52593; http://www.ncbi.nlm.nih.gov). In order to deduce expected surface-exposed regions of the protein which could serve as appropriate antigenic targets, amino acid sequence comprising the catalytically-active transpeptidase domain was analyzed for local hydrophobicity, hydrophilicity, antigenicity and hydropathicity using VectorNTI software (Informax, Invitrogen Corp.). Prediction of likely secondary structure used the NNPREDICT online analysis (http://alexander.compbio.ucsf.edu/~nomi/nnpredict.html). Most probable surface-exposed epitopes were identified based on low hydrophobicity and high hydrophilicity, with bias toward regions with comparatively high antigenic index values. Three regions were identified and custom 20 amino acid peptides were synthesized (ResGen, Invitrogen Corp.). Sequences of the 3 peptides were as follows:

Peptide 1: N-term – TLDDKTSYKIDGKGWQKDKS – C-term (aa pos. 418-437);

Peptide 2: N-term – KDTKNKVWKKNIISKENINL – C-term (aa pos. 551-570);

Peptide 2: N-term – NVKDVQDKGMASYNAKISGK – C-term (aa pos. 632-651).

Antibody Production and Screening

Monoclonal antibodies to PBP2a peptide antigens were produced by the Oklahoma State Hybridoma Research Center. Custom peptides were conjugated via amine coupling to keyhole limpet hemocyanin carrier (Pierce) and pooled for mouse immunization. Immune response was verified by screening against immobilized pooled peptide antigens, and cell fusions were performed using standardized protocols. Supernatants from fusion cultures were tested for reactivity toward individual peptide antigens adsorbed to microplate wells with polyvalent anti-mouse IgG as secondary antibody using blank wells and bovine serum albumin (BSA)-adsorbed wells as controls. Additional screening utilized peptide conjugated to BSA as carrier to allow efficient adsorption in microplates, as well as BSA alone as negative control. Data from colorimetric Enzyme-linked Immunosorbent Assays (ELISAs) were subjected to one-way Analysis of Variance (ANOVA) to determine the three best candidate fusion lines for MAb production. Purified monoclonal antibodies were tested by ELISA and western blot analysis, and class and isotype analysis. Three antibodies were reactive to specific peptides as well as purified, soluble recombinant PBP2a protein: An IgM and two IgG_2 antibodies. Based on suitability for downstream applications the IgG antibodies were chosen for use in assay development. Hybridoma clones expressing these antibodies were grown in batch culture and antibody was purified from culture supernatants using the MAbTrap Kit (Pharmacia) according to manufacturer protocols.

Recombinant Protein Construction, Expression and Purification

Construction of water-soluble PBP2a protein followed the strategy of Wu et al. (1992) wherein the hydrophobic N-terminal 22 amino acids comprising a membrane-spanning region were deleted from the expression construct. The complete PBP2a coding sequence beginning with tyr23 was generated by 3-step polymerase chain reaction amplification of genomic DNA from a methicillin-resistant *S. aureus* reference strain (ATCC 43300) using custom primers:

Forward: 5'-TATGCTTCAAAAGATAAAGAAAT-3';

Reverse: 5'-CATCGTTACGGATTGCTTC-3'.

The reaction was performed using a proofreading polymerase for maximum fidelity (DeepVent®, New England Biolabs) and the reaction was as follows: 200 µM each dNTP, 5 µl reaction buffer, 0.1 µg DNA, 1.5 U enzyme and $MgSO_4$ to a final concentration of 7.5 mM. Final reaction volume was 50 µl and the cycling profile was 94C/5 min.; 30 cycles of 52C/1 min., 72C/1 min., 94C/1 min.; 72C/5 min. The resulting product was purified by gel electrophoresis (QiaQuick Gel Extraction Kit, Qiagen) and incubated with dATP and *Taq* polymerase (1.5 µl AmpliTaq® buffer, 60 mM dATP, 1.5 mM MgCl2 and 1.25U AmpliTaq® polymerase (Applied Biosystems) at room temperature for 10 min.) to produce 3' A-overhangs for ligation into the T7/NT-TOPO vector (Invitrogen). This vector contains a T7 RNA polymerase binding site for high-level transcription, and expressed protein contains an N-terminal fusion domain consisting of an affinity tag, a 6X His region for metal ion chromatography (MIC) and an enterokinase cleavage site for release of the fusion component from solPBP2a protein. The

PCR product was inserted in the expression vector using standard manufacturer protocols and chemically transformed into *E. coli* Top10 One Shot cells (Invitrogen) for screening by restriction analysis of plasmid DNA to determine proper insert orientation relative to vector, followed by DNA sequence analysis to verify correct protein coding sequence.

The complete expression construct was purified (Wizard miniprep kit, Promega) and transformed into *E. coli* pLysS cells (Invitrogen) for protein expression. Cultures were induced with 1 mM IPTG to initiate expression of fusion protein via T7 RNA polymerase originating from host cells, cells were lysed by freeze-fracture, and protein was purified according to manufacturer protocols using Talon® MIC resin (Clontech) and imidazole gradient elution per manufacturer specifications. Purified fusion protein was subjected to SDS-polyacrylamide gel electrophoresis to verify presence of a single band representing the fusion protein product. Excess imidazole was removed by exhaustive dialysis against PBS buffer.

Peptide Displacement Assays

Quencher-labeled peptide displacement assays were performed by competitive elution of labeled peptide from antibody using either unlabeled peptide or solPBP2a protein as displacing agent. Monoclonal antibody was immobilized in protein-G activated microplate wells (Reacti-bind protein G plates, Pierce Bio) at a concentration of 10 µg/well following manufacturer protocols. Quencher-

labeled peptide was custom synthesized (SynPep Corp.) from P2 peptide sequence with a DABCYL label added during synthesis. Microwells were washed twice with PBS buffer and labeled peptide was added at 100-fold molar excess to maximum expected bound antibody (according to manufacturer specifications) and incubated at 4C for 16 hr. Microwells were washed 4 times with PBS buffer and unlabeled peptide or solPBP2a protein was added to wells to initiate antigen displacement. Unlabeled peptide and protein concentration was varied among wells using 10-fold serial dilution ranging from 0.001 to 100 pmol/well. Following a 30 minute total incubation period at room temperature the contents of microplate wells were aspirated and applied to AFP-coated glass microcapillaries in a flow-through format within a bench top fluorometer (Fluoromax 2, Jobin-Yvon, Inc.). AFP was diluted to a final concentration of 0.1 mg/ml wt/vol in toluene and applied by addition of ~40 µl to the inside of a pre-etched capillary with a syringe and 27g needle, followed by spinning of the capillary in a spin-coating device at ~3000 x g for 20 seconds to remove excess AFP solution. Prior to addition of displacement samples capillaries were washed with 500 µl PBS buffer (approximately 50 times internal capillary volume) at a flow rate of approximately 0.25 ml/min. to allow buffer-polymer equilibration, to elute unbound polymer and to facilitate baseline fluorescence values. High between-capillary variability precluded the use of individual capillaries for each displacement assay sample. Instead, samples were applied in succession from lowest to highest concentration of displacing agent within a single capillary. An additional correction factor was applied by running parallel assays using bare

glass capillaries to determine fluorescence associated with assay samples. These values were then subtracted from corresponding sample-AFP values to yield the fluorescence value corrected for intrinsic sample fluorescence.

Results and Discussion

Peptide Antigen Selection

The results of *in silico* selection of potential antigenic peptide antigens are summarized in Figure 3. The selection strategy relied upon selecting peptide sequences in regions with highest likelihood of surface exposure on the intact and correctly folded native protein. Regions with low hydrophobicity and high hydrophilicity are most likely to be exposed on the surface, while the reverse characteristics are more suitable for peptides buried within the hydrophobic interior of the intact protein. Three peptides were selected primarily on hydrophobicity/hydrophilicity characteristics, and to a lesser extent hydropathicity and antigenic value indices. Results of NNPredict analysis (Figure 4) were compared to predicted peptide hydrophobicity plots and regions lacking secondary structure with low hydrophobic potential were selected. During the course of this study the 3-dimensional structure of native PBP2a protein was determined by NMR (Lim and Strynadka, 2002). The location of selected peptide regions, and that of peptide 2 in particular are shown in Figure 5. The results indicate excellent prediction of surface-exposed regions for antigenic peptide

synthesis. The region indicated for peptide 2 is well-exposed and is expected to interact efficiently with antibody in competitive binding assays.

Antibody Screening

Screening of 78 monoclonal antibody fusion stocks yielded 3 candidate antibodies which were reactive to peptide antigens in ELISA assays using peptide adsorbed directly to microplate wells or conjugated to BSA prior to adsorption. Western blot analysis was performed against solPBP2a protein and all antibodies were shown to bind recombinant protein. Further characterization and isotyping of candidate antibodies indicated one antibody was IgM, while the remaining 2 were IgG2. In the interest of downstream assay development the IgM candidate was rejected. The remaining candidates were both identified as reactive and specific to the same immunizing peptide antigen, peptide 2.

Antigen Displacement

Recombinant soluble PBP2a protein was prepared in milligram quantities from large-scale culture. Results of immobilized metal ion chromatography using imidazole gradient were unsatisfactory and resulted in several bands ranging in size from 8 to ~75 kDa. It was necessary to modify protein purification to include 2 steps, an initial imidazole gradient followed by a second round of IMAC purification employing a 50 mM imidazole wash step to remove contaminants prior to final elution of solPBP2a with 100 mM imidazole. Although total protein

yield was greatly reduced, this method did result in a single protein product (Figure 6).

Initial displacement assay experiments utilized a custom capillary tube holder fitted to a bench top fluorometer, with a new AFP-coated glass capillary tube used for each antigen displacement sample. However, fluorescent intensity was highly variable both between capillaries and even within individual capillary tubes as a result of orientation-dependent light scattering due to variations in capillary geometry. Final assay measurements employed a modified capillary holder to facilitate flow-through, stop-flow assays (Figure 7). The capillary holder was fitted to the bench top fluorometer and AFP was interrogated at peak excitation (405 nm) and emission (460 nm) wavelengths. Data was collected via software provided by instrument manufacturer (Jobin-Yvon, Inc.). Following equilibration, samples were applied to the capillary column via syringe, small-bore tubing and a 27 ga. needle piercing a septum holding the capillary in place. In this manner it was possible to apply samples without disturbing the capillary tube and in turn introduce uncontrolled variation in fluorescent intensity from the glass capillary. Baseline polymer response to DABCYL-labeled and unlabeled peptide and solPBP2a protein was determined by application of successively higher concentrations of these analytes to an AFP capillary and determining fluorescent intensity after each addition. In this manner it was possible to evaluate the effect of each of these sample types on AFP fluorescent response. The flow-through

design allowed incoming sample to efficiently and completely replace resident sample in the capillary.

In order to assess the reactivity of the system to pure analyte and to begin to evaluate the sensitivity of a capillary-based AFP detection system the effect of increasing amounts of DABCYL-labeled peptide added to AFP was evaluated (Figure 8). Addition of labeled peptide had little fluorescence quenching effect until the 1 pmol sample suggesting general assay sensitivity in the 0.1-1 pmol range. There was a concentration-dependent quenching effect out to 1 nmol labeled peptide addition, which resulted in nearly a 50% reduction in fluorescence of polymer. A nonlinear effect was noted in the 0.1 to 10 pmol range, which is in agreement with the amplifying characteristics of the polymer. Small concentrations of quencher are expected to have a large effect on polymer fluorescence due to quenching of entire fluorescent polymer chains. It is important to note that polymer coatings within capillaries represent layers of individual polymer strands, and the most rapid quenching effect is expected to occur on the surface of the polymer, with quenching of deeper layers dependent upon diffusion of quencher into the polymer layers. Although some interstrand quenching (i.e., between layers) is possible, the most efficient quenching effect involves the interaction of quencher with individual conjugated polymer chains. At higher concentrations of quencher there is expected to be a concentration-driven shift in diffusion characteristics to enable interaction with deeper polymer layers. This effect is becomes apparent beyond the 10 pmol labeled peptide

sample, resulting in a more extensive quenching effect. The initial increase in fluorescence at lowest sample concentration is of minimal concern and may be representative of the inherent noise in the assay.

An important consideration in the assay is the contribution of the peptide component to the overall quenching effect. In order to evaluate the effect of peptide on AFP fluorescence, increasing concentrations of unlabeled peptide were applied to AFP capillaries (Figure 9). The result was a general linear trend representing a concentration-dependent decrease in fluorescence with increasing peptide concentration, indicating some contribution of peptide component to polymer quenching. However, the result was difficult to quantify due to increased fluorescence associated with the 100 pmol sample in comparison to the 10 pmol sample. Regardless, comparison of lowest-fluorescence sample with starting fluorescence indicated approximately 2.5% quench could be attributable to quenching of polymer by peptide component. These results suggest a better test of assay sensitivity and range could be obtained by applying only the DABCYL quencher to AFP, rather than labeled peptide as described above. However, the interaction of simple quencher with polymer surface is expected to be dissimilar to labeled peptide due to smaller molecular size, which would alter diffusion characteristics into multiple polymer layers. In addition the AFP has a highly hydrophobic nature which, when combined with native hydrophobicity of the DABCYL structure, would introduce

confounding quencher-polymer affinity effects due to hydrophobic interaction at the polymer surface.

The effect of increasing solPBP2a protein on AFP fluorescence was more substantial (Figure 10). As with the peptide samples, a concentration-dependent decrease in AFP fluorescence was observed with increasing protein concentration. The trend appears more linear in comparison to peptide, and maximal quench at highest protein level tested (100 pmol) was 13.6%. In the intended assay, antibody is bound to a solid surface, possibly within a small chamber or flow cell, and incoming PBP2a protein from a clinical sample competes with bound peptide for antibody binding sites. In this scenario the incoming protein becomes bound while liberating labeled peptide, and the free (liquid) sample is transferred to the transduction cell containing AFP. Thus, the impact of the concentration-dependent quenching effect of target protein is diminished somewhat. Of greater concern is the overall purity of the sample and the effect of a potentially higher concentration of contaminating proteins in the sample. However, the availability of the native protein target to participate in the assay is restricted due to its location between the bacterial cell wall and the cytoplasmic membrane. It is anticipated that some level of purification is necessary in the final assay format to liberate the native protein and make it available for detection. If the quench associated with increased protein is indeed directly protein-associated, this scenario could pose significant problems to assay development, as even a purified sample would likely have a large

concentration of contaminating proteins. It is possible that this effect could be diminished by using diluted samples to decrease the effect of total protein on AFP fluorescence, but this would be at the risk of assay sensitivity.

Parallel antigen displacement assays were performed on both candidate IgG antibodies immobilized in protein-G derivatized microplate wells using both unlabeled peptide and recombinant solPBP2a protein as the displacing agent. Displacement assay results for one of the antibodies was highly variable with poor response, particularly with unlabeled peptide as displacing agent. These results suggest this antibody candidate had low affinity for labeled peptide antigen and was deemed unsuitable for continued analysis or assay development. The remaining antibody displayed better performance, and AFP quenching plots for protein and unlabeled peptide as displacing agent is shown in Figure 11. In both cases there is a concentration-dependent quench of the polymer, with the displacement product associated with protein detection approximately 3-fold greater compared to peptide at higher assay concentrations.

Additional testing of monoclonal antibodies against crude lysates from MRSA and MSSA reference strains was performed. Western blot analysis indicated reactivity of both antibodies to a >70 kDa protein in the MRSA strain (expected to be PBP2a), but a much stronger band was observed at ~54 kDa in both strains (data not shown). The identity of the smaller band is unknown, but strong reactivity between both MRSA and MSSA renders the antibodies produced

during this study ineffective at distinguishing between methicillin-resistant and sensitive strains using a displacement component similar to the one described. It is possible there is cross-reactivity with another PBP, possibly the lower molecular weight PBP4 protein, but it was not possible to determine if that was the case as the protein associated with this band was not identified or characterized. Saito et al. (1995) reported development of an anti-PBP2a antibody using synthetic peptides as immunizing antigen. The monoclonal antibodies produced during this study were raised against 20-mer peptides similar to those reported by that group, and one peptide sequence overlapped the peptide sequence of one of peptides used successfully in that study. A key difference may lie in the presentation of antigen during the mouse immunization procedure. In this study the peptides were directly conjugated to hemocyanin via an EDAC linker, whereas they used linkage through an N-terminal cysteine residue and a bifunctional linker to attach it to a BSA carrier. The direct attachment used in this study may have restricted epitope accessibility or physically forced the peptide into a conformation which was non-native, leading to production of antibodies that recognized an incorrect peptide conformation.

However, the displacement assay utilized targets which had been previously shown to react with the antibodies, either during the antibody selection process as with peptide, or by western blot analysis with the recombinant solPBP2a protein. Therefore, the results presented for the displacement assay should be interpreted as a proof-of-concept study to demonstrate the utility of AFP to detect

labeled peptide displaced by incoming antigen. In this context the system appeared to function as intended.

Successful incorporation of a displacement component similar to the one described (utilizing more appropriate antibodies) into a device for a medical application presents additional challenges. The effect of protein on AFP function must be considered, as clinical samples are expected to contain copious amounts of non-PBP2a protein. A significant quench of AFP was apparent when increasing concentration of unlabeled protein was added to the displacement reaction, and future development of an AFP signal transduction system must be able to discriminate true quench associated with PBP2a from that associated with general protein effect. One possible solution is isolation of *S. aureus* from the clinical sample prior to lysing and presenting to the assay platform. This could be accomplished by immunomagnetic separation using antibodies against *Staphylococcus*, while actual discrimination between MRSA and MSSA could occur in the displacement assay. However, addition of purification steps will undoubtedly complicate the assay and increase assay time and may not be feasible for final assay development.

Conclusions

The results of this study demonstrate the potential utility of labeled peptide displacement assays when performed in conjunction with AFP. Proof-of-concept experiments demonstrated displacement and detection of a labeled peptide via fluorescence quenching of AFP. Some limitations may exist in direct incorporation of an assay of this type into a biomedical detection platform due to the effects of extraneous protein on AFP fluorescence. Additional investigation regarding protein-AFP interaction is needed to determine true feasibility of the assay described in this study. Future experiments should include additional testing of AFP with increasing concentrations of contaminating protein. Further development of PBP2a-specific antibodies is also needed. In addition, incorporation into a final flow-based diagnostic antigen displacement assay will require extensive testing of reaction conditions (flow, buffer composition, etc.) and optimization of antigen-antibody affinity to give best sensitivity with lowest possibility of false-positive results.

Figure 1. Features of amplifying fluorescent polymer (AFP). Space-filling model (left) and general chemical structure (right). The AFP backbone is responsible for the intrinsic amplification of AFPs, while the rigid pentiptycene scaffold prevents quenching of the AFP's fluorescence. The pendant side chain substituents are critical for solubility of the AFP and provide a synthetically versatile point to directly modify the AFP, affecting the surface chemistry of AFP films.

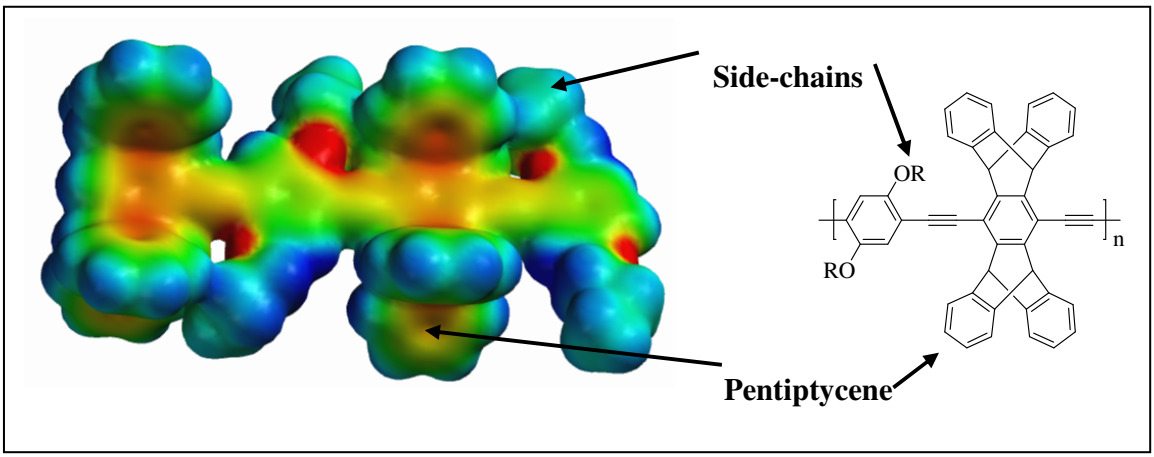
Side-chains
OR
RO
n
Pentiptycene

Figure 2. Comparison of traditional chemosensors to molecularly wired sensors.

Legend

= Emissive polymer

= Quenched polymer

= Analyte molecule

hν = Light at excitation wavelength

hν' = Light at emission wavelength

Traditional chemosensor (isolated chromophores): Binding of an analyte molecule quenches only the chromophore to which it binds.

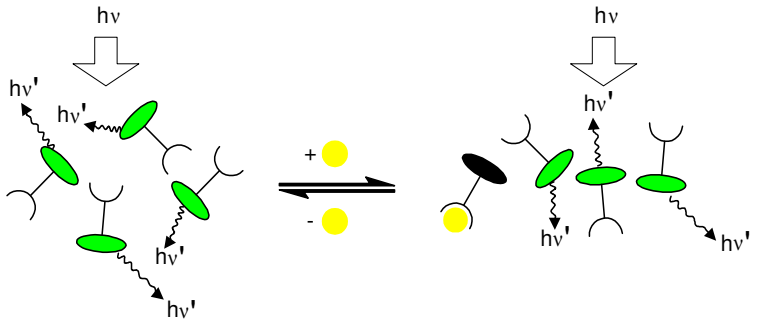

Receptors wired in series (molecular wire arrangement): A single molecular binding event quenches the fluorescence of many chromophores, amplifying the chemosensory response by orders of magnitude.

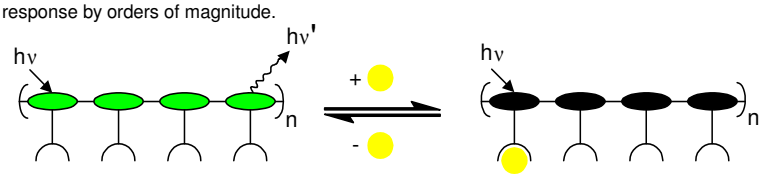

Figure 3: Antigenic peptide prediction based on computer analysis of transpeptidase domain of PBP2a from *Staphylococcus aureus*. Green boxes denote regions containing peptide sequences used in this study.

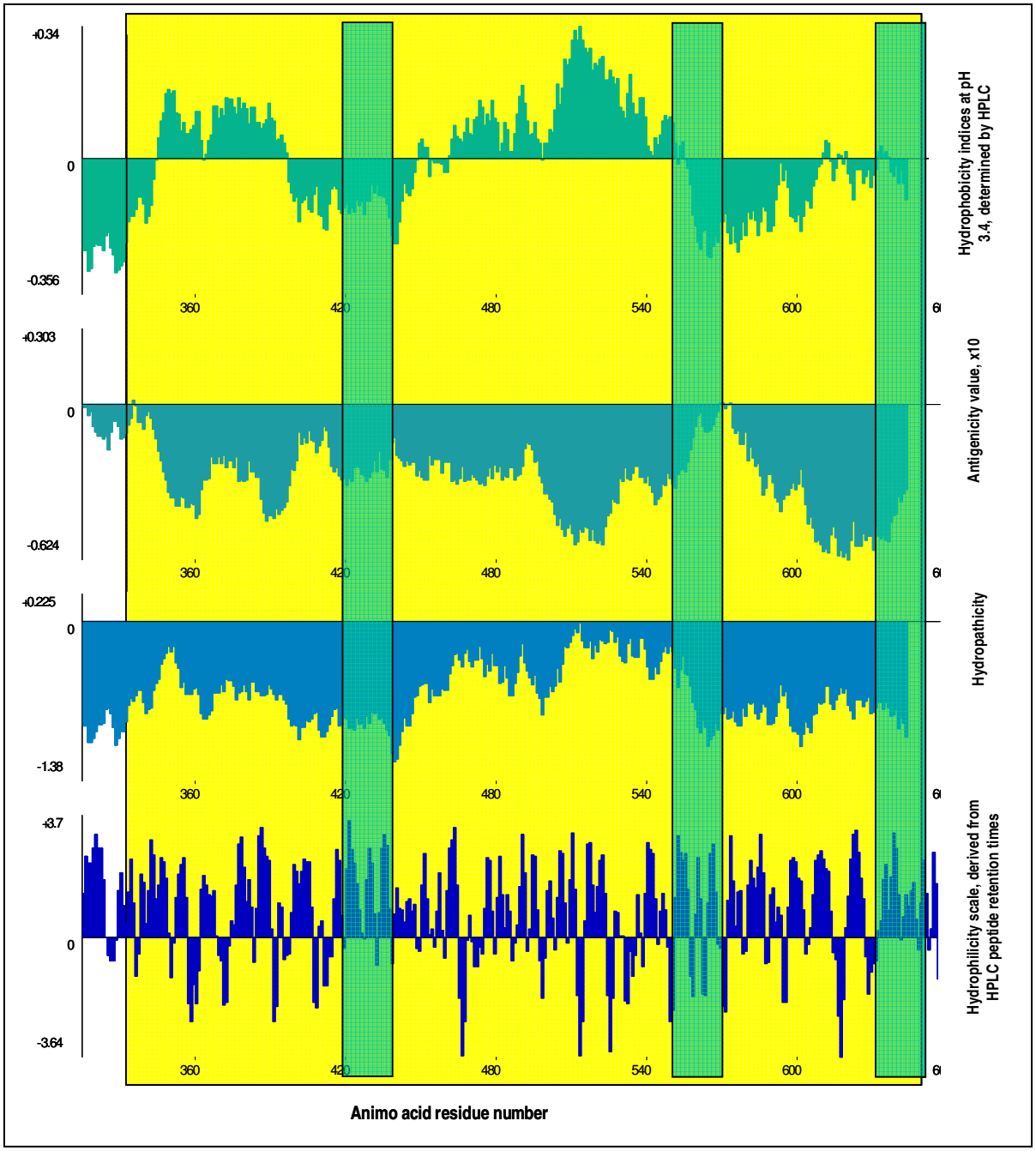
+0.34
0
-0.356
Hydrophobicity indices at pH 3.4, determined by HPLC
360
420
480
540
600
+0.303
0
-0.624
Antigenicity value, x10
+0.225
0
-1.38
Hydropathicity
+3.7
0
-3.64
Hydrophilicity scale, derived from HPLC peptide retention times
Animo acid residue number

Figure 4: Results of NNPredict secondary structure prediction for PBP2a protein. Regions less likely to participate in secondary structure (dashed lines) were targeted as possibly surface-exposed, and hence better antigenic sequences.

```
Results of nnpredict query
Tertiary structure class: none

Sequence saBAA86650:
mkkikivplilivvvvgfgiyfyaskdkeinntidaiedknfkqvykdssyisksdngev
emterpikiynslgvkdiniqdrkikkvsknkkrvdaqykiktnygnidrnvqfnfvked
gmwkldwdhsviipgmqkdqsihienlksergkildrnnvelantgtayeigivpknvsk
kdykaiakelsisedyikqqmdqnwvqddtfvplktvkkmdeylsdfakkfhlttnetes
rnyplekatshllgyvgpinseelkqkeykgykddavigkkgleklydkklqhedgyrvt
ivddnsntiahtliekkkkdgkdiqltidakvqksiynnmkndygsgtaihpqtgellal
vstpsydvypfmygmsneeynkltedkkepllnkfqittspgstqkiltamiglnnktld
dktsykidgkgwqkdkswggynvtryevvngnidlkqaiessdniffarvalelgskkfe
kgmkklgvgedipsdypfynaqisnknldneilladsgygqgeilinpvqilsiysalen
ngninaphllkdtknkvwkkniiskeninlltdgmqqvvnkthkediyrsyanligksgt
aelkmkqgetgrqigwfisydkdnpnmmmainvkdvqdkgmasynakisgkvydelyeng
nkkydide


Secondary structure prediction (H = helix, E = strand, - = no
prediction):
-----E-EEEEEEEEE--EEEEE----------H--HHH----HE-----EE--------
-H----HEEE---------HHHHHHHHHH--------HEEE----------H--------
---E-------E---------EEEE--------E----H-HHH-----EEEEE-------
-HHHHHHHHH---H-HH----------------------HHHHHHHHHHHH---------
-------HHHHHE---------HH-HHH-------HHHH---HHHHHHH--------EEE
EE------HHHHHHHH-------HEEEHHHHH---HH----------EE-----HHEEE
----------EE-----------------------EE-------EEHEHHHH-------
-----EE-----------------EEEE------HHEH------HHEHHHHHHHH-HHHH
HHHHH-----------------------HHHHE--------EEEE---EEEEEEHH---
----------H-----------------HHHH--HHHHH-------HHHHHHHEE-----
HHHHH-------EEEEEEE--------HHEE------------E--------E-HHHH--
```

Figure 5. Three-dimensional structure of PBP2a. (a.) Location of synthesized peptide sequences within the protein structure, (b.) Location, orientation and sequence of antigenic peptide 2.

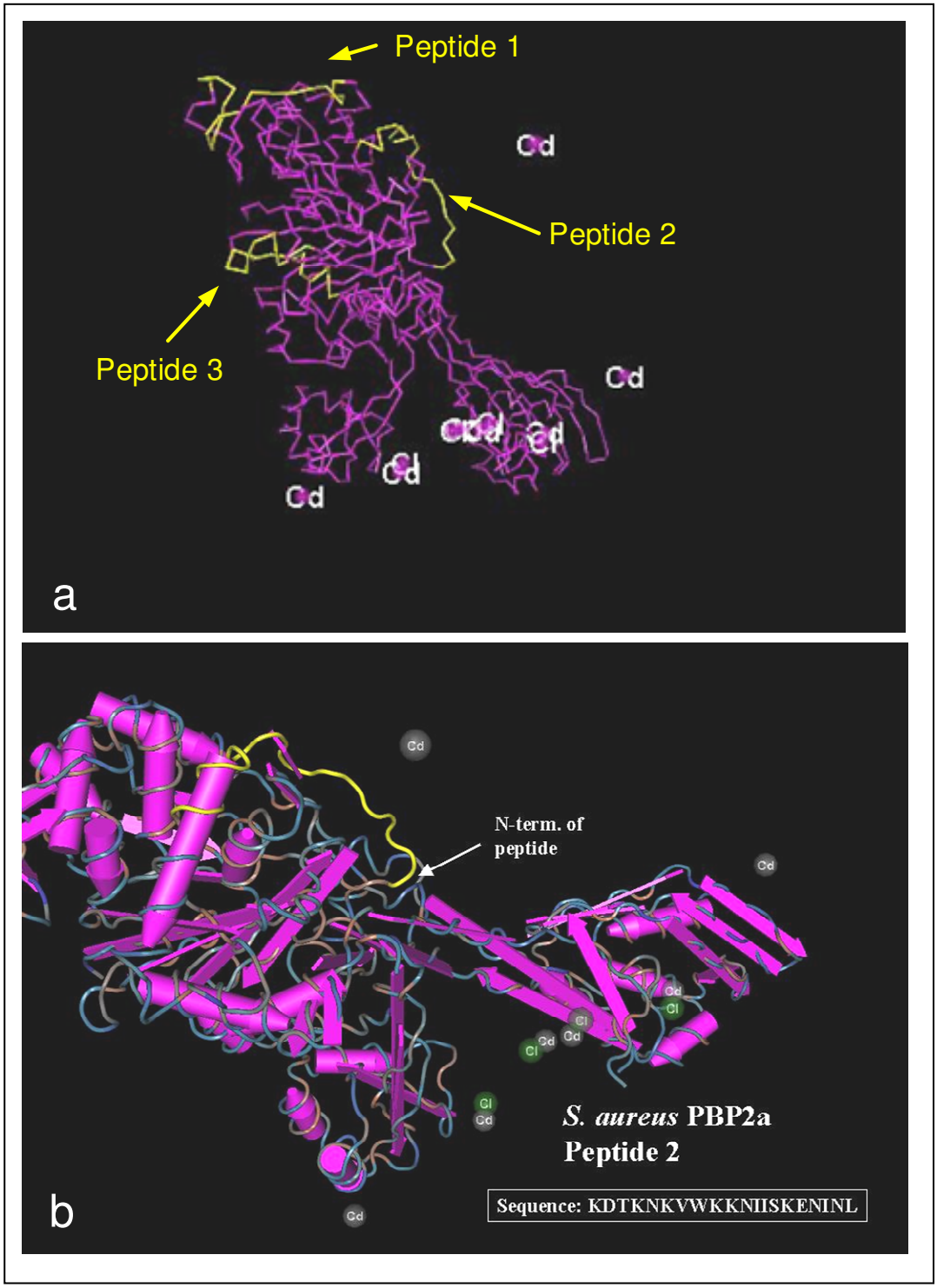
Peptide 1
Peptide 2
Peptide 3
Cd
a
N-term. of peptide
S. aureus PBP2a
Peptide 2
Sequence: KDTKNKVWKKNIISKENINL
b

Figure 6. Results of imidazole pre-wash on purity of solPBP2a protein. (l) Highest purity protein possible with single-step IMAC gradient elution assay, (r) High purity sample following imidazole pre-wash step. M: molecular weight marker; Lanes 1-5: elution with increasing imidazole concentration.

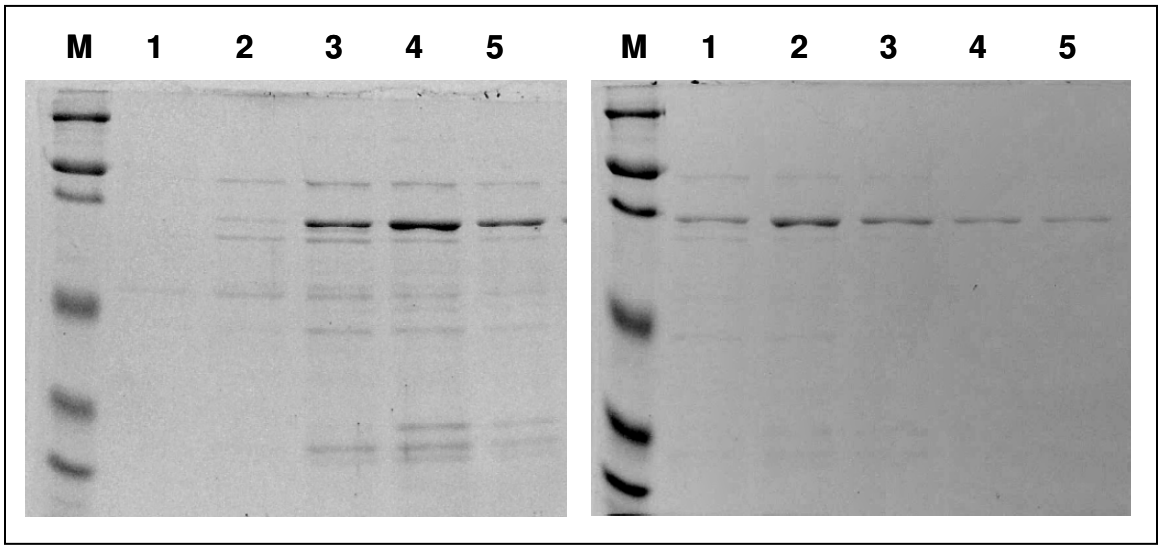
M 1 2 3 4 5
M 1 2 3 4 5

Figure 7. Capillary tube holder used in these assays. AFP-coated glass capillary tube is fitted to holder and samples from displacement reactions flow vertically from tube to bottom through the flow apparatus.

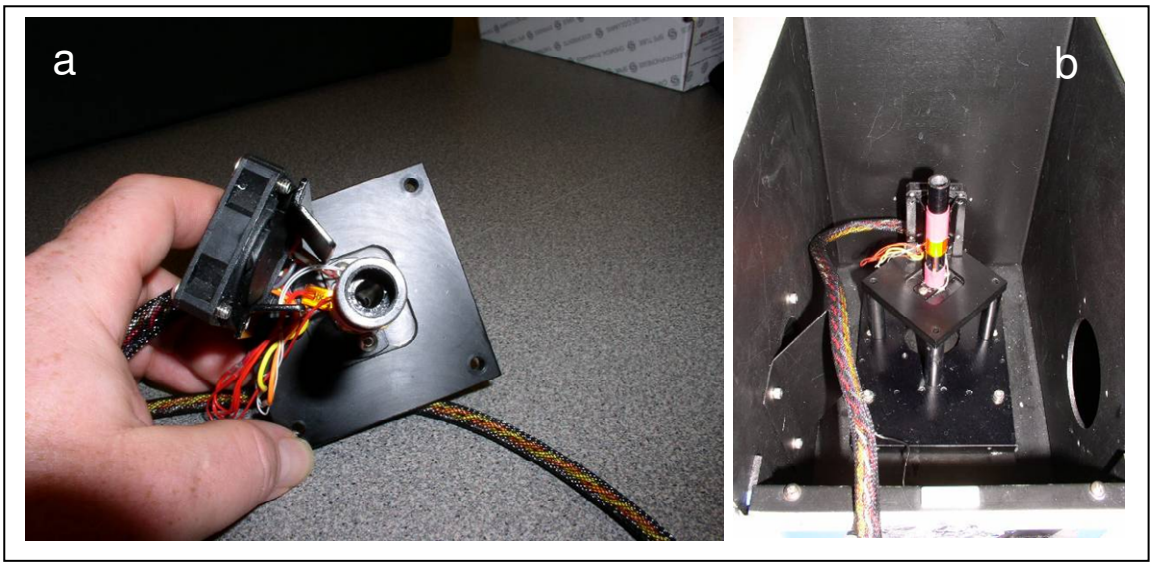
a
b

Figure 8. Effect of increasing DABCYL-labeled peptide on AFP fluorescence in the capillary flow system. In this case there was no displacement reaction. Labeled peptide was added from stock to help estimate sensitivity of the AFP capillary assay.

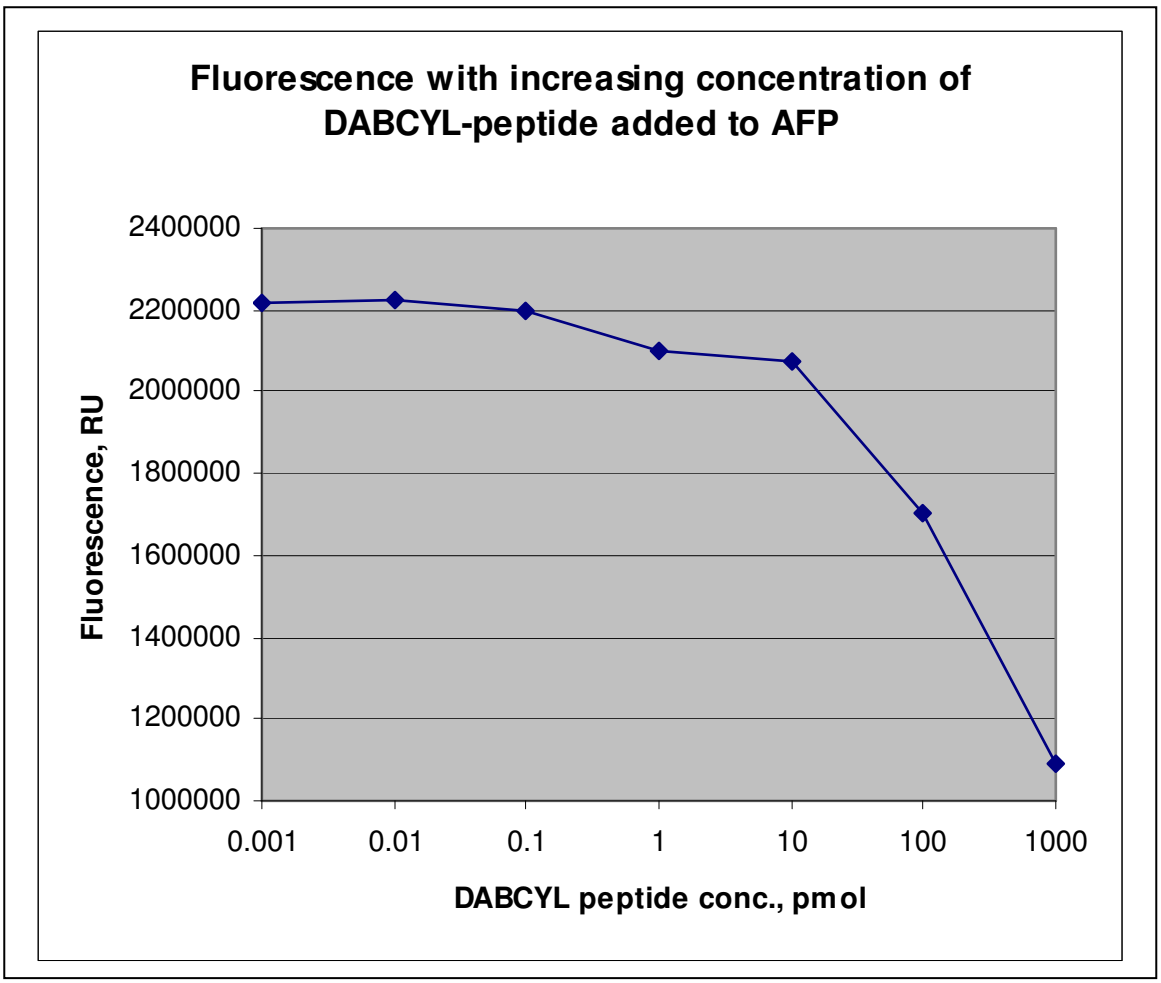
Fluorescence with increasing concentration of DABCYL-peptide added to AFP
Fluorescence, RU
2400000
2200000
2000000
1800000
1600000
1400000
1200000
1000000
0.001
0.01
0.1
1
10
100
1000
DABCYL peptide conc., pmol

Figure 9. Effect of increasing concentration of unlabeled probe on AFP capillary fluorescence.

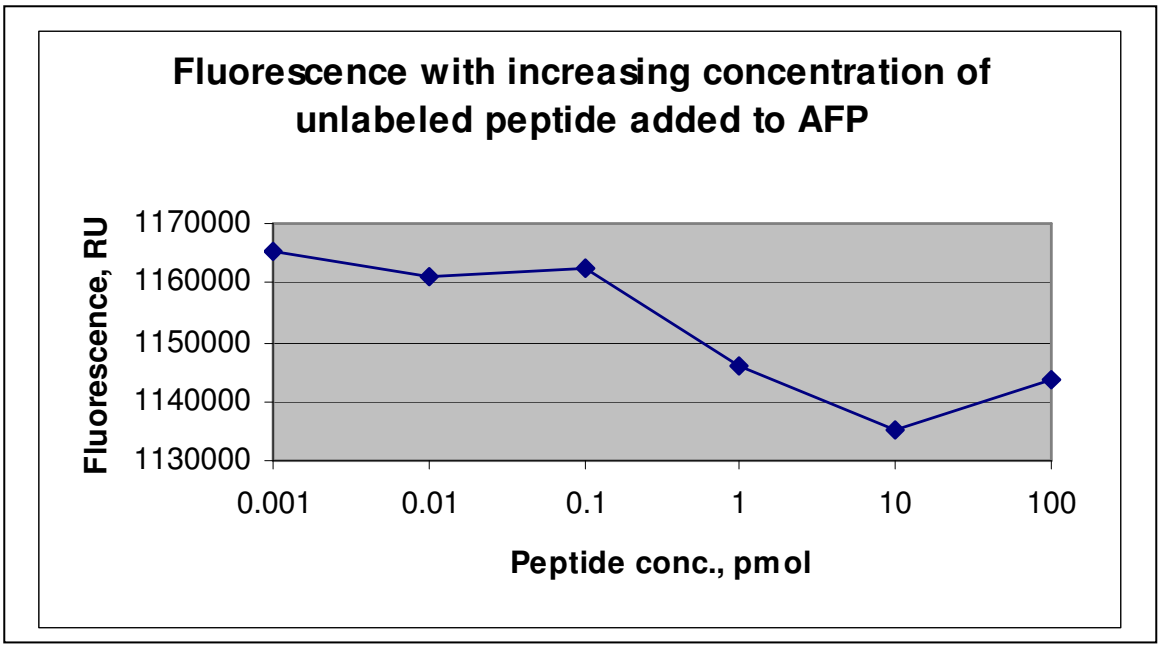
Fluorescence with increasing concentration of unlabeled peptide added to AFP
Fluorescence, RU
1170000
1160000
1150000
1140000
1130000
0.001
0.01
0.1
1
10
100
Peptide conc., pmol

Figure 10. Effect of increasing concentration of unlabeled solPBP2A protein on AFP capillary fluorescence.

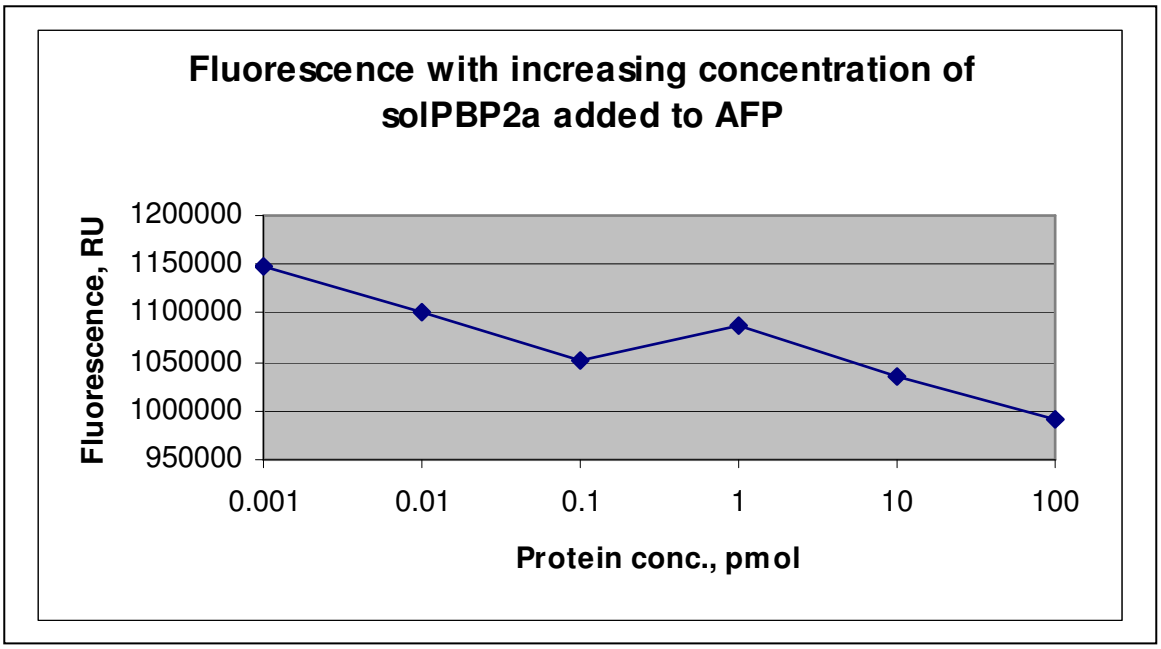
Fluorescence with increasing concentration of solPBP2a added to AFP
Fluorescence, RU
1200000
1150000
1100000
1050000
1000000
950000
0.001
0.01
0.1
1
10
100
Protein conc., pmol

Figure 11. Results of peptide displacement reaction using unlabeled probe or solPBP2a protein as displacing agent. DABCYL-labeled peptide was preloaded onto immobilized antibody and was displaced by peptide or protein for interaction with AFP.

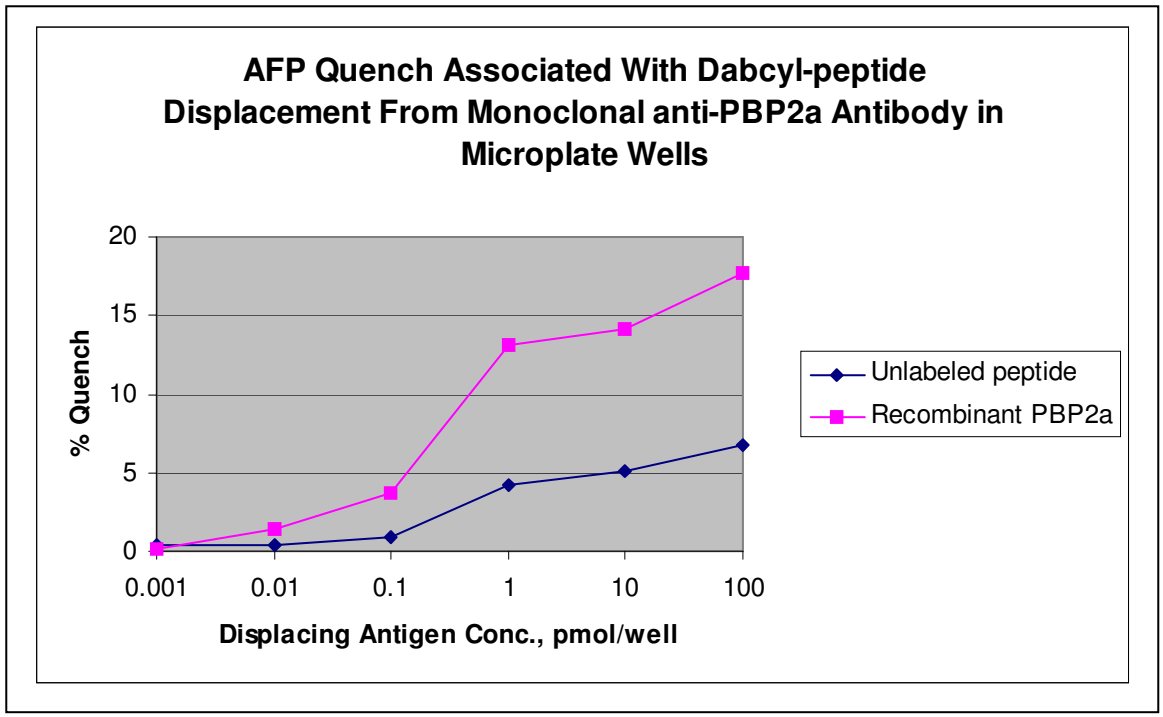
AFP Quench Associated With Dabcyl-peptide Displacement From Monoclonal anti-PBP2a Antibody in Microplate Wells
% Quench
20
15
10
5
0
0.001
0.01
0.1
1
10
100
Displacing Antigen Conc., pmol/well
Unlabeled peptide
Recombinant PBP2a

CHAPTER V

Multiplex Microring Resonator-Based Assay for Detection of *Salmonella* Typhimurium and *Escherichia coli* O157:H7

Introduction

Rapid and simple detection of foodborne pathogens is currently of great interest, both from the standpoint of food production and for rapid diagnosis of clinical disease associated with these organisms. The negative effects of *E. coli* O157:H7 and Salmonella on human health and food production are immense, and they can have serious economic impact. Current methods of detection tend to be laborious and time-consuming, and in some cases a compromise between speed and sensitivity is necessary. New biosensor technologies have the potential to greatly enhance detection capabilities without compromising time to results. Label-free assays are of great interest and a number of platforms are currently in development.

In recent years, different sensor platforms exhibiting enhanced detection capabilities, based on potentiometric, amperometric, magnetic, and optical transducers have been developed (Lazcka et al., 2007). One of these promising new technologies involves the use of microring resonators as optical sensors for detection of biomolecules. Operating as bound mass signal transducers, these devices have the flexibility to be used for a range of biodetection applications. Microring resonators offer several advantages for use as biosensing platforms. They provide label-free, sensitive, and real-time detection capabilities. The small form factor facilitates production of arrays of individually-addressable sensing elements on a single chip using standard photolithographic fabrication methods, enabling multiplexing capabilities. In addition, microring resonator chips can be mass produced at low cost, enabling incorporation into disposable detection/diagnostic devices. This report details the use of microring resonators as a label-free platform for detection of the major foodborne pathogens *E. coli* O157:H7 and *Salmonella* Typhimurium, and demonstrates the utility of the platform as a multiplex assay system.

Materials and Methods

Microring Resonator Chips

Microring resonator sensing chips were obtained from the Little Optics division of ICx Technologies. Chips were created from silicon wafers using optical

photolithography and employed proprietary silicon (glass)-based material called Hydex™ (Yalcin et al., 2006; Hryniewicz et al., 2004). The glass-based Hydex™ material is a low-loss, high-refractive index substrate ideally suited to fabrication of MR devices due to exceptionally low bending losses, enabling fabrication of devices with very tight radii (small diameter). The high-density wafer-based fabrication process results in a large number of chips (>100) diced from a single wafer with high chip-to-chip uniformity in physical specification and optical characteristics. Chips used in this study contained 5 independently-addressable microring structures with a 100 µm diameter and cross-sectional dimensions of 0.75 µm wide by 1.5 µm high. Each ring was optically coupled to individual input and output waveguide buses buried within the chip structure, such that vertical optical coupling of waveguide buses and sensing microring structures was achieved (Figure 1) (Yalcin et al., 2006). Optical fiber cables were used to connect sensing chips with the optical interrogation system. One end of the cable was fitted with a precision-aligned terminator which was butt-coupled to the sensing chip, while the other end was terminated in optical MTP-style connectors.

Reader System and Determination of Resonance Wavelength

In order to determine the initial resonance wavelengths of individual micro-rings on the micro-ring resonator chip, and to monitor shifts in the resonance wavelengths over time, a reader system consisting of an optical spectrum analyzer (OSA, ANDO-AQ6317B), a broadband light source (1.53–1.61 µm,

Thorlabs Inc., ASE-FL7002) and an optical switch (JDS Uniphase) were used. The input and output waveguides of the micro-ring resonator chip were connected to the broadband light source and the OSA, respectively, via the MTP-terminated optical fiber tail of the microring resonator chip. Detecting shifts in resonance peaks was accomplished using OSA-based scanning of the output waveguide wavelengths, with data collected in real-time and displayed on a desktop computer using a dedicated software package created by Little Optics. The optical switch facilitated repeated sequential channeling of light to the five rings. The scan rate for the system was approximately 15 seconds per microring channel.

Microring Resonator Chip Functionalization

Antibodies were coupled to the microring surface via covalent attachment of surface-exposed antibody amine groups to epoxy-modified sensing surfaces. When new chips were used they were first cleaned by immersion in 1% sodium hydroxide in a 60% ethanol/40% water solution for 30 minutes. Preparing chips which had been used previously was similar, with the exception of a preliminary etching in 100 mM aqueous sodium hydroxide solution for 30 minutes at room temperature to remove any contaminating material. Chips were thoroughly rinsed in deionized water followed by 95% ethanol. Epoxysilane groups were generated on the chip surface by immersing cleaned chips in a solution containing 10% GPTS (3-glycidoxylpropyltrimethoxysilane) and 10mM acetic acid in 95% ethanol for 30 minutes. Following silanization, the chips were rinsed

thoroughly with 95% ethanol. Epoxysilane-modified surfaces were cured by baking in an oven at 120ºC for 1 hour. Chips were stored in a desiccator until antibody attachment.

E. coli Whole-Cell Binding Experiments

Initial experiments were directed toward detection of whole bacterial cells in broth suspensions to demonstrate feasibility of microring-based bacterial detection. Paired microrings on a chip (rings 1 and 2 or rings 4 and 5) were functionalized with monoclonal antibody specific for LPS oligosaccharide of *E. coli* O157:H7 (Abcam Inc., Cambridge, MA, USA) or with a negative control antibody previously shown to be nonreactive to *E. coli*. Antibodies were suspended in phosphate-buffered saline (PBS), pH 7, to a concentration of 1 µg/µl and mixed with 10mM sodium hydroxide in 5:1 ratio to give an antibody solution with a final pH of 10. Antibody solution (~0.5 µl) was applied over each of the micro-rings and allowed to bind overnight at 4ºC in a humidified chamber.

Following antibody binding, microring resonator chips were subjected to a blocking and washing cycle in order to neutralize unreacted epoxysilane groups on the chip surface and to remove any excess unbound fraction of antibodies. Chips were washed in PBS buffer (pH 7) then the chip surface was blocked with 1% bovine serum albumin (BSA) in PBS for 30–45 min and rinsed with PBS–Tween solution (PBS, pH 7 with 0.5% Tween-20) followed by two rinses with

PBS alone. Each rinse procedure was performed for 10 minutes. In this manner, the untreated ring to be used as reference (ring 3) was blocked with BSA.

The MR chips were connected to the reader system via the optical fiber tail using standard MTP connectors. Chips were immersed in a 2 ml cryovial tube containing 2ml PBS to determine initial resonance wavelengths and to establish a baseline. *E. coli* O157:H7 cells in broth culture (~$2x10^9$ cells/ml) were spiked into the buffer at a final ratio of 1:1 culture:buffer to yield a final concentration of 10^9 cells/ml. Solutions were continuously stirred using a magnetic micro-stir bar while monitoring resonance wavelength shift over time to detect target-binding events. As with other RI sensing methods, where RI is a function of temperature, the microring resonator signal is also temperature-sensitive. To minimize temperature-induced signal drift, all experiments were performed at room temperature, with samples and buffers pre-incubated at room temperature prior to detection. In addition, the temperature-induced drifts were minimized by subtracting the reference ring signal (BSA blocked, no antibody) from the antibody-activated sensing ring signal. A parallel assay was performed on identically-treated but non-connecterized chips (no optical fiber cable), and these chips were used for scanning electron microscopy (SEM) analysis to confirm bacterial binding to relevant microrings.

Multiplexed Whole Bacterial Cell Detection Assays

The ability to function in multiplexed whole cell assays was determined by functionalization of MR chips with monoclonal antibody directed toward *E. coli* or *Salmonella* Typhimurium LPS, followed by sequential whole cell binding assays. Although not a multiplexed assay *per se*, as the detection process does not involve simultaneous detection of different targets, the term multiplex is used in the context of this report to indicate capability to be incorporated into a multiplex assay following demonstration of specificity to multiple targets in sequential binding assays. Initial assays used high concentrations of target cells in buffer in a stirred-tube assay format. Further experiments were performed with lower cell concentration either applied directly to the microring sensing surface or in conjunction with a dedicated custom microflow cell apparatus.

High Concentration Multiplex Assay

Monoclonal antibody to *E. coli* O157:H7 (described above) and *S. typhimurium* LPS (0-4 serotype specific; Abcam Inc., Cambridge, MA, USA) was diluted to a final concentration of 0.1 mg/ml in PBS buffer (pH 10) and spotted (>0.5 µl) onto epoxysilane-activated rings (described above). Pairs consisting of adjacent rings (rings 1 and 2, or rings 4 and 5) were spotted with like antibody, while the center reference ring was spotted with 1 mg/ml BSA in PBS (pH 10). Covalent coupling of antibody or BSA to microring surface was accomplished by overnight incubation at 4ºC in a humidified chamber. Following overnight incubation, chips were washed with PBS (pH 7) with gentle agitation. Because high antibody

concentration was used in conjunction with direct covalent coupling of BSA to the reference ring, additional BSA blocking steps, as described for initial whole cell detection assays, were omitted.

Antibody-derivatized chips were placed in 2 ml PBS buffer (pH 7) in a stirred cryovial tube for initial resonance peak detection and to establish a 30-minute buffer baseline. Half of the buffer was removed and replaced with bacterial suspension culture as described above, to yield a final cell concentration of approximately 10^9 CFU/ml. Resonance shift was continuously monitored for 45 minutes. Following first bacterial binding, recording was halted momentarily to aspirate away the bacterial test suspension and replaced with PBS. This procedure was repeated twice more to remove as much of the first bacterial suspension as possible. Two ml of PBS was then added to the tube and resonance wavelength monitoring was resumed. After approximately 1 hr. the second (alternate) bacterial test suspension was added in the same manner as the first suspension to achieve ~10^9 CFU/ml cell density. Wavelength monitoring continued for 45 minutes, followed by washing and re-equilibration in fresh PBS buffer. Results of wavelength scans were averaged across antibodies (measurements from rings with like antibodies) and were corrected for temperature by subtraction of reference ring scan values.

Low Concentration, Direct Application Multiplex Assay

In an effort to enhance response time during whole cell multiplex assays, lower concentrations of bacterial test suspensions were applied directly to the MR sensing chip. Preparation of chips was as described above for the high concentration assay, as was the initial baseline measurement, except baseline collection time was extended to 1 hr. Presentation of the first whole cell bacterial suspension was accomplished by halting scanning, removing excess buffer from the chip and placing the chip in a horizontal position in a high-humidity chamber. Twenty microliters of bacterial cell suspension at a concentration of $1x10^5$ CFU/ml (2000 cells total) was pipetted directly on to the surface of the MR chip, completely covering the sensing rings. Wavelength scanning resumed for approximately 25 minutes, then halted to remove bacterial suspension and to transfer the chip back to the stirred cryovial. Wavelength scanning resumed for 2 hrs. to ensure stable baseline and to remove all unbound cells. Scanning was again halted to allow presentation of the second (alternate) bacterial suspension in the same manner as the first. Scanning resumed and after approximately 30 minutes the chip was re-equilibrated in PBS buffer in the manner following the first sample presentation. Measurement averaging and reference subtraction were as described for high concentration multiplex assays.

Low Concentration Flow Cell Multiplex Assays

In order to further enhance mass transport of analyte (bacterial cells) to the sensing surface, a custom flow cell was fabricated to hold a microring resonator

chip (Figure 2). The format for the cell is input and output microchannels connected to a small chamber volume defined by a channel cut from gasket material. The gasket channel is fabricated such that when the MR chip is mounted all active rings are within the channel volume. Initial attempts utilized an acetate film as the gasket material, which was then replaced by skived Teflon™ sheeting. The flow channel was cut manually under magnification using a template, and the dimensions of the channel were 5.5 mm long by approximately 1.2-1.4 mm wide by 100 µm high (the thickness of the skived Teflon™), for a total volume of approximately 650-750 nl. Sensing chips were prepared as previously described for multiplex assays and mounted in flow cell apparatus. Flow rate and volume of cell suspension were controlled by syringe pump, and small-bore Teflon™ tubing connected a disposable plastic syringe to the flow cell. The flow cell cover containing the input and waste pathways was machined from polyetheretherketone (PEEK), while the base was aluminum for efficient heat conductivity to the MR chip.

Multiplex MR chips were prepared as described above and mounted into the flow cell by sandwiching between the cover and base, with the gasket material between the chip surface and the flow channel cover. Maximum flow rate was set at 0.1 ml/min. with a total volume of 1 ml. During the assay, sample was infused with constant wavelength scanning, followed by static-phase incubation for a total time ranging from 25-45 min. at each step. Bacterial suspensions of 10^4 or 10^5 cells/ml were prepared in PBS (pH 7) by dilution from bacterial culture.

Wavelength scanning was continuous except for when sample or buffer syringes were being changed at the beginning of each infusion/incubation phase. General assay design was as described for previous multiplex assays wherein there is an initial buffer calibration/baseline measurement, infusion of the first bacterial cell sample, buffer wash/equilibration, infusion of alternate bacterial sample and a final wash/equilibration phase. All assays were performed at room temperature with the flow cell resting on a plastic rack or mounted in a Styrofoam holder for thermal isolation from the bench top surface. It is important to note that the flow cell is reliant upon compression of the MR chip for efficient sealing. In many cases rings failed to respond or displayed extreme, erratic resonance shifts for no apparent reason. It was determined post-assay that sensing microrings had failed, presumably as a result of compression when mounted in the flow cell. Therefore, averaging and reference subtraction were not performed, although reference ring values are provided where available.

Results and Discussion

The microring resonator chip design used in the present study consisted of five micro-ring resonators integrated on a single chip. Each of the microring structures was vertically coupled to individual sets of input and output waveguides that were buried beneath the surface of the chip. This design is ideal for biosensing applications as it prevents analyte-interaction with input and

output waveguides, thereby ensuring that any specific shift in the resonance spectrum resulted from analyte interactions with the micro-ring structure alone. The OSA-based reader system used in the present study for monitoring resonance wavelength had a noise level of ~1 picometer. Assuming a detection resolution 3× the noise level, the minimum shift in wavelength that could be accurately detected would be ~3 pm. Detection of binding of whole bacterial cells was achieved using this design, and species-specific binding of 2 enteric pathogens was demonstrated through the use of LPS-specific monoclonal antibody functionalization of individually-addressed rings, suggesting the utility of MR sensing methods in multiplex bacterial whole cell detection assays.

E. coli Whole Cell Binding Experiments

In order to demonstrate the ability to detect whole bacterial cell binding to microring resonator sensing devices, resonator chips were exposed to a high concentration (10^9 CFU) of *E. coli* O157:H7. Resonance wavelength values associated with test rings functionalized with anti-*E. coli* antibody and control rings functionalized with non-*E. coli* antibody were similar during initial baseline collection in buffer and are shown in Figure 3. When bacterial culture suspension was added, both treatment groups showed an initial rapid shift in resonance wavelength. However, after a few scan cycles the resonance wavelength associated with the control group stabilized in comparison to the test rings, which displayed a continuous rise in wavelength over time. Following transfer back to buffer the control group returned to values near those observed

during baseline data collection, while the test group remained elevated but stable.

The rapid rise in resonance wavelength in both groups upon addition of culture was the result of a bulk refractive index shift caused by differing refractive index of equilibration buffer and the culture medium. Microring resonators function as refractive index sensors and, as such, are extremely sensitive to changes in refractive index of the medium immediately surrounding the microring. The composition of the bacterial test suspension is expected to have substantially different refractive index properties compared to buffer due to the presence of proteins and other components. In addition, whole bacterial cells themselves can be expected to impart altered refractive index properties to the test suspension by virtue of their large size and relatively high mass. Therefore, it is essential to return the test chip to equilibration buffer in order to determine the net change in resonance wavelength shift in test rings compared to control rings, and in turn determine if binding of whole bacterial cells to the microring surface has occurred. The data in Figure 3 indicate bacterial cells did indeed bind to the test ring resulting in a large wavelength shift which was maintained following return to buffer. Continuous wavelength scanning allowed visualization of bacterial binding over time as evidenced by the steady rise in resonance wavelength shift during bacterial culture incubation stage. However, the bulk refractive index phenomenon can easily confound this observation. Therefore, actual determination of cell binding should be determined after re-equilibration in buffer.

Parallel test rings treated in the same manner and subjected to SEM indicated binding of bacterial cells to the ring structure (Figure 4). Cells were also bound to areas surrounding the ring due to the imprecise antibody application process which floods the epoxysilane-activated area surrounding the ring and in turn functionalizes these surfaces with antibody as well. SEM comparison to control rings was dramatic, with no bacterial cells associated with these control ring structures.

High Concentration Multiplex Assay

The design of the MR chip allows independently-addressable sensing rings to be scanned continuously and independently over time. Functionalization of individual microrings within an array, with antibodies specific for a particular bacterial species or even strains within a species, can facilitate multiplex assays capable of identifying one or more bacterial pathogens within a clinical sample simultaneously. In order to determine the utility of microring resonators in multiplexed assays high concentration (10^9 CFU/ml) cultures of *S.* Typhimurium or *E. coli* were tested sequentially while monitoring resonance wavelength peaks of microrings functionalized with species-specific antibody for species-specific bacterial binding to sensing surfaces. The results of the assay are shown in Figure 5. Addition of *Salmonella* culture resulted in a rapid wavelength shift in anti-*Salmonella* treated rings, with a comparatively small shift observed in anti-*E. coli* treated microrings as a result of bulk refractive index effects. Interestingly, the bulk refractive index effect appeared to be of lower magnitude than observed

previously during single culture *E. coli* binding assays. Following transfer to buffer the *E. coli* rings returned to baseline level while the *S.* Typhimurium rings remained elevated, indicating specific binding of *Salmonella* to cognate microrings. Addition of *E. coli* culture caused a rapid upward shift in resonance wavelength in *E. coli*-specific rings with a small increase in *S.* Typhimurium rings. Following transfer to buffer the resonance wavelength of *E. coli* rings remained elevated relative to pre-*E. coli* values. Wavelength values for *Salmonella* rings returned to levels similar to those observed during the intermediate buffer stage, indicating no binding of *E. coli* to *Salmonella* rings had occurred. The net wavelength shift relative to baseline was less in *E. coli* rings compared to *Salmonella* rings. The difference cannot readily be explained, although it may be a function of different antibody-antigen binding characteristics resulting in differing binding capacity or binding rate, or possibly due to degradation or loss of *E. coli*-specific antibody during the course of the assay. Regardless, these results demonstrate the utility of application of microring arrays to a multiplex assay format for detection and identification for specific pathogens in samples containing high concentrations of bacteria. The rapid increase at each sample addition step suggests the assay binding time could be shortened substantially with little likelihood of compromising final assay results.

Low Concentration, Direct Application Multiplex Assay

Previous experiments relied on the introduction of bacterial cell samples in a proportionately large assay volume (2 ml), which can be expected to seriously

impact speed of assay due to the need for mass transfer of analyte (cells) through a large volume to reach the sensing surface. In an effort to improve mass transfer, assays were performed with low bacterial cell concentration suspensions (2000 cells in 20 µl) in PBS buffer applied directly to the MR chip surface. Overall results were similar to those observed for high-concentration assays but data had sharper transitions due to transfer of the chip in and out of buffer (Figure 6). Addition of *Salmonella* resulted in a positive shift in resonance wavelength in rings specific for that organism, while the *E. coli* rings showed a slight resonance shift in the opposite direction, a result which cannot be readily explained. However, those assay rings returned to near baseline values when the chip was transferred back to PBS while the *Salmonella*-specific rings maintained the elevated resonance wavelength relative to baseline. The addition of *E. coli* resulted in a positive bulk refractive index shift in both samples, and the resonance shift was maintained in *E. coli* microrings following transfer to buffer, and resonance shift was maintained in *Salmonella* rings as well. As observed previously with high concentration assays the shift in resonance wavelength for *E. coli*-specific rings was of lower magnitude compared to *Salmonella* rings.

Overall assay binding time at each step was approximately half that used for high concentration tube assays. Net results were similar, but total shift in resonance wavelength was substantially less suggesting fewer cells, and hence less mass and lower RI, were bound to the sensing surface. However, in most cases a peak was observed during binding suggesting some other unexplained factors

may be influencing binding capacity when samples are applied directly to the chip surface. The surface of the chip is fairly hydrophobic, presumably due to unblocked epoxysilane groups, and samples applied to the surface tended to rest on the surface as drops with high surface tension. Under these circumstances bacterial cells may be drawn to the perimeter of the drop and mass transfer may be hindered. Influence of the unblocked surface on spontaneous covalent coupling of bacteria in the test sample to the chip surface via amine groups on the bacterial surface could not be determined. Although this did not appear to affect high concentration assays there could be some effect at lower cell concentrations. It is interesting to note that during binding, the apparent rate of cell binding which could be roughly deduced from the steepness of the binding curve was similar to that seen in high concentration assays. Results from these assays demonstrate successful species-specific detection of whole bacterial cells at concentrations as low as 10^5 CFU/ml in a label-free assay system.

Low Concentration Flow Cell Multiplex Assays

In an effort to further enhance mass transport to the MR sensing surface, a microfluidic flow cell was incorporated into assays similar to those previously described. Obtaining good multiplex assay data using the flow cell was challenging due to the loss of activity of some sensing rings after the MR chip was fitted to the flow cell apparatus. An initial experiment employed a 10^5 CFU/ml *S.* Typhimurium bacterial suspension to determine if cell-specific binding could be achieved at higher rates with high sensitivity. The results showed a

rapid positive shift in resonance wavelength in both *S.* Typhimurium and *E. coli* microrings when cell suspension was applied (Figure 7). Interestingly, the shift in the *E. coli* rings was almost 2-fold greater than in *Salmonella* microrings. However, when flow was transitioned back to buffer the resonance wavelength for both samples dropped to below-baseline levels. Nonetheless, a net increase in resonance wavelength in *Salmonella*-specific microrings was observed compared to *E. coli* rings. The unexpected wavelength shift characteristics could not be readily explained and may be the result of microfluidic effects associated with the flow cell. Unfortunately, a functional reference ring was not available for this assay. The overall response time based on steepness of the curve during binding suggested the flow cell substantially aided mass transport of bacteria to the cell surface.

Further experiments were conducted to determine the utility of the flow cell device in multiplex assays. In most cases it was difficult to obtain complete multiplex data due to inactivation of rings following fitment to the flow cell. One experiment is shown in Figure 8, and in this case the reference ring is plotted rather than subtracted to illustrate flow cell characteristics, and only a single cell-specific treatment ring was available for each group. In this case, initial buffer flow caused an abrupt increase in reference and *E. coli* rings. When flow was transitioned to a 10^4 CFU/ml suspension of *E. coli*, a bulk refractive index shift was noted in all samples. Following transition to buffer there was a decrease in resonance wavelength for all microrings, with the *E. coli* ring higher than the

Salmonella ring. Transition to a 10^4 CFU/ml suspension of *Salmonella* resulted in a positive wavelength shift in that treatment ring, but a decrease in reference and *E. coli* rings which continued into the buffer recovery phase. The results following the first buffer recovery phase suggested an *E. coli* specific to that analyte. However, initial noise in the PBS equilibration step, and in steps following *E. coli* binding and wash make overall results difficult to interpret. Although enhanced mass transport is expected in the flow cell apparatus due to much smaller sample volume, the steep slope observed at the onset of the bacterial presentation phase was also apparent in the reference ring, suggesting the observation may be an artifact of the overall bulk refractive index shift. Further experimentation using the flow cell device was not possible due to the potential damage to valuable sensing chips. Nonetheless, the potential for improvement in response, as a result of lower assay volume and improved mass transport, is significant and warrants further investigation into improved flow cell design and testing.

Overall performance of the system based on data for 1 x 10^5 CFU/ml in the low concentration, direct application experiment was about an order of magnitude more sensitive than previously reported for a *Salmonella*-specific electrochemical sensor (Yang et al., 2004) and the Love-wave surface acoustic wave (SAW) device described by Moll et al., (2007). Linear bacterial detection range from 10^2-10^8 CFU/ml have been demonstrated using a quartz crystal microbalance device (Huang and Cooper, 2006). Linear range was not determined in this

study, but based on the data presented it appears the lower limit of detection range lies below 10^5 CFU/ml. When compared to cantilever devices the performance was slightly better than deflection mode microcantilevers (Zhang and Ji, 2004), but was nowhere near the 500-700 CFU/ml claimed for millimeter sized cantilever devices (Zhu et al., 2007b; Campbell and Mutharasan, 2005b).

When compared with the most popular optical platform, surface plasmon resonance (SPR), performance was equal or slightly better than the direct binding assay reported by Subramanian et al. (2006). In their SPR system they reported sensitivity down to 10^4 CFU/ml using a sandwich binding assay. The microring system described here operates on sensing refractive index changes as a result of bound mass, much the same as SPR functions. It is reasonable to assume our system will have similar performance enhancement if a sandwich assay is used. However, to date those experiments have not been performed and it is unclear exactly what performance enhancement could be achieved with this strategy. The addition of another binding step would also add time and complexity to the assay which would not be desirable.

The best SPR whole cell binding results reported to date claim sensitivity of around 25 CFU/ml (Waswa et al., 2006) which, if accurate, rival high-efficiency PCR for assay sensitivity. Modifying our current system from a broad band light source and a scanning detector (the OSA) to a scanning light source and fixed detector is expected to provide at least an order of magnitude higher sensitivity.

This design would employ a tunable diode laser at the front end as the excitation source. Such a reader design would have a much smaller form factor, and a portable microring sensor platform could be developed.

In addition to flow cell design improvements and addition of a tunable diode laser, another important area for improvement revolves around application of antibody to the microring sensing surface. As demonstrated by the SEM data in Figure 4b substantial area of the chip surface surrounding the ring becomes functionalized with antibody using the current spotting procedure. Antibody not associated with the sensing surface competes for bacterial binding with that on the ring surface. This can result in lack of sensitivity, which can be of great concern when attempting to maximize assay sensitivity. Possible solutions are direct-writing of antibody on the surface of the microring. One commercial example of this technology, dip pen nanolithography, involves the modification of an atomic force microscope to facilitate writing or “tapping” of antibody to precise regions on the sensing surface. It is expected that precise functionalization methods will yield a significant gain in whole cell detection sensitivity, particularly when used in conjunction with a small assay chamber.

Conclusions

The results of this study clearly demonstrate the ability to detect whole bacterial cells in a label-free assay format with species specificity, and suggest high utility for a microring array-based multiplexed bacterial detection system. In this work, the organisms used constituted enteric pathogens of high importance both for their potential to cause serious disease and for their impact on food safety. A sensitive, rapid and label-free multiplex assay to detect a range of pathogens in a sample is of great value. Further efforts to develop the microring resonator platform for diagnostic and biomedical uses should be considered, with further optimization of low-volume flow cell devices and specific activation of sensing surfaces to maximize sensitivity and minimize competition for bacterial binding associated with non-sensing regions.

Figure 1. Photograph of the five-ringed microring resonator chip. A magnified view of the 5 rings with input and output ports are depicted in the drawing. The input and output waveguides are “U” shaped with a single microring at the base of the U.

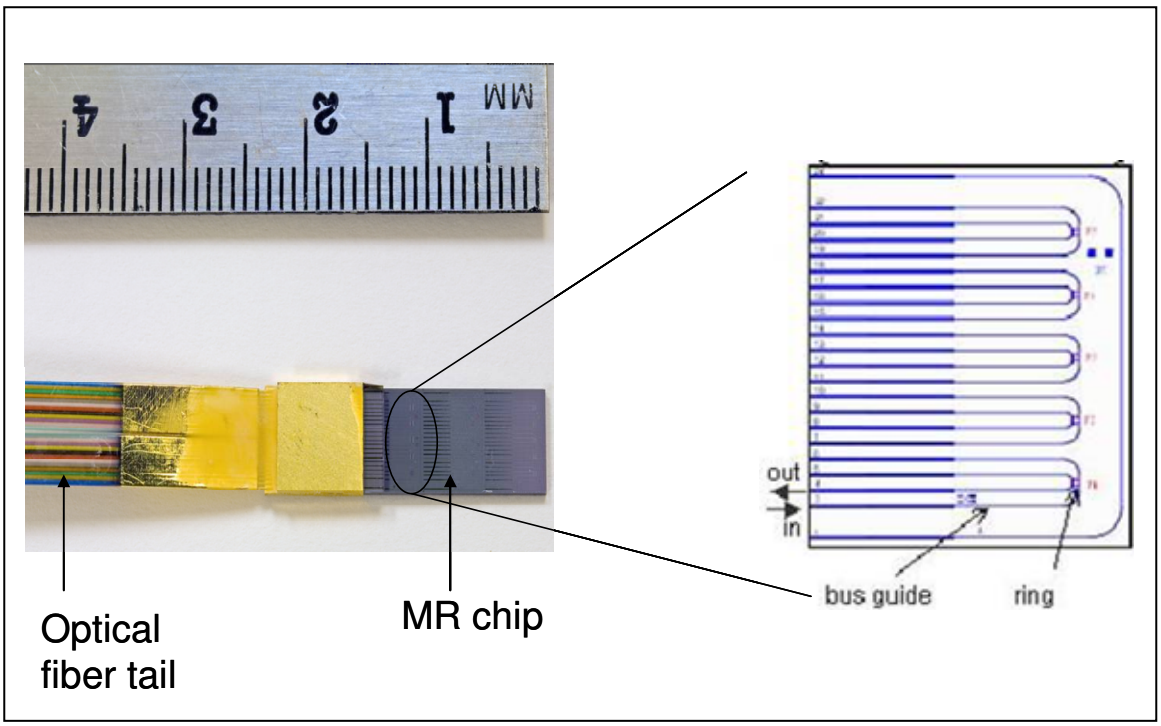
MM
1
2
3
4
out
in
bus guide
ring
Optical
fiber tail
MR chip

Figure 2. Flow-cell for microring resonator assays. Clockwise from left: Disassembled flow cell showing microchannels in cover, machined base and gasket defining flow channel; Base with chip and flow channel gasket; Assembled flow cell apparatus with connectorized MR sensing chip.

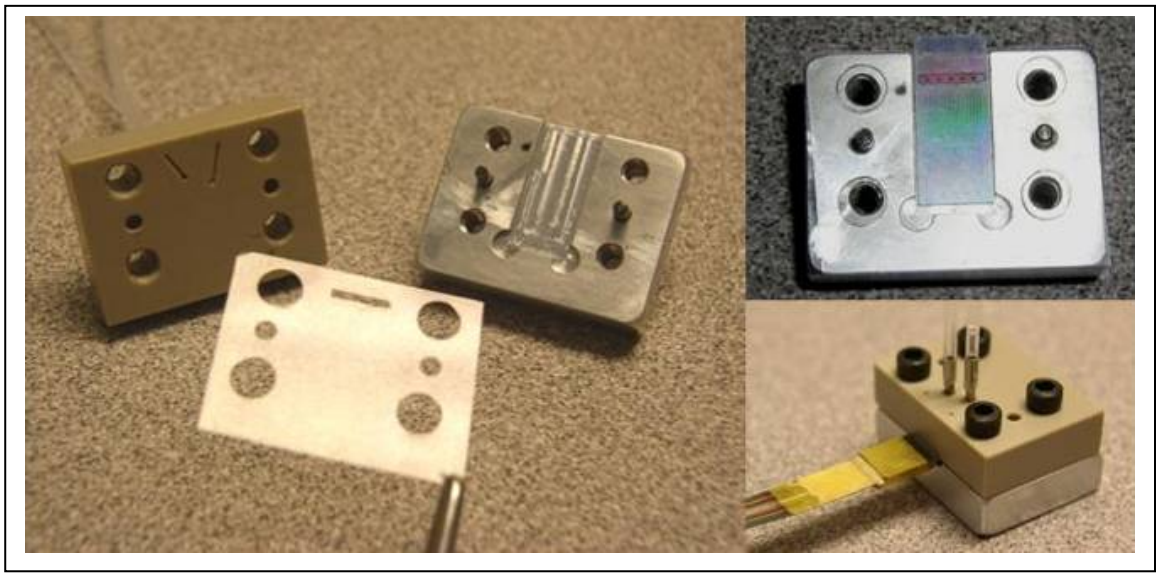

Figure 3. Microring resonator detection of *E. coli* O157:H7. Test: Microrings functionalized with antibody to *E. coli* O157:H7; Control: Microrings functionalized with non-*E. coli*-specific antibody. Bacterial suspension used was *E. coli* O157:H7 at 10^9 CFU/ml.

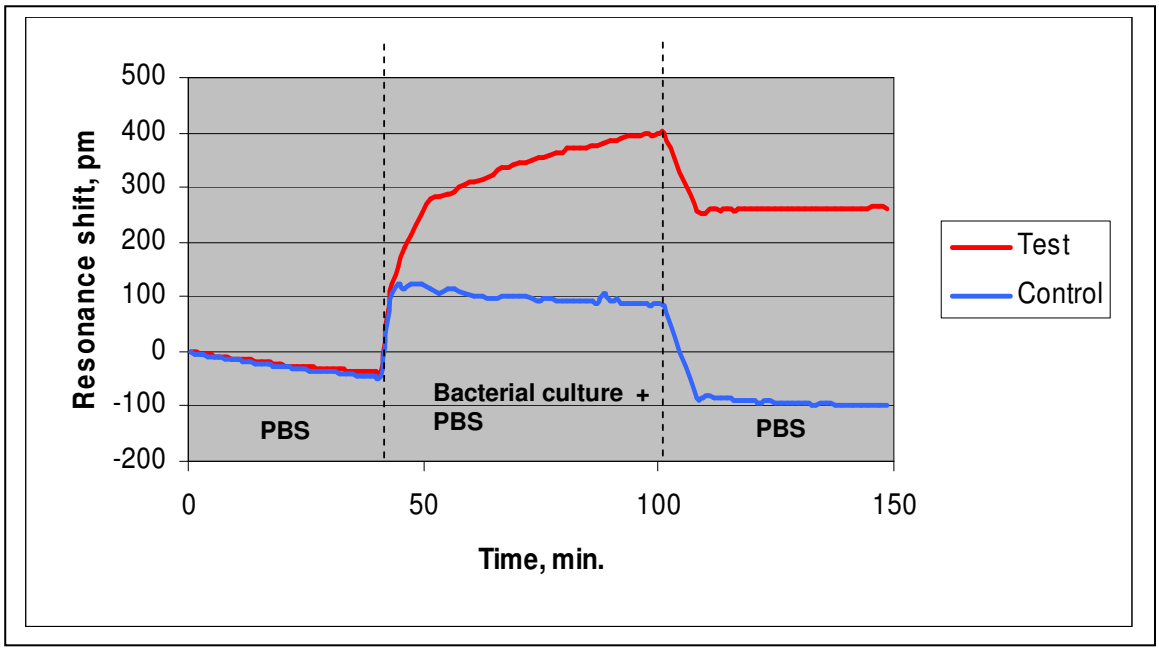
500
400
300
200
100
0
-100
-200
Resonance shift, pm
0
50
100
150
Time, min.
PBS
Bacterial culture + PBS
PBS
Test
Control

Figure 4. Scanning electron micrographs of bacteria bound to MR sensing chip. *E. coli* cells are bound to ring surface functionalized with anti-*E. coli* antibody (Test, bottom) and not to non-*E. coli* antibody microrings (Control, top). Magnification: 2200X

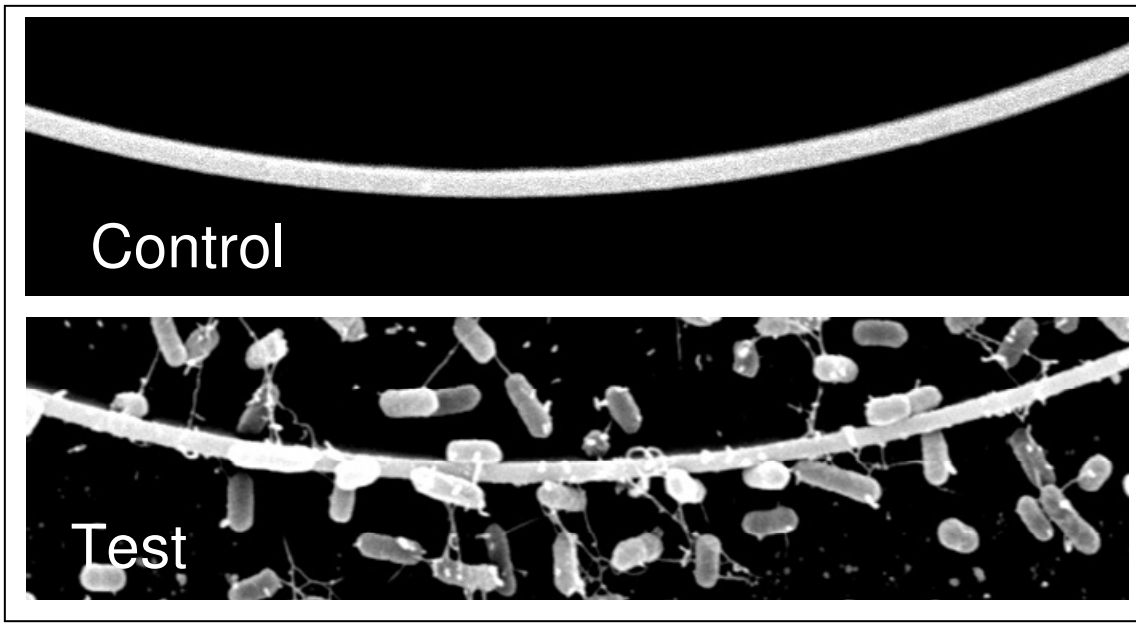
Control
Test

Figure 5. Sequential detection of *S.* Typhimurium and *E. coli* with microring resonator device. Rings were functionalized with species-specific anti-LPS antibodies. Results are averaged across 2 treatment microrings per group and corrected for reference.

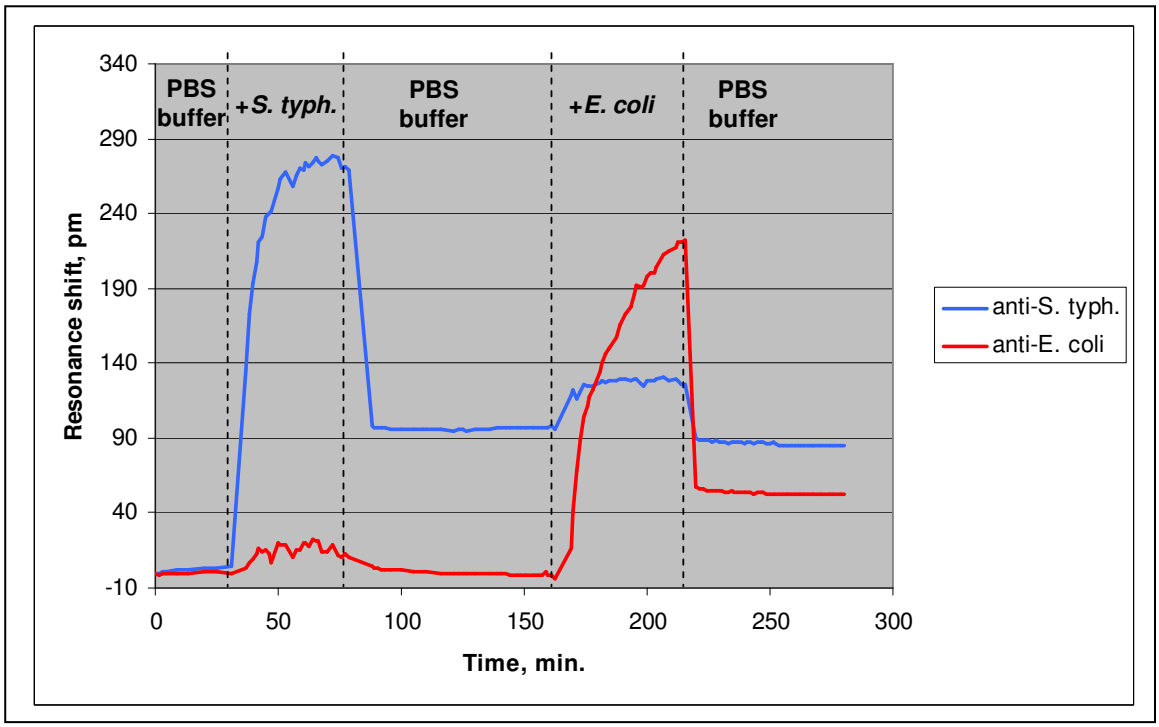
PBS buffer
+S. typh.
PBS buffer
+E. coli
PBS buffer
340
290
240
190
140
90
40
-10
Resonance shift, pm
0
50
100
150
200
250
300
Time, min.
anti-S. typh.
anti-E. coli

Figure 6. Multiplex detection of *E. coli* or *S.* Typhimurium on MR chips by direct application of sample to sensing surface. Chips were transferred from buffer to humidity chamber during cell binding phases. Data are averaged across 2 microrings per group and corrected for reference microring response.

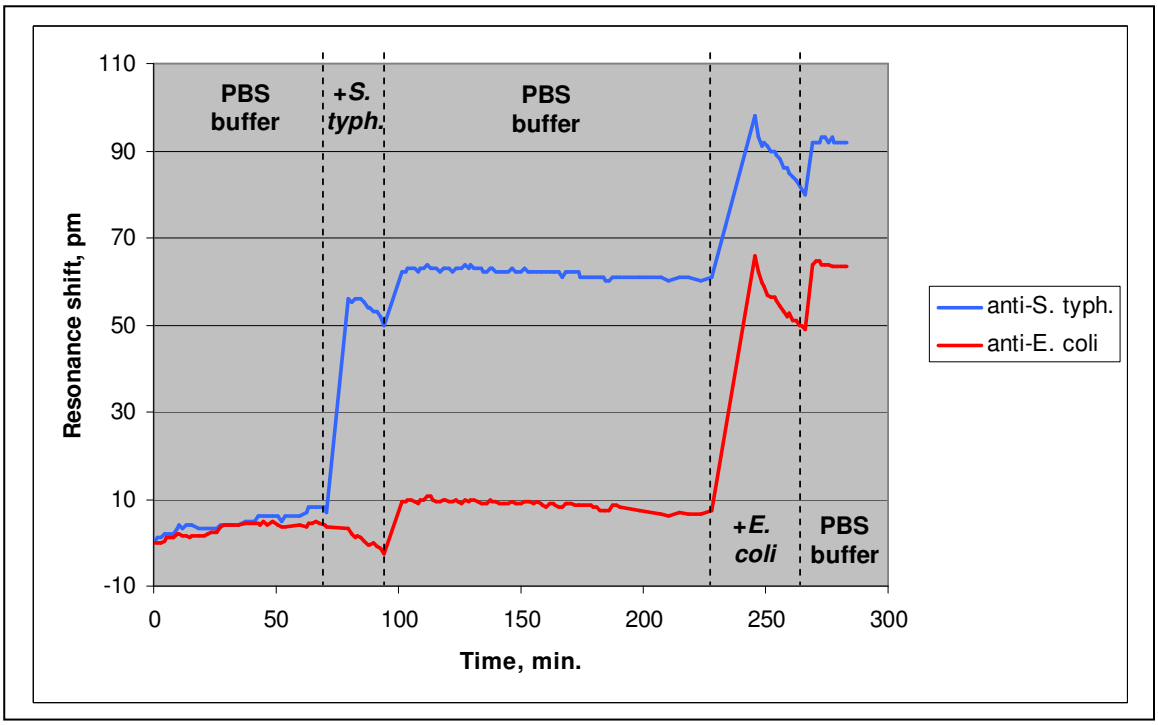
PBS buffer
+S. typh.
PBS buffer
+E. coli
PBS buffer
Resonance shift, pm
Time, min.
110
90
70
50
30
10
-10
0
50
100
150
200
250
300
anti-S. typh.
anti-E. coli

Figure 7. Detection of *S.* Typhimurium whole bacterial cells on MR chips in a flow cell apparatus. Rings were functionalized with antibodies specific for *E. coli* or *S. typhimurium* LPS. Reference ring data not available in this assay.

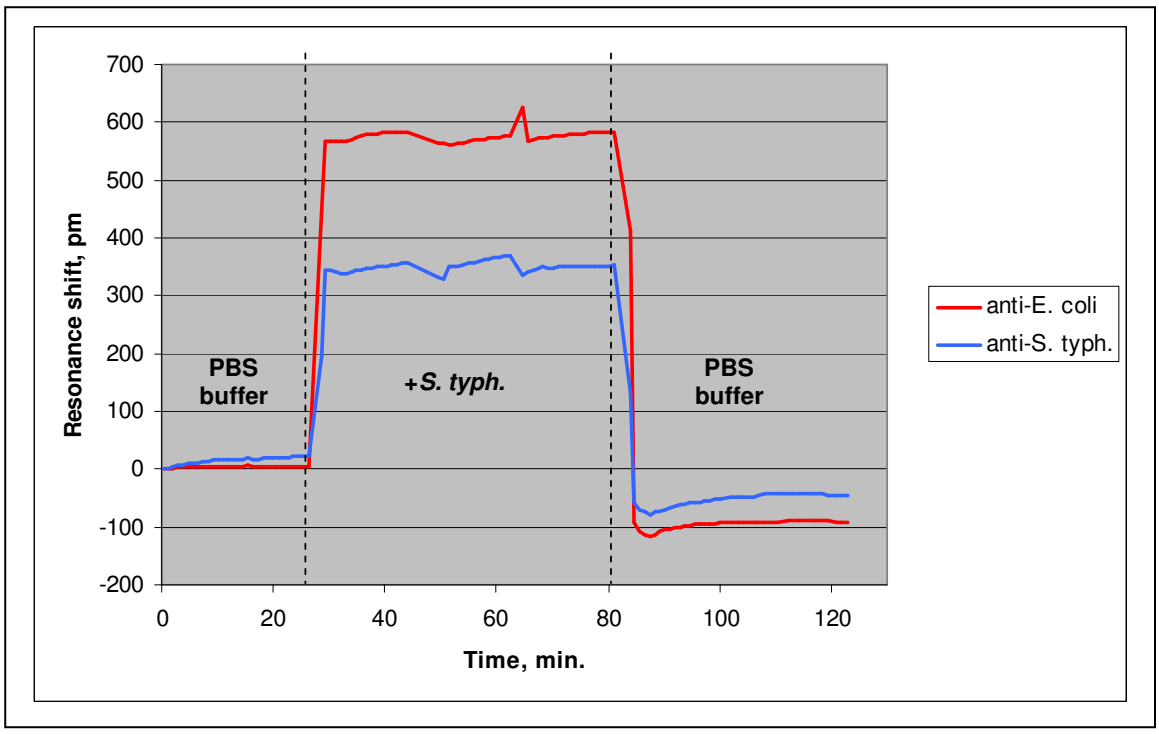
700
600
500
400
300
200
100
0
-100
-200
Resonance shift, pm
0
20
40
60
80
100
120
Time, min.
PBS buffer
+S. typh.
PBS buffer
anti-E. coli
anti-S. typh.

Figure 8. Multiplex detection of *E. coli* or *S.* Typhimurium on microring resonators using a microfluidic flow cell apparatus.

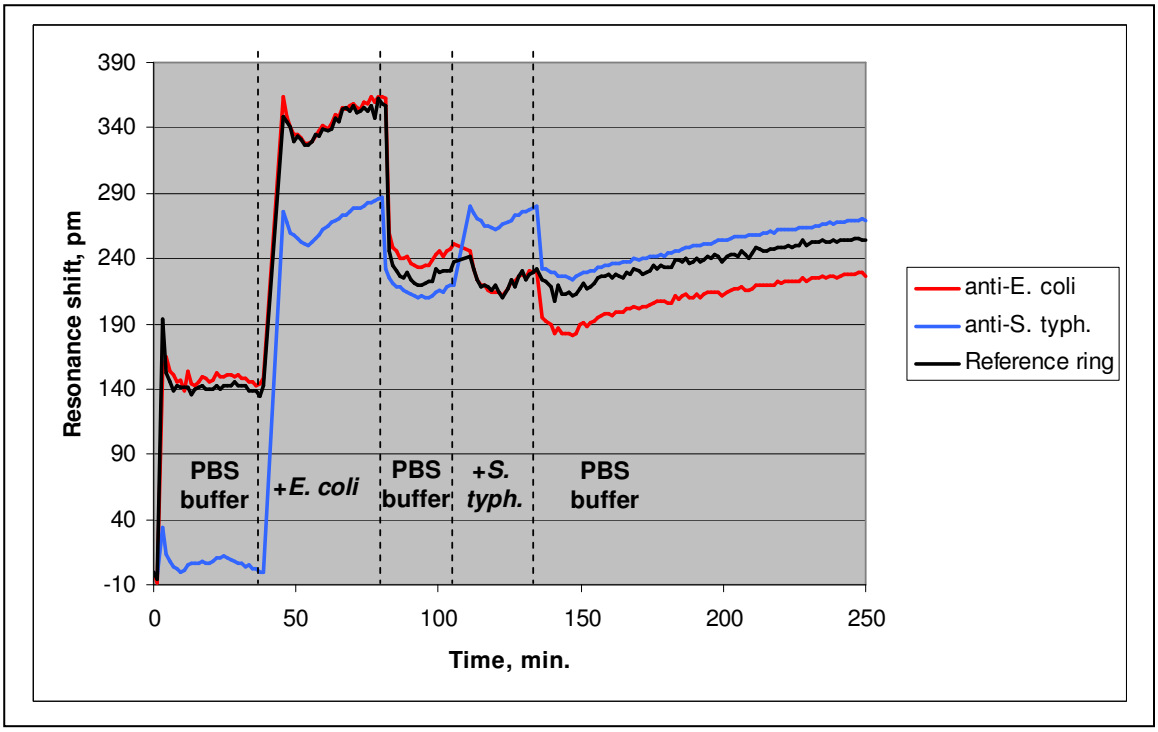
390
340
290
240
190
140
90
40
-10
Resonance shift, pm
0
50
100
150
200
250
Time, min.
PBS buffer
+E. coli
PBS buffer
+S. typh.
PBS buffer
anti-E. coli
anti-S. typh.
Reference ring

CHAPTER VI

CONCLUSION

The results of the described research address the major points introduced at the beginning of this dissertation. The ability to identify useful genomic sequences which can serve as genetic markers for nucleic acid-based detection protocols has been discussed. Although the original goal of finding genomic markers associated with increased cytoxicity of the H1 isolate of *C. piliforme* was unsuccessful, the final result was highly useful in that new markers were identified. These markers can be transitioned into assays for highly specific detection of this pathogen, particularly if a multiplex assay is performed. It is anticipated that a system of this type will far outperform the current assays based on amplification of 16S ribosomal sequences.

The ability to detect phenotypic markers associated with pathogenic organisms was shown, at least as proof-of-concept, in peptide displacement assays for MRSA, and the application of AFP to detection protocols has tremendous potential. The major advantage of this type of assay is the detection of the protein product which is actually responsible for the phenotype, in this case

methicillin resistance. Protein detection assays of this nature are in some cases actually preferable to genetic tests because the result is not only detection of the marker, but also assurance that the protein is being expressed, creating the highly pathogenic phenotype.

The application of label-free detection methods is the current area of most interest in diagnostic platforms, detection systems for medical and biodefense applications and animal health. The application of optical microring resonator devices to whole bacterial cell detection in a multiplex assay design has not been previously reported. The results presented here clearly demonstrate the utility of the platform, and provide credence for continued development into a fieldable device.

Taken together, the data presented here give a broad view of detection schemes for pathogenic bacteria, including animal and human pathogens. Further, both label-free and label-dependent assays were investigated, as were genetic and protein based assays.

REFERENCES

Appelbaum, P. C. 2007. Microbiology of antibiotic resistance in *Staphylococcus aureus*. *Clin. Infect. Dis.* **45**(Suppl 3):S165-170.

Barken, K. B., Haagensen, J. A. and Tolker-Nielsen, T. 2007. Advances in nucleic acid-based diagnostics of bacterial infections. *Clin. Chim. Acta.* **384**:1-11.

Barrios, C. A., Bañuls, M. J., González-Pedro, V., Gylfason, K. B., Sánchez, B., Griol, A., Maquieira, A., Sohlström, H., Holgado, M. and Casquel, R. 2008. Label-free optical biosensing with slot-waveguides. *Opt. Lett.* **33**:708-710.

Barrios, C. A., Gylfason, K. B., Sánchez, B., Griol, A., Sohlström, H., Holgado, M. and Casquel, R. 2007. Slot-waveguide biochemical sensor. *Opt. Lett.* **32**:3080-3082.

Berger-Bächi, B. and Rohrer, S. 2002. Factors influencing methicillin resistance in staphylococci. *Arch. Microbiol.* **178**:165-171.

Berkenpas, E., Millard, P. and Pereira da Cunha, M. 2006. Detection of *Escherichia coli* O157:H7 with langasite pure shear horizontal surface acoustic wave sensors. *Biosens. Bioelectron.* **21**:2255-2262.

Boivin, G. P., Hook, R. R. Jr. and Riley, L. K. 1994. Development of a monoclonal antibody-based competitive inhibition enzyme-linked immunosorbent assay for detection of *Bacillus piliformis* isolate-specific antibodies in laboratory animals. *Lab Anim. Sci.* **44**:153-158.

Boivin, G. P., Hook, R. R. and Riley, L. K. 1993. Antigenic diversity in flagellar epitopes among *Bacillus piliformis* isolates. *J. Med. Microbiol.* **38**:177-182.

Bokken, G. C., Corbee, R. J., van Knapen, F. and Bergwerff, A. A. 2003. Immunochemical detection of *Salmonella* group B, D and E using an optical surface plasmon resonance biosensor. *FEMS Microbiol. Lett.* **222**:75-82.

Borchers, A., Magdesian, K. G., Halland, S., Pusterla, N. and Wilson, W. D. 2006. Successful treatment and polymerase chain reaction (PCR) confirmation of Tyzzer's disease in a foal and clinical and pathologic characteristics of 6 additional foals (1986-2005). *J. Vet. Intern. Med.* **20**:1212-1218.

Boschert, K. R., Allison, N., Allen, T. L. and Griffin, R. B. 1988. *Bacillus piliformis* infection in an adult dog. *J. Am. Vet. Med. Assoc.* **192**:791-792.

Boyle-Vavra, S. and Daum, R. S. Community-acquired methicillin-resistant *Staphylococcus aureus*: the role of Panton-Valentine leukocidin. *Lab. Invest.* **87**:3-9.

Branch, D. W. and Brozik, S. M. Low-level detection of a *Bacillus anthracis* simulant using Love-wave biosensors on 36 degrees YX LiTaO3. *Biosens. Bioelectron.* **19**:849-859.

Brooks, J. W., Whary, M. T., Hattel, A. L., Shaw, D. P., Ge, Z., Fox, J. G. and Poppenga, R. H. 2006. *Clostridium piliforme* infection in two farm-raised white-tailed deer fawns (*Odocoileus virginianus*) and association with copper toxicosis. *Vet. Pathol.* **43**:765-768.

Brown, D. F., Edwards, D. I., Hawkey, P. M., Morrison, D., Ridgway, G. L., Towner, K. J., Wren, M. W.; Joint Working Party of the British Society for Antimicrobial

Chemotherapy; Hospital Infection Society; Infection Control Nurses Association. 2005. Guidelines for the laboratory diagnosis and susceptibility testing of methicillin-resistant *Staphylococcus aureus* (MRSA). *J. Antimicrob. Chemother.* **56**:1000-1018.

Campbell, G. A. and Mutharasan, R. 2007. A method of measuring *Escherichia coli* 0157:H7 at 1 cell/mL in 1 liter sample using antibody functionalized piezoelectric-excited millimeter-sized cantilever sensor. *Environ. Sci. Technol.* **41**:1668-1674.

Campbell, G. A., Uknalis, J., Tu, S. I. and Mutharasan, R. 2007. Detection of *Escherichia coli* O157:H7 in ground beef samples using piezoelectric excited millimeter-sized cantilever (PEMC) sensors. *Biosens. Bioelectron.* **22**:1296-1302.

Campbell, G. A. and Mutharasan, R. 2005a. Detection of pathogen *Escherichia coli* O157:H7 using self-excited PZT-glass microcantilevers. *Biosens. Bioelectron.* **21**:462-473.

Campbell, G. A. and Mutharasan, R. 2005b. *Escherichia coli* O157:H7 detection limit of millimeter-sized PZT cantilever sensors is 700 cells/mL. *Anal. Sci.* **21**:355-357.

Canfield, P. J. and Hartley, W. J. 1991. Tyzzer's disease (*Bacillus piliformis*) in Australian marsupials. *J. Comp. Pathol.* **105**:167-173.

Carroll, K. C. 2008. Rapid diagnostics for methicillin-resistant *Staphylococcus aureus*: current status. *Mol. Diagn. Ther.* **12**:15-24.

Chalmers, G. A. and MacNeill, A. C. 1977. Tyzzer's disease in wild-trapped muskrats in British Columbia. *J. Wildl. Dis.* **13**:114-116.

Chambers, H. F. 1997. Methicillin resistance in staphylococci: molecular and biochemical basis and clinical implications. *Clin. Microbiol. Rev.* **10**:781-791.

Chao, C.-Y., Fung, W. and Guo, L. J. 2006. Polymer microring resonators for biochemical sensing applications. *IEEE J. Sel. Top. Quant. Electron.* **12**:134–142.

Chu, S. T., Little, B. E., Pan, W., Kaneko, T., Sato, S. and Kokubun, Y. 1999. An eight-channel add-drop filter using vertically coupled microring resonators over a cross grid. *IEEE Photon. Technol. Lett.* **11**:691–693.

Coburn, B., Grassl, G. A. and Finlay BB. 2007. *Salmonella*, the host and disease: a brief review. *Immunol. Cell Biol.* **85**:112-118.

Cooper, M. A. 2003. Label-free screening of bio-molecular interactions. *Anal. Bioanal. Chem.* **377**:834-42.

Cooper, M. A. and Singleton, V. T. 2007. A survey of the 2001 to 2005 quartz crystal microbalance biosensor literature: applications of acoustic physics to the analysis of biomolecular interactions. *J. Mol. Recognit.* **20**:154-184.

Dancer, S. J. 2008. The effect of antibiotics on methicillin-resistant *Staphylococcus aureus*. *J. Antimicrob. Chemother.* **61**:246-253.

Deisingh, A. K. and Thompson M. 2004a. Strategies for the detection of *Escherichia coli* O157:H7 in foods. *J. Appl. Microbiol.* **96**:419-429.

Deisingh, A. K and Thompson, M. 2004. Biosensors for the detection of bacteria. *Can. J. Microbiol.* **50**:69-77.

de Jonge, B. L. and Tomasz, A. 1993. Abnormal peptidoglycan produced in a methicillin-resistant strain of *Staphylococcus aureus* grown in the presence of

methicillin: functional role for penicillin-binding protein 2A in cell wall synthesis. *Antimicrob. Agents Chemother.* **37**:342-346.

de Lencastre, H., Oliveira, D. and Tomasz, A. 2007. Antibiotic resistant *Staphylococcus aureus*: a paradigm of adaptive power. *Curr. Opin. Microbiol.* **10**:428-435.

Deng, S., Cai, W. and Astratov, V. 2004. Numerical study of light propagation via whispering gallery modes in microcylinder coupled resonator optical waveguides. *Opt. Express* **12**:6468–6480.

Deurenberg, R. H., Vink, C., Kalenic, S., Friedrich, A. W., Bruggeman, C. A. and Stobberingh, E. E. 2007. The molecular evolution of methicillin-resistant *Staphylococcus aureus*. *Clin. Microbiol. Infect.* **13**:222-235.

Dhayal, B., Henne, W. A., Doorneweerd, D. D., Reifenberger, R. G. and Low, P. S. 2006. Detection of *Bacillus subtilis* spores using peptide-functionalized cantilever arrays. *J. Am. Chem. Soc.* **128**:3716-3721.

Diatchenko, L., Lau, Y. F., Campbell, A. P., Chenchik, A., Moqadam, F., Huang, B., Lukyanov, S., Lukyanov, K., Gurskaya, N., Sverdlov, E. D. and Siebert, P. D. 1996. Suppression subtractive hybridization: a method for generating differentially regulated or tissue-specific cDNA probes and libraries. *Proc. Natl. Acad. Sci. U S A.* **93**:6025-6030.

Duncan, A. J., Carman, R. J., Olsen, G. J. and Wilson, K. H. 1993. Assignment of the agent of Tyzzer's disease to *Clostridium piliforme* comb. *nov.* on the basis of 16S rRNA sequence analysis. *Int. J. Syst. Bacteriol.* **43**:314-318.

Ekinci, K. L., Huang, M. H. and Roukes, M. L. 2004. Ultrasensitive nanoelectromechanical mass detection. *Appl. Phys. Lett.* **84**:4469-4471.

Feldman, S. H., Kiavand, A., Seidelin, M.and Reiske, H. R. 2006. Ribosomal RNA sequences of *Clostridium piliforme* isolated from rodent and rabbit: re-examining the phylogeny of the Tyzzer's disease agent and development of a diagnostic polymerase chain reaction assay. *J. Am. Assoc. Lab Anim. Sci.* **45**:65-73.

Fosgate, G. T., Hird, D. W., Read, D. H. and Walker, R. L. 2002. Risk factors for *Clostridium piliforme* infection in foals. *J. Am. Vet. Med. Assoc.* **220**:785-790.

Franklin, C. L., Motzel, S. L., Besch-Williford, C. L., Hook, R. R. Jr. and Riley, L. K. 1994. Tyzzer's infection: host specificity of *Clostridium piliforme* isolates. *Lab Anim. Sci.* **44**:568-572.

Franklin, C. L., Kinden, D. A., Stogsdill, P.L. and Riley, L. K. 1993. In vitro model of adhesion and invasion by *Bacillus piliformis*. *Infect. Immun.* **61**:876-883.

Fuda, C., Suvorov, M., Vakulenko, S. B. and Mobashery, S. 2004. The basis for resistance to beta-lactam antibiotics by penicillin-binding protein 2a of methicillin-resistant *Staphylococcus aureus*. *J. Biol. Chem.* **279**:40802-40806.

Fujiwara, K. 1978. Tyzzer's disease. *Jpn. J. Exp. Med.* **48**:467-480.

Furukawa, T., Furumoto, K., Fujieda, M. and Okada, E. 2002. Detection by PCR of the Tyzzer's disease organism (*Clostridium piliforme*) in feces. *Exp. Anim.* **51**:513-516.

Ganaway, J. R., Allen, A. M. and Moore, T. D. 1971. Tyzzer's disease. *Am. J. Pathol.* **64**:717-730.

Giesbrecht, P., Kersten, T., Maidhof, H. and Wecke, J. 1998. Staphylococcal cell wall: morphogenesis and fatal variations in the presence of penicillin. *Microbiol. Mol. Biol. Rev.* **62**:1371-1414.

Goldman, R. 2006. *Escherichia coli*. *Pediatr. Rev.* **27**:114-115.

Goto, K. and Itoh, T. 1994. Detection of *Bacillus piliformis* by specific amplification of ribosomal sequences. *Jikken Dobutsu.* **43**:389-394.

Gronewold, T. M. 2007. Surface acoustic wave sensors in the bioanalytical field: recent trends and challenges. *Anal. Chim. Acta.* **603**:119-128.

Gyles, C. L. 2007. Shiga toxin-producing *Escherichia coli*: an overview. *J. Anim. Sci.* **85**(Suppl):E45-62.

Hansen, K. M. and Thundat, T. 2005. Microcantilever biosensors. *Methods.* **37**:57-64.

Hansen, A. K., Andersen, H. V. and Svendsen, O. 1994. Studies on the diagnosis of Tyzzer's disease in laboratory rat colonies with antibodies against *Bacillus piliformis* (*Clostridium piliforme*). *Lab Anim. Sci.* **44**:424-429.

Harrington, D. D. 1976. *Bacillus piliformis* infection (Tyzzer's disease) in two foals. *J. Am. Vet. Med. Assoc.* **168**:58-60.

Harrington, D. D. 1975. Naturally-occurring Tyzzer's disease (*Bacillus piliformis* infection) in horse foals. *Vet. Rec.* **96**:59-63.

Hartman, B. J. and Tomasz, A. 1984. Low-affinity penicillin-binding protein associated with beta-lactam resistance in *Staphylococcus aureus*. *J. Bacteriol.* **158**:513-516.

Herzog, G and Arrigan, D. W. 2007. Electrochemical strategies for the label-free detection of amino acids, peptides and proteins. *Analyst* **132**:615-632.

Hiramatsu, K. 2001. Vancomycin-resistant *Staphylococcus aureus*: A new model of antibiotic resistance. *Lancet Infect. Dis.* **1**:147-155.

Homola, J. 2008. Surface plasmon resonance sensors for detection of chemical and biological species. *Chem. Rev.* **108**:462-93.

Homola, J. 2003. Present and future of surface plasmon resonance biosensors. *Anal. Bioanal. Chem.* **377**:528-39.

Homola, J., Yee, S. S. and Gauglitz, G. 1999. Surface plasmon resonance sensors: review. *Sens. Actuators B*. **54**:3-15.

Hook, R. R., Riley, L. K., Franklin, C. L. and Besch-Williford, C. L. 1995. Seroanalysis of Tyzzer's disease in horses: implications that multiple strains can infect Equidae. *Equine Vet. J.* **27**:8-12.

Huang, X., Li, Y., Niu, Q. and Zhang, K. 2007. Suppression Subtractive Hybridization (SSH) and its modifications in microbiological research. *Appl. Microbiol. Biotechnol.* **76**:753-760.

Huang, L. and Cooper, M. A. 2006. Real-time label-free acoustic technology for rapid detection of *Escherichia coli* O157:H7. *Clin. Chem.* **52**:2148-2151.

Ibrahim, T.A., Cao, W., Kim, Y., Li, J., Goldhar, J., Ho, P. T. and Lee, C. H. 2003. All-optical switching in a laterally coupled microring resonator by carrier injection. *IEEE Photon. Technol. Lett.* **15**:36–38.

Ilic, B., Craighead, H. G., Krylov, S., Senaratne, W., Ober, C. and Neuzil, P. 2004. Attogram detection using nanoelectromechanical oscillators. *J. Appl. Phys.* **95**:3694-3703.

Ilic, B, Czaplewski, D., Craighead, H. G., Neuzil, P., Campagnolo, C. and Batt, C. 2000. Mechanical resonant immunospecific biological detector. *Appl. Phys. Lett.* **77**:450-452.

Jevons, M. P. 1961. Celbenin-resistant Staphylococci. *Br. Med. J.* **i**:124-125.

Kaper, J. B., Nataro, J. P. and Mobley, H. L. 2004. Pathogenic *Escherichia coli*. *Nat. Rev. Microbiol.* **2**:123-140.

Karch, H., Tarr, P. I. and Bielaszewska, M. 2005. Enterohaemorrhagic *Escherichia coli* in human medicine. *Int. J. Med. Microbiol.* **295**:405-418.

Ksendzov, A. and Lin, Y. 2005. Integrated optics ring-resonator sensors for protein detection. *Opt. Lett.* **30**:3344-3346.

Kültz, D., Fiol, D., Valkova, N., Gomez-Jimenez, S., Chan, S. Y. and Lee, J. 2007. Functional genomics and proteomics of the cellular osmotic stress response in 'non-model' organisms. *J. Exp. Biol.* **210**:1593-1601.

Lambrianou, A., Demin, S.and Hall, E.A. 2008. Protein engineering and lectrochemical biosensors. *Adv. Biochem. Eng. Biotechnol.* **109**:65-96.

Langan, J., Bemis, D., Harbo, S., Pollock, C. and Schumacher, J. 2000. Tyzzer's disease in a red panda (*Ailurus fulgens fulgens*). *J. Zoo Wildl. Med.* **31**:558-562.

Lazcka, O., Del Campo, F.J. and Munoz, F.X. 2007. Pathogen detection: a perspective of traditional methods and biosensors. *Biosens. Bioelectron.* **22**:1205–1217.

Lewis, R. A. and Dyke, K. G. MecI represses synthesis from the beta-lactamase operon of *Staphylococcus aureus*. *J. Antimicrob. Chemother.* **45**:139-144.

Lim, D. and Strynadka, N. C. 2002. Structural basis for the beta lactam resistance of PBP2a from methicillin-resistant *Staphylococcus aureus*. *Nat. Struct. Biol.* **9**:870-876.

Lina, G., Piémont, Y., Godail-Gamot, F., Bes, M., Peter, M. O., Gauduchon, V., Vandenesch, F. and Etienne, J. 1999. Involvement of Panton-Valentine leukocidin-producing *Staphylococcus aureus* in primary skin infections and pneumonia. *Clin. Infect. Dis.* **29**:1128-1132.

Little, B. E., Chu, S. T., Absil, P. P., Hryniewicz, J. V., Johnson, F. G., Seiferth, F., Gill, D., Van, V., King, O. and Trakalo, M. 2004. Very high-order microring resonator filters for WDM applications. *IEEE Photon. Technol. Lett.* **16**:2263–2265.

Little, B. E., Chu, S. T., Pan, W. and Kokubun, Y. 2000. Microring resonator arrays for VLSI photonics. *IEEE Photon. Technol. Lett.* **12**:323–325.

Little, B. E., Chu, S. T., Haus, H. A., Foresi, J. and Laine, J. P. 1997. Microring resonator channel dropping filters. *J. Lightwave Technol.* **15**:998–1005.

Lucarelli, F., Tombelli, S., Minunni, M., Marrazza, G. and Mascini, M. 2008. Electrochemical and piezoelectric DNA biosensors for hybridisation detection. *Anal. Chim. Acta* **609**:139-159.

Maalouf, R., Fournier-Wirth, C., Coste, J., Chebib, H., Saïkali, Y., Vittori, O., Errachid, A., Cloarec, J. P., Martelet, C. and Jaffrezic-Renault, N. 2007. Label-free detection of bacteria by electrochemical impedance spectroscopy: comparison to surface plasmon resonance. *Anal. Chem.* **79**:4879-4886.

Malhotra-Kumar, S., Haccuria, K., Michiels, M., Ieven, M., Poyart, C., Hryniewicz, W., Goossens, H.; MOSAR WP2 Study Team. 2008. Current trends in rapid

diagnostics for methicillin-resistant *Staphylococcus aureus* and glycopeptide-resistant enterococcus species. *J. Clin. Microbiol.* **46**:1577-1587.

Maraldo, D. and Mutharasan, R. 2007. 10-minute assay for detecting *Escherichia coli* O157:H7 in ground beef samples using piezoelectric-excited millimeter-size cantilever sensors. *J. Food Prot.* **70**:1670-1677.

Marler, R. J. and Cook, J. E. 1976. Tyzzer's disease in two coyotes. *J. Am. Vet. Med. Assoc.* **169**:940-941.

Martins, A. and Cunha, M. de L. R. S. Cunha. 2007. Methicillin resistance in *Staphylococcus aureus* and coagulase-negative staphylococci: Epidemiological and molecular aspects. *Microbiol. Immunol.* **51**:787-795.

McKinney, T. K., Sharma, V. K., Craig, W. A. and Archer, G. L. 2001. Transcription of the gene mediating methicillin resistance in *Staphylococcus aureus* (*mecA*) is corepressed but not coinduced by cognate mecA and beta-lactamase regulators. *J. Bacteriol.* **183**:6862-6868.

McQuade, D. T., Pullen, A. E., and Swager, T. M. 2000. Conjugated polymer-based chemical sensors. *Chem. Rev.* **100**:2537.

Mead, P. S., Slutsker, L., Dietz, V., McCaig, L. F., Bresee, J. S., Shapiro, C., Griffin, P. M. and Tauxe, R. V. 1999. Food-related illness and death in the United States. *Emerg. Infect. Dis.* **5**:607-625.

Moll, N., Pascal, E., Dinh, D. H., Pillot, J. P., Bennetau, B., Rebière, D., Moynet, D., Mas, Y., Mossalayi, D., Pistré, J. and Déjous C. 2007. A Love wave immunosensor for whole *E. coli* bacteria detection using an innovative two-step immobilisation approach. *Biosens. Bioelectron.* **22**:2145-2150.

Motzel, S. L. and Riley, L. K. 1992. Subclinical infection and transmission of Tyzzer's disease in rats. *Lab Anim. Sci.* **42**:439-443.

Motzel, S. L., Meyer, J. K. and Riley, L. K. 1991. Detection of serum antibodies to *Bacillus piliformis* in mice and rats using an enzyme-linked immunosorbent assay. *Lab Anim. Sci.* **41**:26-30.

Nakatomi, Y. and Sugiyama, J. 1998. A rapid latex agglutination assay for the detection of penicillin-binding protein 2'. *Microbiol. Immunol.* **42**:739-743.

Nugen, S. R. and Baeumner, A. J. 2008. Trends and opportunities in food pathogen detection. *Anal. Bioanal. Chem.* **391**:451–454.

Odenthal, K. J. and Gooding, J. J. 2007. An introduction to electrochemical DNA biosensors. *Analyst* **132**:603-610.

Oh, B. K., Lee, W., Kim, Y. K., Lee, W. H. and Choi, J. W. 2004a. Surface plasmon resonance immunosensor using self-assembled protein G for the detection of *Salmonella paratyphi*. *J. Biotechnol.* **111**:1-8.

Oh, B.K., Kim, Y. K., Park, K. W., Lee, W. H. and Choi, J. W. 2004b. Surface plasmon resonance immunosensor for the detection of *Salmonella typhimurium*. *Biosens. Bioelectron.* **19**:1497-504.

Olsen, E. V., Pathirana, S. T., Samoylov, A. M., Barbaree, J. M., Chin, B.A., Neely, W.C. and Vodyanoy, V. 2003. Specific and selective biosensor for *Salmonella* and its detection in the environment. *J. Microbiol. Methods.* **53**:273-285.

Otto, G. and Franklin, C. L. 2006. Medical management and diagnostic approaches. In: The Laboratory Rat, 2nd ed. Academic Press. pp. 547-565.

Pathirana, S. T., Barbaree, J., Chin, B. A., Hartell, M. G., Neely, W. C. and Vodyanoy, V. 2000. Rapid and sensitive biosensor for *Salmonella*. *Biosens. Bioelectron.* **15**:135-141.

Pinho, M. G., Filipe, S. R., de Lencastre, H. and Tomasz, A. 2001. Complementation of the essential peptidoglycan transpeptidase function of penicillin-binding protein 2 (PBP2) by the drug resistance protein PBP2A in *Staphylococcus aureus*. *J. Bacteriol.* **183**:6525-6531.

Ramachandran, A., Wang, S., Clarke, J., Ja, S. J., Goad, D., Wald, L., Flood, E. M., Knobbe, E., Hryniewicz, J. V., Chu, S. T., Gill, D., Chen, W., King, O. and Little, B. E. 2008. A universal biosensing platform based on optical micro-ring resonators. *Biosens. Bioelectron.* **23**:939-944.

Raymond, J. T., Topham, K., Shirota, K., Ikeda, T. and Garner, M. M. 2001. Tyzzer's disease in a neonatal rainbow lorikeet (*Trichoglossus haematodus*). *Vet. Pathol.* **38**:326-327.

Ricci, F., Volpe, G., Micheli, L. and Palleschi, G. 2007. A review on novel developments and applications of immunosensors in food analysis. *Anal. Chim. Acta.* **605**:111-29.

Riley, L. K., Caffrey, C. J., Musille, V. S. and Meyer, J. K. 1992. Cytotoxicity of *Bacillus piliformis*. *J. Med. Microbiol.* **37**:77-80.

Riley, L. K., Besch-Williford, C. and Waggie, K. S. 1990. Protein and antigenic heterogeneity among isolates of *Bacillus piliformis*. *Infect. Immun.* **58**:1010-1016.

Rohrer, S., Bischoff, M., Rossi, J. and Berger-Bachi, B. 2003. Mechanisms of methicillin resistance. *In:* MRSA: Current Perspectives. *Eds.* Fluit, A. C. and Schmitz, F-J, Caister Academic Press. pp. 31-53.

Røsok, Ø. and Sioud, M. 2007. Discovery of differentially expressed genes: technical considerations. *Methods Mol. Biol.* **360**:115-129.

Sabath, L. D., Wallace, S. J. and Gerstein, D. A. 1972. Suppression of intrinsic resistance to methicillin and other penicillins in *Staphylococcus aureus*. *Antimicrob. Agents Chemother.* **2**:350-355.

Saito, M., Sekiguchi, K., Yajima, R., Hina, M., Doss, R. C. and Kanno, H. 1995. Immunological detection of penicillin-binding protein 2' of methicillin-resistant staphylococci by using monoclonal antibodies prepared from synthetic peptides. *J. Clin. Microbiol.* **33**:2498-2500.

Sasseville, V. G., Simon, M. A., Chalifoux, L. V., Lin, K. C. and Mansfield, K. G. 2007. Naturally occurring Tyzzer's disease in cotton-top tamarins (*Saguinus oedipus*). *Comp. Med.* **57**:125-127.

Saunders, G. K., Sponenberg, D. P. and Marx, K. L. 1993. Tyzzer's disease in a neonatal cockatiel. *Avian Dis.* **37**:891-894.

Schmidt, R. E., Eisenbrandt, D. L. and Hubbard, G. B. 1984. Tyzzer's disease in snow leopards. *J. Comp. Pathol.* **94**:165-167.

Serra, B., Gamella, M., Reviejo, A. J. and Pingarrón, J. M. 2008. Lectin-modified piezoelectric biosensors for bacteria recognition and quantification. *Anal. Bioanal. Chem.* **391**:1853-1860.

Smith, K. J., Skelton, H. G., Hilyard, E. J., Hadfield, T., Moeller, R. S., Tuur, S., Decker, C., Wagner, K. F. and Angritt, P. 1996. *Bacillus piliformis* infection (Tyzzer's disease) in a patient infected with HIV-1: confirmation with 16S ribosomal RNA sequence analysis. *J. Am. Acad. Dermatol.* **34**:343-348.

Smotrova, E. I., Nosich, A. I., Benson, T. M. and Sewell, P. 2006. Optical coupling of whispering-gallery modes of two identical microdisks and its effect on photonic molecule lasing. *IEEE J. Sel. Top. Quant. Electron.* **12**:78–85.

Sobel, J., Griffin, P. M., Slutsker, L., Swerdlow, D. L. and Tauxe, R. V. 2002a. Investigation of multistate foodborne disease outbreaks. *Public Health Rep.* **117**:8-19.

Sobel , J., Khan, A. S. and Swerdlow, D. L. 2002b. Threat of a biological terrorist attack on the US food supply: the CDC perspective. *Lancet* **359**:874-880.

Stanley, S. M., Flatt, R. E. and Daniels, G. N. 1978. Naturally occurring Tyzzer's disease in the gray fox. *J. Am. Vet. Med. Assoc.* **173**:1173-1174.

Sternberg, M. B. and Gepstein, S. 2007. Subtractive hybridization techniques to study cellular senescence. *Methods Mol. Biol.* **371**:289-305.

Subramanian, A., Irudayaraj, J. and Ryan, T. A mixed self-assembled monolayer-based surface plasmon immunosensor for detection of *E. coli* O157:H7. *Biosens. Bioelectron.* **21**:998-1006.

Sun, Y., Shopova, S. I., Frye-Mason, G. and Fan, X. 2008. Rapid chemical-vapor sensing using optofluidic ring resonators. *Opt. Lett.* **33**:788-790.

Swager, T. M. 1998. The molecular wire approach to sensory signal amplification. *Acc. Chem. Res.* **31**:201.

Taylor, A. D., Ladd, J., Yu, Q., Chen, S., Homola, J. and Jiang, S. 2006. Quantitative and simultaneous detection of four foodborne bacterial pathogens with a multi-channel SPR sensor. *Biosens. Bioelectron.* **22**:752-8.

Tenover, F. C. 2007. Rapid detection and identification of bacterial pathogens using novel molecular technologies: infection control and beyond. *Clin. Infect. Dis.* **44**:418-423.

Török, T. J., Tauxe, R. V., Wise, R. P., Livengood, J. R., Sokolow, R., Mauvais, S., Birkness, K. A., Skeels, M. R., Horan, J. M. and Foster, L. R. 1997. A large community outbreak of salmonellosis caused by intentional contamination of restaurant salad bars. *JAMA* **278**:389-395.

Tyzzer, E. E. 1917. A fatal disease of the Japanese waltzing mouse caused by a spore-bearing bacillus (*Bacillus piliformis*, N. Sp.). *J. Med. Res.* **37**:307-338.

Turk, M. A., Gallina, A. M. and Perryman, L. E. 1981. *Bacillus piliformis* infection (Tyzzer's disease) in foals in northwestern United States: a retrospective study of 21 cases. *J. Am. Vet. Med. Assoc.* **178**:279-281.

Van Andel, R. A., Hook. R. R. Jr, Franklin, C. L., Besch-Williford, C. L. and Riley, L. K. 1998. Interleukin-12 has a role in mediating resistance of murine strains to Tyzzer's disease. *Infect. Immun.* 66:4942-4946.

Van Andel, R. A., Hook, R. R. Jr, Franklin, C. L., Besch-Williford, C. L., van Rooijen, N. and Riley, L. K. 1997. Effects of neutrophil, natural killer cell, and macrophage depletion on murine *Clostridium piliforme* infection. *Infect. Immun.* **65**:2725-2731.

Vollmer, F., Arnold, S., Braun, D., Teraoka, I. and Libchaber, A. 2003. Multiplexed DNA quantification by spectroscopic shift of two microsphere cavities. *Biophys. J.* **85**:1974–1979.

Vollmer, F., Braun, D., Libchaber, A., Khoshsima, M., Teraoka, I. and Arnold, S. 2002. Protein detection by optical shift of a resonant microcavity. *Appl. Phys. Lett.* **80**:4057–4059.

Waggoner, P. S. and Craighead, H. G. 2007. Micro- and nanomechanical sensors for environmental, chemical, and biological detection. *Lab. Chip.* **7**:1238-1255.

Wang, L. J., Wu, C. S., Hu, Z. Y., Zhang, Y. F., Li, R. and Wang, P. 2008. Sensing *Escherichia coli* O157:H7 via frequency shift through a self-assembled monolayer based QCM immunosensor. *J. Zhejiang Univ. Sci. B* **9**:121-131.

Waswa, J. W., Debroy, C. and Irudayaraj, J. 2006. Rapid detection of *Salmonella enteritidis* and *Escherichia coli* using surface plasmon resonance biosensor. *J. Food Proc. Eng.* **29**:373-385.

Webb, D. M., Harrington, D. D. and Boehm, P. N. 1987. *Bacillus piliformis* infection (Tyzzer's disease) in a calf. *J. Am. Vet. Med. Assoc.* **191**:431-434.

Weeks, B. L., Camarero, J., Noy, A., Miller, A. E., Stanker, L. and De Yoreo, J. J. 2003. A microcantilever-based pathogen detector. *Scanning.* **25**:297-299.

White, I. M., Hanumegowda, N. M. and Fan, X. 2005. Subfemtomole detection of small molecules with microsphere sensors. *Opt. Lett.* **30**:3189–3191.

Whitwell, K. E. 1976. Four cases of Tyzzer's disease in foals in England. *Equine Vet. J.* **8**:118-122.

Winstanley. C. 2002. Spot the difference: applications of subtractive hybridisation to the study of bacterial pathogens. *J. Med. Microbiol.* **51**:459-467.

Wojcinski, Z. W. and Barker, I. K. 1986. Tyzzer's disease as a complication of canine distemper in a raccoon. *J. Wildl. Dis.* **22**:55-59.

World Health Organization. "Drug resistant Salmonella". http://www.who.int/mediacentre/factsheets/fs139/en/ 2005. WHO website.

CDC. 2008. CDC Update, "Investigation of Outbreak of Infections Caused by *Salmonella* Saintpaul", http://www.cdc.gov/salmonella/saintpaul/index.html CDC website.

Wu, C. Y., Hoskins, J., Blaszczak, L. C., Preston, D. A. and Skatrud, P. L. 1992. Construction of a water-soluble form of penicillin-binding protein 2a from a methicillin-resistant *Staphylococcus aureus* isolate. *Antimicrob. Agents Chemother.* **36**:533-539.

Yalcin, A., Popat, K. C., Aldridge, J. C., Desai, T. A., Hryniewicz, J., Chbouki, N., Little, B. E., King, O., Van, V., Chu, S., Gill, D., Anthes-Washburn, M. Unlu, M. S. and Goldberg, B. B. 2006. Optical Sensing of Biomolecules Using Microring Resonators. *IEEE Journal of Selected Topics In Quantum Electronics.* **12**:148-155.

Yanagase, Y., Suzuki, S., Kokubun, Y. and Sai, T. C. 2002. Box-like filter response and expansion of FSR by a vertically triple coupled microring resonator filter. *J. Lightwave Technol.* **20**:1525–1529.

Yang, L. 2008. Electrical impedance spectroscopy for detection of bacterial cells in suspensions using interdigitated microelectrodes. *Talanta* **74**:1621-1629.

Yang, L. and Bashir, R. 2008. Electrical/electrochemical impedance for rapid detection of foodborne pathogenic bacteria. *Biotechnol. Adv.* **26**:135-150.

Yang, Y. T, Callegari, C., Feng, X. L., Ekinci, K. L. and Roukes, M. L. 2006. Zeptogram-scale nanomechanical mass sensing. *Nano. Lett.* **6**:583-586.

Yang, L., Li, Y., Griffis, C. L., Johnson, M. G. 2004. Interdigitated microelectrode (IME) impedance sensor for the detection of viable *Salmonella typhimurium*. *Biosens. Bioelectron.* **19**:1139-1147.

Young, J. K., Baker, D. C. and Burney, D. P. 1995. Naturally occurring Tyzzer's disease in a puppy. *Vet. Pathol.* **32**:63-65.

Yu, X., Xu, D. and Cheng, Q. 2006. Label-free detection methods for protein microarrays. *Proteomics.* **6**:5493-503.

Zeng, K. C., Dai, L., Lin, J. Y. and Jiang, H. X. 1999. Optical resonance modes in InGaN/GaN multiple-quantum-well microring cavities. *Appl. Phys. Lett.* **75**:2563.

Zhang, J. and Ji, H. F. 2004. An anti *E. coli* O157:H7 antibody-immobilized microcantilever for the detection of *Escherichia coli* (*E. coli*). *Anal. Sci.* **20**:585-587.

Zhu, Q., Shih, W. Y. and Shih, W.-H. 2007a. Real-time, label-free, all-electrical detection of *Salmonella typhimurium* using lead titanate zirconate/gold-coated glass cantilevers at any relative humidity. *Sens. Actuators, B.* **125**:379-388.

Zhu, Q., Shih, W. Y.and Shih, W. H. 2007b. In situ, in-liquid, all-electrical detection of *Salmonella typhimurium* using lead titanate zirconate/gold-coated glass cantilevers at any dipping depth. *Biosens. Bioelectron.* **22**:3132-3138.

Zhu, H., Suter, J. D., White, I. M. and Fan, X. 2006. Aptamer Based Microsphere Biosensor for Thrombin Detection. *Sensors* **6**:795.

APPENDIX

Nucleotide Sequences and BLAST Homology Search Results for DNA Insert Sequences Generated By *Clostridium Piliforme* isolate H1 Suppression Subtractive Hybridization

DNA Insert Sequence for *C. Piliforme* Suppression Subtractive Hybridization Clone A1:

```
AGCGGCCGCCCGGGCAGGTCTCCAAGGCGGGTCCTTCGCTTTATTTTATTCTTTTTGTTT
1.......10........20........30........40........50........60

TTAATTGTTAAAGATTTGTTTTTTTGNTCGCTTGTTTGTTACCGCCCTCCGCACCACGCC
........70........80........90.......100.......110.......120

CT
..
```

Computer Output of BLAST Homology Search for Insert Sequence A1:

BLAST Basic Local Alignment Search Tool

Job Title: A1T7

Sequences producing significant alignments: (Click headers to sort columns)		Max score	Total score	Query coverage	E value	Max ident.	
AJ640141.1	Homo sapiens mRNA for ceramide kinase-like protein (CERKL gene)	53.6	53.6	63%	1e-04	76%	U G
AF000670.1	Homo sapiens elf-1 related protein (ELFR) mRNA, complete cds	50.0	50.0	58%	0.002	75%	U E G
AJ272202.1	Arabidopsis thaliana mRNA for mitochondrial half-ABC transporter (STA1 gene)	48.2	48.2	59%	0.006	75%	U E G
AJ616905.1	Glomeris marginata partial mRNA for hedgehog protein (hh gene)	46.4	46.4	20%	0.022	100%	
AB286673.1	Lethenteron japonicum LjHox10s gene for LjHox10s homeobox, parital cds	44.6	44.6	19%	0.078	100%	
AJ279849.1	Mus musculus partial mRNA for hypothetical protein, clone mvx2010	44.6	44.6	19%	0.078	100%	U E
AJ279846.1	Mus musculus partial mRNA for hypothetical protein, clone mvx2002	44.6	44.6	26%	0.078	90%	U E G
DQ204620.1	Diospyros kaki microsatellite 5 sequence	42.8	42.8	18%	0.27	100%	
DQ204619.1	Diospyros kaki microsatellite 4 sequence	42.8	42.8	21%	0.27	96%	
DQ204617.1	Diospyros kaki microsatellite 2 sequence	42.8	42.8	21%	0.27	96%	
DQ204605.1	Diospyros kaki ISSR marker 807 genomic sequence	42.8	42.8	18%	0.27	100%	
AY754861.1	Metarhizium anisopliae clone cag5 putative cell wall plasma membrane linker protein-like mRNA, partial sequence	42.8	160	21%	0.27	100%	
AF373712.1	Ovis aries clone 2G8 bone morphogenetic protein receptor-IB (BMPR-IB) mRNA, 5'UTR, partial sequence	42.8	42.8	18%	0.27	100%	U
AB095996.1	Gallus gallus Ghsr1aV mRNA for growth hormone secretagogue receptor type 1a variant, complete cds	42.8	42.8	18%	0.27	100%	U G
AB095995.1	Gallus gallus Ghsr1a mRNA for growth hormone secretagogue receptor type 1a, complete cds	42.8	42.8	18%	0.27	100%	U G
AF074706.1	Bos taurus 11-beta-hydroxysteroid dehydrogenase type 2 mRNA, complete cds	42.8	42.8	18%	0.27	100%	U E G
AF118784.1	Glycine max ribonucleotide reductase large subunit A mRNA, complete cds	42.8	42.8	18%	0.27	100%	U G
AF326687.1	Vigna radiata cysteine-rich protein mRNA, complete cds	42.8	42.8	18%	0.27	100%	
AB090165.1	Sus scrofa mRNA for receptor activity-modifying protein, complete cds	42.8	42.8	18%	0.27	100%	U G
AJ010750.1	Rattus norvegicus mRNA for Castration Induced Prostatic Apoptosis Related protein-1 (CIPAR-1)	42.8	42.8	18%	0.27	100%	U E G
AJ279852.1	Mus musculus partial mRNA for hypothetical protein, clone mvx2017	42.8	42.8	18%	0.27	100%	E
AJ279847.1	Mus musculus partial mRNA for hypothetical protein, clone mvx2005	42.8	42.8	18%	0.27	100%	U G
AJ279835.1	Mus musculus partial mRNA for hypothetical protein, clone mvx11002	42.8	42.8	18%	0.27	100%	U E G
AJ279833.1	Mus musculus partial mRNA for hypothetical protein, clone mv12x1	42.8	42.8	18%	0.27	100%	U E
AB049620.1	Halocynthia roretzi AsFCN2 mRNA for filcolin 2, complete cds	42.8	42.8	49%	0.27	76%	
AB019569.1	Homo sapiens mRNA expressed only in placental villi, clone SMAP84	42.8	42.8	18%	0.27	100%	U E G
AB019566.1	Homo sapiens mRNA expressed only in placental villi, clone SMAP67	42.8	42.8	18%	0.27	100%	U E
DQ222242.2	Lycopersicon esculentum cryptochrome 3 (Cry3) gene, complete cds	41.0	41.0	18%	0.95	100%	
DQ204616.1	Diospyros kaki microsatellite 1 sequence	41.0	41.0	18%	0.95	100%	
DQ204610.1	Diospyros kaki ISSR marker 850-2 genomic sequence	41.0	41.0	18%	0.95	100%	
DQ204609.1	Diospyros kaki ISSR marker 861 genomic sequence	41.0	41.0	20%	0.95	96%	
AF075584.1	Homo sapiens transforming growth factor alpha precursor (TGFA) gene, exon 2 and partial cds	41.0	41.0	22%	0.95	92%	G

DNA Insert Sequence for *C. Piliforme* Suppression Subtractive Hybridization Clone A2:

```
TTAGGGCGNGGNAGCTGNAGGNANGTCATCATGTNTACCATTTCGNGNANTGCTCATGTA
1.......10........20........30........40........50........60

TGGGTTGCGACGATGNGCTACTTATAACGGTNTGNNATNACAGNAACTAAAGGTGTTTGC
........70........80........90.......100.......110.......120

TTATGTCATGTGNAGGTTNATGGNNCTACCCTCAACTTCTCATGTNCTGAGATTACCTGC
.......130.......140.......150.......160.......170.......180

CCGNGCGGTCG
.......190.
```

Computer Output of BLAST Homology Search for Insert Sequence A2:

BLAST Basic Local Alignment Search Tool

Job Title: A2T7

Sequences producing significant alignments: (Click headers to sort columns)		Max score	Total score	Query coverage	E value	Max ident.
AC154551.2	Mus musculus BAC clone RP23-238B16 from chromosome 16, complete sequence	42.8	83.7	16%	0.48	92%
AC154188.2	Mus musculus BAC clone RP24-455C11 from chromosome 16, complete sequence	42.8	42.8	14%	0.48	92%
CT033776.8	Mouse DNA sequence from clone RP24-83D14 on chromosome 16, complete sequence	42.8	126	16%	0.48	92%
AL358942.6	Human DNA sequence from clone RP1-159M24 on chromosome 6 Contains a proliferation-associated 2G4, 38kD (PA2G4) pseudogene, complete sequence	41.0	41.0	14%	1.7	89%
AL844852.11	Mouse DNA sequence from clone RP23-260N23 on chromosome 2 Contains the 5' end of the Ncoa6 gene for nuclear receptor coactivator 6, a carnitine deficiency-associated gene expressed in ventricle 3 (Cdv3) pseudogene, a cytochrome c somatic (Cycs) pseudogene, the Ggtl3 gene for gamma-glutamyltransferase-like 3, the Acss2 gene for acyl-CoA synthetase short-chain family member 2, a gene (4930471I20Rik), the Gss gene for glutathione synthetase, a novel gene(0610038P03Rik), two novel genes, a novel gene (possible orthologue of human myosin heavy polypeptide 7B cardiac muscle beta (MYH7B)), the Trpc4ap gene for transient receptor potential cation channel subfamily C member 4 associated protein and three CpG islands, complete sequence	41.0	41.0	13%	1.7	92%
AC160936.2	Mus musculus BAC clone RP23-300E17 from chromosome 12, complete sequence	39.2	39.2	15%	5.9	86%
AC160561.2	Mus musculus BAC clone RP23-102D22 from chromosome 12, complete sequence	39.2	39.2	15%	5.9	86%

DNA Insert Sequence for *C. Piliforme* Suppression Subtractive Hybridization Clone A3:

```
AGGGCGTGGTGCGGAGGGCGGTAATCTGGGTTAATAAAAGATTTAAGTCTAAAGATGCGT
1.......10........20........30........40........50........60

CCATTTCTAAAATATCTTTTTCCAGATATACCTAAAAATCATAAATCTCTTGACTATATA
........70........80........90.......100.......110.......120

TCAACAAATGTTATAGCAAATATACTTGGTCTTGGTTGGGCTGCAACTCCAGCTGGTATA
.......130.......140.......150.......160.......170.......180

AAAGCTATGGAAAGTTTACAGACGCTAAATTGATAAAAAAGATGAAGCCAGTAGATCACC
.......190.......200.......210.......220.......230.......240

TGCCCGGGCGGCCGCTCGA
.......250.........
```

Computer Output of BLAST Homology Search for Insert Sequence A3:

BLAST Basic Local Alignment Search Tool

Job Title: A3

Sequences producing significant alignments: (Click headers to sort columns)		Max score	Total score	Query coverage	E value	Max ident.	
CP000679.1	Caldicellulosiruptor saccharolyticus DSM 8903, complete genome	64.4	64.4	28%	2e-07	78%	
CP000885.1	Clostridium phytofermentans ISDg, complete genome	59.0	59.0	52%	9e-06	70%	
CP001034.1	Natranaerobius thermophilus JW/NM-WN-LF, complete genome	51.8	51.8	35%	0.001	73%	
CP000383.1	Cytophaga hutchinsonii ATCC 33406, complete genome	51.8	51.8	59%	0.001	67%	
CP000685.1	Flavobacterium johnsoniae UW101, complete genome	50.0	50.0	48%	0.005	70%	
AE001437.1	Clostridium acetobutylicum ATCC 824, complete genome	50.0	50.0	32%	0.005	72%	
AJ251660.1	Girardia tigrina mRNA for homeodomain transcription factor (so gene)	48.2	48.2	10%	0.017	100%	
AF169248.2	Opsanus beta acetylglutamate-activated carbamoyl phosphate synthase III mRNA, complete cds	48.2	48.2	10%	0.017	100%	
AE016877.1	Bacillus cereus ATCC 14579, complete genome	48.2	87.3	52%	0.017	100%	
CP000962.1	Clostridium botulinum A3 str. Loch Maree, complete genome	46.4	46.4	45%	0.059	69%	
CP000853.1	Alkaliphilus oremlandii OhILAs, complete genome	46.4	46.4	28%	0.059	73%	
CP000107.1	Ehrlichia canis str. Jake, complete genome	46.4	46.4	26%	0.059	75%	
AJ279852.1	Mus musculus partial mRNA for hypothetical protein, clone mvx2017	46.4	87.3	21%	0.059	100%	E
AB019563.1	Homo sapiens mRNA expressed only in placental villi, clone SMAP42	46.4	46.4	10%	0.059	96%	
AC116358.2	Homo sapiens chromosome 5 clone RP11-679B13, complete sequence	44.6	44.6	17%	0.21	84%	
AC114283.2	Homo sapiens chromosome 5 clone CTD-2319M2, complete sequence	44.6	44.6	17%	0.21	84%	
AF403384.2	Homo sapiens LGR8 mRNA, complete cds	44.6	44.6	10%	0.21	96%	U E G
AB182645.1	Anguilla japonica eDmc1 mRNA for RecA homolog DMC1, complete cds	44.6	44.6	10%	0.21	96%	
AJ272202.1	Arabidopsis thaliana mRNA for mitochondrial half-ABC transporter (STA1 gene)	44.6	44.6	9%	0.21	100%	U E G
AJ223715.1	Squalus acanthias mRNA for sgk-1 serine-threonine protein kinase	44.6	44.6	9%	0.21	100%	
BA000028.3	Oceanobacillus iheyensis HTE831 DNA, complete genome	44.6	44.6	44%	0.21	68%	
AC126345.11	Homo sapiens chromosome 11, clone RP11-100E23, complete sequence	44.6	44.6	12%	0.21	91%	
AC092915.7	Homo sapiens 3 BAC RP11-585P20 (Roswell Park Cancer Institute Human BAC Library) complete sequence	44.6	44.6	13%	0.21	88%	
AF133675.1	Populus tremula x Populus tremuloides retinoblastoma-related protein 1 (RB1) mRNA, complete cds	44.6	44.6	9%	0.21	100%	U
AJ276466.1	Klebsiella pneumoniae contig region pSL004	44.6	44.6	12%	0.21	90%	
AB088073.1	Oryza barthii DNA, retroposon p-SINE1-r607, repeat sequence	44.6	44.6	11%	0.21	93%	
AF133731.2	Rattus norvegicus 11-zinc finger protein (CTCF) mRNA, complete cds	44.6	44.6	9%	0.21	100%	U E G
AJ279849.1	Mus musculus partial mRNA for hypothetical protein, clone mvx2010	44.6	85.5	17%	0.21	100%	U E
AB019569.1	Homo sapiens mRNA expressed only in placental villi, clone SMAP84	44.6	85.5	21%	0.21	100%	U E G
CP001078.1	Clostridium botulinum E3 str. Alaska E43, complete genome	42.8	42.8	25%	0.72	74%	
CP001056.1	Clostridium botulinum B str. Eklund 17B, complete genome	42.8	42.8	25%	0.72	74%	
CP000939.1	Clostridium botulinum B1 str. Okra, complete genome	42.8	42.8	29%	0.72	72%	
CU442713.16	Pig DNA sequence from clone CH242-405H5 on chromosome 3, complete sequence	42.8	42.8	11%	0.72	93%	
EF648567.1	Riftia pachyptila clone TRbwC21 ubiquinol cytochrome reductase mRNA, partial cds	42.8	42.8	8%	0.72	100%	
CP000820.1	Frankia sp. EAN1pec, complete genome	42.8	42.8	12%	0.72	87%	
CP000728.1	Clostridium botulinum F str. Langeland, complete genome	42.8	42.8	28%	0.72	72%	

DNA Insert Sequence for *C. Piliforme* Suppression Subtractive Hybridization Clone B3:

```
TGTAGCGTGAAGACGACAGAAGCCCTATAGTGAGTCGTATTACACCTGCCCGGGCGGCCG
1.......10........20........30........40........50........60

CTCGA
.....
```

Computer Output of BLAST Homology Search for Insert Sequence B3:

BLAST Basic Local Alignment Search Tool

Job Title: B3T7

Sequences producing significant alignments: (Click headers to sort columns)		Max score	Total score	Query coverage	E value	Max ident.	
AJ306902.1	Ricinus communis mRNA for iron transport protein 2 (ipt2 gene)	53.6	94.5	69%	6e-05	100%	
DQ423779.1	Kryptolebias marmoratus Rhesus glycoprotein (RhCG2) mRNA, complete cds	46.4	46.4	38%	0.009	100%	
AB182999.1	Danio rerio mRNA for RecA homolog Dmc1, complete cds	46.4	87.3	69%	0.009	100%	U G
AB091786.1	Lemur catta AMELY gene for amelogenin, partial cds	46.4	46.4	52%	0.009	91%	
AJ289605.1	Mus musculus partial Lancl1 gene for LanC-like protein 1, exon 4	46.4	46.4	52%	0.009	91%	G
AP006628.2	Onion yellows phytoplasma OY-M DNA, complete genome	44.6	126	36%	0.030	100%	
AY961924.2	Picea abies dehydrin 1 (Dhn) mRNA, complete cds	44.6	44.6	41%	0.030	96%	
AM712630.1	Ostertagia ostertagi mRNA for activation associated secreted protein (al2 gene)	44.6	44.6	36%	0.030	100%	
AB181949.1	Glycine max GmChl 3 gene for Chlorophyllase 3, complete cds	44.6	44.6	36%	0.030	100%	
AB181947.1	Glycine max GmChl 1 gene for Chlorophyllase 1, complete cds	44.6	44.6	36%	0.030	100%	
AY737284.1	Yeast TAP expression vector pYL435, complete sequence	44.6	44.6	41%	0.030	96%	
AY428072.1	Expression vector pYES263 complete sequence	44.6	44.6	41%	0.030	96%	
AY428071.1	Expression vector pYES260 complete sequence	44.6	44.6	41%	0.030	96%	
AF258578.2	Homo sapiens PP4519 mRNA, complete cds	44.6	87.3	67%	0.030	100%	E G
D50399.1	Unidentified cloning vector Phagemid pFABC DNA for murine immunoglobulin gammal chain CH1 domain	44.6	44.6	36%	0.030	100%	
AF106913.1	Homo sapiens CRL3 protein (CRL3) mRNA, complete cds	44.6	44.6	36%	0.030	100%	U E G
AB032017.1	Homo sapiens mRNA for KPG_003 protein, complete cds	44.6	85.5	69%	0.030	100%	U G
Y12236.1	D.rerio mRNA for Cu/Zn-superoxide dismutase	44.6	44.6	36%	0.030	100%	U E G
AJ310908.1	Fucus vesiculosus mRNA for ALA dehydratase (hemB gene)	44.6	85.5	70%	0.030	100%	
AJ277562.1	Lycopersicon esculentum partial mRNA for cyclophilin-like protein (pi2 gene)	44.6	44.6	36%	0.030	100%	U G
AJ277560.1	Lycopersicon esculentum partial mRNA for putative asparaginyl-tRNA synthetase (ats1 gene)	44.6	87.3	38%	0.030	100%	U G
AY822457.1	Yeast expression vector pJG518 chloramphenicol resistance protein (CmR) and CcdB (ccdB) genes, complete cds	44.6	44.6	41%	0.030	96%	
AY822456.1	Yeast expression vector pJG516 chloramphenicol resistance protein (CmR) and CcdB (ccdB) genes, complete cds	44.6	44.6	41%	0.030	96%	
AY822455.1	Yeast expression vector pJG484 chloramphenicol resistance protein (CmR) and CcdB (ccdB) genes, complete cds	44.6	44.6	41%	0.030	96%	
AY822454.1	Yeast expression vector pJG485 chloramphenicol resistance protein (CmR) and CcdB (ccdB) genes, complete cds	44.6	44.6	41%	0.030	96%	
AK188447.1	Mus musculus cDNA, clone:Y0G0145D23, strand:minus, reference:ENSEMBL:Mouse-Transcript-ENST:ENSMUST00000066401, based on BLAT search	44.6	44.6	36%	0.030	100%	
AK182294.1	Mus musculus cDNA, clone:Y0G0121H22, strand:plus, reference:ENSEMBL:Mouse-Transcript-ENST:ENSMUST00000070905, based on BLAT search	44.6	44.6	60%	0.030	87%	U
AK177326.1	Mus musculus cDNA, clone:Y0G0102G07, strand:minus, reference:ENSEMBL:Mouse-Transcript-ENST:ENSMUST00000026262, based on BLAT search	44.6	44.6	36%	0.030	100%	U
AB098525.1	Petunia x hybrida mRNA for PHCLF3, complete cds	44.6	85.5	69%	0.030	100%	
AF133675.1	Populus tremula x Populus tremuloides retinoblastoma-related protein 1 (RB1) mRNA, complete cds	44.6	44.6	41%	0.030	96%	U
AJ276066.1	Rattus norvegicus mRNA for putative GDP-L-fucose pyrophosphorylase	44.6	44.6	36%	0.030	100%	U E G
AJ277561.1	Lycopersicon esculentum partial mRNA for putative glutamine synthase (gts1 gene)	44.6	87.3	38%	0.030	100%	U E G
AJ277558.1	Lycopersicon esculentum partial mRNA for CGI-144 like protein (cgi1 gene)	44.6	44.6	36%	0.030	100%	U G
D50400.1	Unidentified cloning vector Phagemid pLINK DNA for flexible peptide used as scFv linker	44.6	44.6	36%	0.030	100%	
D50401.1	Unidentified cloning vector Phagemid pPDS DNA for fusion protein of murine immunoglobulin kappa chain constant region and the carboxy-terminal half of coat protein III of M13mp18	44.6	44.6	36%	0.030	100%	
AJ251833.1	Homo sapiens mRNA for hypothetical protein (ORF1 DNA)	44.6	44.6	36%	0.030	100%	U G
AB091179.1	Botryotinia fuckeliana BMR5 gene for ABC-transporter, complete cds	44.6	44.6	41%	0.030	96%	

DNA Insert Sequence for *C. Piliforme* Suppression Subtractive Hybridization Clone C5:

```
GCGCTGGTGCCGTGGCTCGNACCTGCGCCGGTGCGGTCGGGGCGCTACCGCCCGNTGTTC
1.......10........20........30........40........50........60

AAGNATCTACTTGCTGGCTGCTCGCGGCGGACTTCGTGATCCTGACCTGGGTCGGCGCCC
........70........80........90.......100.......110.......120

AGCAGACCACCTTCNCCTACGACTGGATCTCGCTCATCGCATCGGCCTACTGGTTCGCCT
.......130.......140.......150.......160.......170.......180

ACTTCCTGGTGATCCTGCCGATCCTCGGCGCGATCGAGAAGCCGGTGGCTCCGCCCGCGA
.......190.......200.......210.......220.......230.......240

CCCATCGAAGAAGACTTTCAACGCCCCACTACTCGCCGGCGACCCGGNGGCACGAAAACG
.......250.......260.......270.......280.......290.......300

GNTCGTGGCAGNAGTTATCTAAGAGGAGCATGGCGACCGTTCGGGGCCCCANTTTCGGCC
.......310.......320.......330.......340.......350.......360

CCTNTNGGGAGGNCGANTTTNCAATTTCNACTGGGCCGNNNGNTTTTAACAAACGN
.......370.......380.......390.......400.......410......
```

Computer Output of BLAST Homology Search for Insert Sequence C5:

BLAST Basic Local Alignment Search Tool

Job Title: C5T7

Sequences producing significant alignments: (Click headers to sort columns)

		Max score	Total score	Query coverage	E value	Max ident.
CP000143.1	Rhodobacter sphaeroides 2.4.1 chromosome 1, complete sequence	479	479	74%	5e-132	95%
X56157.1	R. sphaeroides fbc operon for cytochrome bc1 complex reductase (EC 1.10.2.2)	479	479	74%	5e-132	95%
CP000577.1	Rhodobacter sphaeroides ATCC 17029 chromosome 1, complete sequence	470	512	74%	3e-129	95%
CP000661.1	Rhodobacter sphaeroides ATCC 17025, complete genome	363	363	74%	3e-97	87%
CP000830.1	Dinoroseobacter shibae DFL 12, complete genome	169	169	63%	1e-38	75%
X05630.1	Rhodopseudomonas capsulata petABC operon	161	161	54%	2e-36	76%
X03476.1	Rhodopseudomonas sphaeroides fbc operon (fbcF, fbcB, fbcC genes)	161	161	54%	2e-36	76%
CP000031.1	Silicibacter pomeroyi DSS-3, complete genome	136	136	65%	7e-29	71%
CP000264.1	Jannaschia sp. CCS1, complete genome	131	131	62%	3e-27	72%
CP000489.1	Paracoccus denitrificans PD1222 chromosome 1, complete sequence	125	125	63%	1e-25	71%
X05799.1	P. denitrificans bc1 gene for cytochrome bc1 complex (EC 1.10.2.2)	125	125	63%	1e-25	71%
M17522.1	P.denitrificans bc1 operon genes encoding three subunits (FeS, b and c1) of the cytochrome bc1 complex, complete cds	125	125	63%	1e-25	71%
CP000377.1	Silicibacter sp. TM1040, complete genome	120	120	30%	5e-24	83%
AP007255.1	Magnetospirillum magneticum AMB-1 DNA, complete genome	80.6	80.6	17%	5e-12	83%
CP000362.1	Roseobacter denitrificans OCh 114, complete genome	73.4	73.4	60%	7e-10	67%
AL591788.1	Sinorhizobium meliloti 1021 complete chromosome; segment 7/12	69.8	69.8	52%	8e-09	68%
BA000012.4	Mesorhizobium loti MAFF303099 DNA, complete genome	60.8	60.8	53%	4e-06	66%
AE005673.1	Caulobacter crescentus CB15, complete genome	57.2	57.2	12%	5e-05	83%
CP000699.1	Sphingomonas wittichii RW1, complete genome	55.4	55.4	47%	2e-04	67%
CP000115.1	Nitrobacter winogradskyi Nb 255, complete genome	53.6	53.6	14%	6e 04	80%
CP000463.1	Rhodopseudomonas palustris BisA53, complete genome	50.0	50.0	46%	0.008	67%
CP000248.1	Novosphingobium aromaticivorans DSM 12444, complete genome	50.0	50.0	52%	0.008	66%
AF109172.1	Rhizobium galegae ubiquinol-cytochrome c reductase iron-sulfur subunit (fbcF), ubiquinol-cytochrome c reductase cytochrome b subunit (fbcB), cytochrome c1 (fbcC), and adenine phosphoribosyltransferase (aprt) genes, complete cds	50.0	50.0	13%	0.008	78%
CP000440.1	Burkholderia ambifaria AMMD chromosome 1, complete sequence	48.2	48.2	9%	0.027	87%
CP000157.1	Erythrobacter litoralis HTCC2594, complete genome	48.2	48.2	13%	0.027	78%
CP000301.1	Rhodopseudomonas palustris BisB18, complete genome	46.4	46.4	14%	0.096	80%
AP008229.1	Xanthomonas oryzae pv. oryzae MAFF 311018 DNA, complete genome	46.4	46.4	11%	0.096	82%
CP000086.1	Burkholderia thailandensis E264 chromosome I, complete sequence	46.4	46.4	8%	0.096	88%
AE013598.1	Xanthomonas oryzae pv. oryzae KACC10331, complete genome	46.4	46.4	11%	0.096	82%
CP000868.1	Burkholderia multivorans ATCC 17616 chromosome 1, complete sequence	44.6	44.6	10%	0.33	83%
CP000458.1	Burkholderia cenocepacia HI2424 chromosome 1, complete sequence	44.6	85.5	22%	0.33	84%
CP000378.1	Burkholderia cenocepacia AU 1054 chromosome 1, complete sequence	44.6	85.5	22%	0.33	84%
CP000076.1	Pseudomonas fluorescens Pf-5, complete genome	44.6	44.6	8%	0.33	88%
CP000908.1	Methylobacterium extorquens PA1, complete genome	42.8	42.8	9%	1.2	82%
CP000494.1	Bradyrhizobium sp. BTAi1, complete genome	42.8	42.8	12%	1.2	78%
CU234118.1	Bradyrhizobium sp. ORS278,complete sequence	42.8	42.8	12%	1.2	80%
CP000572.1	Burkholderia pseudomallei 1106a chromosome I, complete sequence	42.8	42.8	8%	1.2	86%
CP000556.1	Methylibium petroleiphilum PM1 plasmid RPME01, complete sequence	42.8	42.8	10%	1.2	83%

DNA Insert Sequence for *C. Piliforme* Suppression Subtractive Hybridization Clone C7:

```
GAGGGCCGCCCGGGCAGGTACCTGCCTGTAATACGACTCACTATAGGGCTCGACCGCCCT
1.......10........20........30........40........50........60

CCGCACCACGCCCT
........70....
```

Computer Output of BLAST Homology Search for Insert Sequence C7:

BLAST Basic Local Alignment Search Tool

Job Title: C7T7

Sequences producing significant alignments: (Click headers to sort columns)		Max score	Total score	Query coverage	E value	Max ident.	
AB094665.1	Seriola quinqueradiata YGHL1 gene for putative growth hormone like protein-1, complete cds	57.2	57.2	60%	6e-06	89%	
AB112919.1	Cucumis sativus sdhB mRNA for succinate dehydrogenase iron-sulfur protein subunit, partial cds	55.4	55.4	47%	2e-05	94%	
AB067639.1	Daucus carota Dc2ox1 mRNA for gibberellin 2-oxidase1, complete cds	50.0	50.0	40%	9e-04	96%	
Y10472.1	N.tabacum mRNA for ornithine decarboxylase	50.0	50.0	47%	9e-04	91%	U
AF092132.1	Homo sapiens PAK2 mRNA, complete cds	50.0	50.0	40%	9e-04	96%	U E
AF019411.1	Charybdis feriatus Mn-superoxide dismutase mRNA, complete cds	50.0	50.0	40%	9e-04	96%	
AF039201.1	Pinus caribaea germin-like protein (PcGER1) mRNA, complete cds	50.0	50.0	47%	9e-04	91%	
AB264540.1	Phalacrocorax carbo arnt 2 mRNA for aryl hydrocarbon receptor nuclear translocator 2, complete cds	48.2	48.2	45%	0.003	91%	
AB284983.1	Bombyx mori bmST1 mRNA for sulfotransferase, complete cds	48.2	48.2	45%	0.003	91%	U G
AF034643.3	Haematobia irritans irritans putative cdc2-related kinase (CDRK) mRNA, partial cds	48.2	48.2	45%	0.003	91%	
Z86091.1	Fragaria x ananassa mRNA for TCTP protein	48.2	48.2	41%	0.003	93%	
AB182999.1	Danio rerio mRNA for RecA homolog Dmc1, complete cds	48.2	48.2	45%	0.003	91%	U G
AB182645.1	Anguilla japonica eDmc1 mRNA for RecA homolog DMC1, complete cds	48.2	48.2	45%	0.003	91%	
AB057371.1	Daucus carota CSCP mRNA for cysteine proteinase, partial cds	48.2	48.2	45%	0.003	91%	
AB070845.1	Aspergillus oryzae metR gene for positive-acting master sulfur regulatory, complete cds	48.2	85.5	50%	0.003	95%	
AB032017.1	Homo sapiens mRNA for KPG_003 protein, complete cds	48.2	48.2	45%	0.003	91%	U G
AJ272202.1	Arabidopsis thaliana mRNA for mitochondrial half-ABC transporter (STA1 gene)	48.2	48.2	45%	0.003	91%	U E G
AJ223716.1	Squalus acanthias mRNA for sgk-2 serine-threonine protein kinase	48.2	48.2	45%	0.003	91%	
AJ223715.1	Squalus acanthias mRNA for sgk-1 serine-threonine protein kinase	48.2	48.2	45%	0.003	91%	
AJ009799.1	Gallus gallus mRNA for ABC transporter protein	48.2	48.2	45%	0.003	91%	U G
AJ004937.1	Phascolion strombi mRNA for cytoplasmic intermediate filament protein	48.2	48.2	45%	0.003	91%	
AF050198.1	Homo sapiens putative mitochondrial space protein 32.1 mRNA, nuclear gene encoding mitochondrial protein, complete cds	48.2	48.2	45%	0.003	91%	U E G
AF139835.1	Populus tremula x Populus tremuloides F-box containing protein TIR1 (TIR1) mRNA, complete cds	48.2	48.2	45%	0.003	91%	U
AB121211.1	Marsupenaeus japonicus mjTSPc mRNA for thrombospondin, complete cds	48.2	48.2	45%	0.003	91%	
AB121210.1	Marsupenaeus japonicus mjTSPb mRNA for thrombospondin, complete cds	48.2	48.2	45%	0.003	91%	
AB121209.1	Marsupenaeus japonicus mjTSPa mRNA for thrombospondin, complete cds	48.2	48.2	45%	0.003	91%	
AB098525.1	Petunia x hybrida mRNA for PHCLF3, complete cds	48.2	48.2	45%	0.003	91%	
AF072534.1	Capsicum annuum pepper MADS-box protein (PepMADS) mRNA, complete cds	48.2	48.2	45%	0.003	91%	
Z93765.1	M.domestica mRNA for lignostilbene dioxygenase-like protein	48.2	48.2	45%	0.003	91%	U
L77146.1	Danio rerio heat shock cognate (hsc70) mRNA, complete cds	48.2	48.2	45%	0.003	91%	U E G
AJ293852.1	Klebsiella pneumoniae partial EVGS gene for putative sensor protein EVGS precursor, contig region pSL026	48.2	48.2	39%	0.003	96%	
AJ306902.1	Ricinus communis mRNA for iron transport protein 2 (ipt2 gene)	48.2	48.2	45%	0.003	91%	
AF026274.1	Mus musculus Sumiko (sumiko) mRNA, complete cds	48.2	48.2	45%	0.003	91%	U E G

DNA Insert Sequence for *C. Piliforme* Suppression Subtractive Hybridization Clone D2:

```
AGGGCGTGGTGCGGAGGACGGTGATCTGCATCTGCTAAATGGACTATACTTGCACCAGTA
1.......10........20........30........40........50........60

TTTATACCTATGTTTATGAAACTTGGTTATTCACCAGAGCTTACACAGGTTGCATATCGT
........70........80........90.......100.......110.......120

ATAGGTGACTACCTGCCCGGGCGGCCGCTCGA
.......130.......140.......150..
```

Computer Output of BLAST Homology Search for Insert Sequence D2:

BLAST Basic Local Alignment Search Tool

Job Title: D2T7

Sequences producing significant alignments: (Click headers to sort columns)		Max score	Total score	Query coverage	E value	Max ident.	
AM180355.1	Clostridium difficile 630 complete genome	86.0	86.0	67%	3e-14	78%	
CP000853.1	Alkaliphilus oremlandii OhILAs, complete genome	84.2	84.2	68%	1e-13	77%	
AE015927.1	Clostridium tetani E88, complete genome	84.2	137	73%	1e-13	89%	
BA000028.3	Oceanobacillus iheyensis HTE831 DNA, complete genome	73.4	73.4	65%	2e-10	76%	
CP000724.1	Alkaliphilus metalliredigens QYMF, complete genome	71.6	121	68%	7e-10	75%	
CR954246.1	Pseudoalteromonas haloplanktis str. TAC125 chromosome I, complete sequence	50.0	50.0	46%	0.002	75%	
Y10552.1	H.sapiens mRNA for calpain-like protease	48.2	48.2	19%	0.009	96%	U G
CR378665.1	Photobacterium profundum SS9; segment 3/12	48.2	48.2	68%	0.009	70%	
CT029336.1	Poplar cDNA sequences	46.4	46.4	21%	0.030	90%	
CT029125.1	Poplar cDNA sequences	46.4	46.4	21%	0.030	90%	
CT028739.1	Poplar cDNA sequences	46.4	46.4	21%	0.030	90%	
CT028316.1	Poplar cDNA sequences	46.4	46.4	21%	0.030	90%	
DQ459385.1	Nicotiana tabacum serine/threonine kinase mRNA, partial cds	46.4	46.4	19%	0.030	93%	U
NM_001097447.1	Sus scrofa retinoid x receptor interacting protein (RAP80), mRNA >dbj|AB248750.1| Sus scrofa RAP80 mRNA for retinoid x receptor interacting protein, complete cds	44.6	44.6	15%	0.10	100%	U G
AJ009799.1	Gallus gallus mRNA for ABC transporter protein	44.6	44.6	15%	0.10	100%	U G
AF139835.1	Populus tremula x Populus tremuloides F-box containing protein TIR1 (TIR1) mRNA, complete cds	44.6	44.6	17%	0.10	96%	U
AJ293760.1	Agaricus bisporus mRNA for putative beta glucosidase (bg1 gene), strain D649	44.6	44.6	15%	0.10	100%	
AF005654.1	Homo sapiens actin-binding double-zinc-finger protein (abLIM) mRNA, complete cds	44.6	44.6	17%	0.10	96%	U E G
AB013101.1	Solanum lycopersicum LE-ACO4 mRNA for 1-aminocyclopropane-1-carboxylate oxidase, complete cds	44.6	44.6	15%	0.10	100%	U G
D78130.1	Homo sapiens mRNA for squalene epoxidase, complete cds	44.6	44.6	22%	0.10	91%	U E G
AB072357.1	Homo sapiens mRNA for hSSH-1B, complete cds	44.6	44.6	15%	0.10	100%	U E G
EF648525.1	Riftia pachyptila clone BWbrC20 hypothetical protein bw5 mRNA sequence	42.8	42.8	15%	0.36	100%	
EU022152.1	Montipora capitata clone DCMU1L5 unknown mRNA	42.8	42.8	17%	0.36	96%	
AB296066.1	Rousettus leschenaulti FcRn mRNA for neonatal Fc recepter, complete cds	42.8	42.8	15%	0.36	100%	
AM231542.1	Photorhabdus asymbiotica subsp. asymbiotica partial sopB for inositol phosphate phosphatase, clone 214	42.8	42.8	15%	0.36	100%	
AM748509.1	Vigna unguiculata partial mRNA for putative single-stranded nucleic acid binding R3H (MtrDRAFT_AC183371g11v1 gene), clone 54	42.8	42.8	15%	0.36	100%	
AM748484.1	Vigna unguiculata partial mRNA for putative ATP synthase CF1 epsilon subunit (atpE gene), clone 29	42.8	42.8	15%	0.36	100%	
AM748466.1	Vigna unguiculata partial mRNA for putative single-stranded nucleic acid binding R3H (MtrDRAFT_AC183371g11v1 gene), clone 11	42.8	42.8	15%	0.36	100%	
AM748416.1	Vigna unguiculata partial mRNA for putative proton-dependent oligopeptide transport (POT) family protein (AT3G54140 gene), clone 30	42.8	42.8	15%	0.36	100%	
AM748403.1	Vigna unguiculata partial mRNA for putative rubisco activase (Rca gene), clone 17	42.8	42.8	15%	0.36	100%	
AB307741.1	Antheraea yamamai vdp mRNA for vitellin-degrading protease, partial cds	42.8	42.8	15%	0.36	100%	
AM706434.1	Eristalis tenax mRNA for hypothetical protein (ORF1), isolate 26	42.8	42.8	15%	0.36	100%	
AM706411.1	Eristalis tenax partial mRNA for hypothetical protein	42.8	42.8	15%	0.36	100%	

DNA Insert Sequence for *C. Piliforme* Suppression Subtractive Hybridization Clone D6:

```
AGGGCGTGGTGCGGAGGGCGGTGATCATGTAGACCATTTCAGGAAATCTTAGGTATGGGT
1.......10........20........30........40........50........60

TGAGAGAGAAGATGTCCTACTTATAAGGCTGGTATTACAGAAACTAAAGCTGCTTGCTTA
........70........80........90.......100.......110.......120

TGTCATTGGAGGTTCATGAAACTACCTCAACTCTCATGTACTGAGATTACCTGCCCGGGC
.......130.......140.......150.......160.......170.......180

GGCCGCTCGA
.......190
```

Computer Output of BLAST Homology Search for Insert Sequence D6:

BLAST Basic Local Alignment Search Tool

Job Title: D6T7

Sequences producing significant alignments: (Click headers to sort columns)		Max score	Total score	Query coverage	E value	Max ident.	
AF133093.2	Mus musculus chromosome X clones CT7-116D19, CT7-309B4, CT7-567G9, MGSPI-15528, MGSPI-15530 complete sequence	149	209	74%	4e-33	89%	E
AL672094.11	Mouse DNA sequence from clone RP23-373N8 on chromosome X Contains the 3' end of the Abcd1 gene for ATP-binding cassette, sub-family D, member 1, the Plxnb3 gene for plexin B3, the Stk23 gene for serine/threonine kinase 23, the Idh3g gene for isocitrate dehydrogenase 3 NAD+, gamma, the Ssr4 gene for signal sequence receptor, delta, the Pdzd4 gene for PDZ domain containing 4, a novel gene, the L1cam gene for L1 cell adhesion molecule and two CpG islands, complete sequence	149	209	74%	4e-33	89%	
CT028193.1	Poplar cDNA sequences	48.2	48.2	16%	0.011	93%	
AF403384.2	Homo sapiens LGR8 mRNA, complete cds	48.2	48.2	20%	0.011	87%	U E G
AB182645.1	Anguilla japonica eDmc1 mRNA for RecA homolog DMC1, complete cds	46.4	46.4	15%	0.039	93%	
AJ010090.1	Arabidopsis thaliana mRNA for MAP3K alpha protein kinase	46.4	46.4	15%	0.039	96%	U
AF095771.1	Homo sapiens PTH-responsive osteosarcoma B1 protein (B1) mRNA, complete cds	46.4	46.4	13%	0.039	100%	U E G
U58918.1	Arabidopsis thaliana MEK kinase (MAP3Ka) mRNA, complete cds	46.4	46.4	15%	0.039	96%	U E G
AM422099.2	Danio rerio tf2a mRNA, 3'UTR	44.6	44.6	15%	0.14	93%	U G
AM422096.1	Danio rerio partial mRNA for retinol dehydrogenase 10 (rdh10 gene)	44.6	44.6	14%	0.14	96%	U G
AM422870.1	Fagopyrum esculentum gFeAP9 gene for aspartic proteinase, exons 1-13	44.6	44.6	12%	0.14	100%	
AB264540.1	Phalacrocorax carbo arnt 2 mRNA for aryl hydrocarbon receptor nuclear translocator 2, complete cds	44.6	44.6	12%	0.14	100%	
AB266320.1	Musa acuminata AAA Group MA-EIL3 mRNA for ethylene signal transcription factor, complete cds	44.6	44.6	12%	0.14	100%	
CT028404.1	Poplar cDNA sequences	44.6	44.6	16%	0.14	90%	
AB194775.1	Solanum lycopersicum AUREA gene for phytochromobilin synthase, complete cds	44.6	44.6	12%	0.14	100%	G
Y11312.1	H.sapiens mRNA for phosphoinositide 3-kinase	44.6	44.6	12%	0.14	100%	U E G
AF107491.1	Hexamita sp. carbamate kinase (CBK) gene, complete cds	44.6	44.6	12%	0.14	100%	
AF483014.2	Boltenia villosa muscle actin mRNA, partial cds	44.6	44.6	15%	0.14	93%	
AJ276466.1	Klebsiella pneumoniae contig region pSL004	44.6	44.6	14%	0.14	96%	
AF002248.2	Pisum sativum PSI light-harvesting antenna chlorophyll a/b-binding protein (lhcA-P4) mRNA, complete cds	44.6	44.6	12%	0.14	100%	
AF118559.1	Avena fatua puroindoline precursor, mRNA, complete cds	44.6	44.6	12%	0.14	100%	
AF061027.1	Vernicia fordii omega-3 fatty acid desaturase precursor, mRNA, partial cds	44.6	44.6	12%	0.14	100%	
AJ535757.1	Bactrocera oleae ovoB gene for zinc finger transcription factor	44.6	44.6	12%	0.14	100%	
AJ535756.1	Bactrocera oleae ovoA gene for zinc finger transcription factor	44.6	44.6	12%	0.14	100%	
AJ293391.1	Homo sapiens mRNA differentially expressed in malignant melanoma, clone MM J9	44.6	44.6	14%	0.14	96%	U
AJ293390.1	Homo sapiens mRNA, differentially expressed in malignant melanoma, clone MM A2	44.6	44.6	14%	0.14	96%	U E
EF648525.1	Riftia pachyptila clone BWbrC20 hypothetical protein bw5 mRNA sequence	42.8	42.8	12%	0.48	100%	
EU022152.1	Montipora capitata clone DCMU1L5 unknown mRNA	42.8	42.8	13%	0.48	96%	
AB296066.1	Rousettus leschenaulti FcRn mRNA for neonatal Fc recepter, complete cds	42.8	42.8	12%	0.48	100%	
D89732.1	Cucumis sativus mRNA for 1-aminocyclopropane-1-carboxylate	42.8	83.7	15%	0.48	100%	

DNA Insert Sequence for *C. Piliforme* Suppression Subtractive Hybridization Clone D7:

```
TCGAGCGGCCGCCCGGGCAGGTCTCCAAGGCGGGTCCTTCGCTTTATTTTATTCTTTTTG
1.......10........20........30........40........50........60

TTTTTAATTGNTAAAGATTTGTTTTTTTGTTCGTTTGTTTGCTACCGTCCTCCGCACCAC
........70........80........90.......100.......110.......120

GCCCT
.....
```

Computer Output of BLAST Homology Search for Insert Sequence D7:

BLAST Basic Local Alignment Search Tool

Job Title: D7T7

Sequences producing significant alignments: (Click headers to sort columns)

		Max score	Total score	Query coverage	E value	Max ident.	
AJ640141.1	Homo sapiens mRNA for ceramide kinase-like protein (CERKL gene)	59.0	59.0	73%	4e-06	75%	UG
AF000670.1	Homo sapiens elf-1 related protein (ELFR) mRNA, complete cds	57.2	57.2	59%	1e-05	76%	UEG
AJ616905.1	Glomeris marginata partial mRNA for hedgehog protein (hh gene)	51.8	51.8	22%	5e-04	100%	
AB286673.1	Lethenteron japonicum LjHox10s gene for LjHox10s homeobox, parital cds	50.0	50.0	21%	0.002	100%	
AJ272202.1	Arabidopsis thaliana mRNA for mitochondrial half-ABC transporter (STA1 gene)	50.0	50.0	60%	0.002	75%	UEG
AB095996.1	Gallus gallus Ghsr1aV mRNA for growth hormone secretagogue receptor type 1a variant, complete cds	48.2	48.2	20%	0.007	100%	UG
AB095995.1	Gallus gallus Ghsr1a mRNA for growth hormone secretagogue receptor type 1a, complete cds	48.2	48.2	20%	0.007	100%	UG
AF074706.1	Bos taurus 11-beta-hydroxysteroid dehydrogenase type 2 mRNA, complete cds	48.2	48.2	20%	0.007	100%	UEG
AF118784.1	Glycine max ribonucleotide reductase large subunit A mRNA, complete cds	48.2	48.2	20%	0.007	100%	UG
AB090165.1	Sus scrofa mRNA for receptor activity-modifying protein, complete cds	48.2	48.2	20%	0.007	100%	UG
AJ010750.1	Rattus norvegicus mRNA for Castration Induced Prostatic Apoptosis Related protein-1 (CIPAR-1)	48.2	48.2	20%	0.007	100%	UEG
AB049620.1	Halocynthia roretzi AsFCN2 mRNA for filcolin 2, complete cds	48.2	48.2	52%	0.007	76%	
DQ222242.2	Lycopersicon esculentum cryptochrome 3 (Cry3) gene, complete cds	46.4	46.4	20%	0.023	100%	
AF075584.1	Homo sapiens transforming growth factor alpha precursor (TGFA) gene, exon 2 and partial cds	46.4	46.4	24%	0.023	93%	G
AF093414.1	Saguinus oedipus estrogen response element binding protein mRNA, complete cds	46.4	46.4	53%	0.023	74%	
AF093139.1	Rattus norvegicus tip associating protein (TAP) mRNA, complete cds	46.4	46.4	25%	0.023	93%	UEG
AF079314.1	Rattus norvegicus nuclear factor kappa B subunit p65 (NFkB) mRNA, partial cds	46.4	46.4	20%	0.023	100%	UEG
AB000814.1	Homo sapiens mRNA for BMAL1f, partial cds	46.4	46.4	54%	0.023	75%	UEG
AB266595.1	Plutella xylostella PxSP1 mRNA for methionine-rich storage protien 1, complete cds	44.6	44.6	21%	0.080	96%	
AB265796.1	Pyrus x bretschneideri PbACS3 mRNA for 1-aminocyclopropane-1-carboxylate synthase, complete cds	44.6	44.6	19%	0.080	100%	
X96789.2	Sporosarcina sp. genes for Sse9I restriction-modification system	44.6	44.6	19%	0.080	100%	
AY273895.1	Brugia malayi transglutaminase mRNA, partial cds	44.6	44.6	19%	0.080	100%	
AB240529.1	Eublepharis macularius ERb mRNA for estrogen receptor beta, complete cds	44.6	44.6	19%	0.080	100%	
AJ238855.1	Rattus norvegicus mRNA for type A/B hnRNP protein p38	44.6	44.6	19%	0.080	100%	UG
AJ238854.1	Rattus norvegicus mRNA for type A/B hnRNP protein p40	44.6	44.6	19%	0.080	100%	UEG
AF039086.1	Pseudomicrothorax dubius articulin 1 mRNA, complete cds	44.6	44.6	19%	0.080	100%	
AB032017.1	Homo sapiens mRNA for KPG_003 protein, complete cds	44.6	44.6	29%	0.080	86%	UG
AJ252088.1	Solanum dulcamara mRNA for gibberellin 20-oxidase (ga20ox1 gene)	44.6	87.3	52%	0.080	100%	
AJ223716.1	Squalus acanthias mRNA for sgk-2 serine-threonine protein kinase	44.6	44.6	19%	0.080	100%	
AB066448.1	Closterium ehrenbergii scdip-1 mRNA for sexual cell division-inducing pheromone, complete cds	44.6	44.6	19%	0.080	100%	
AF026274.1		44.6	44.6	52%	0.080	76%	

DNA Insert Sequence for *C. Piliforme* Suppression Subtractive Hybridization Clone E1:

```
TCGAGCGGCCGCCCGGGCAGGTGATCAACCCTTAAAAACCAGCCATATTCTGCATCTGCA
1.......10........20........30........40........50........60

ACAACAAGTTTATTGCTACCATTTTGTATAGAATGGTGTGCAAGTGCCATGTCATCTGTA
........70........80........90.......100.......110.......120

ATAGGATTTAAGTCACAACCTATCTGCCATTCTAAGAAGAGTTTCTCCACCTGTTGTAAT
.......130.......140.......150.......160.......170.......180

ATTGGTTCCTAAAAGAAGCTTACCATCTTCCTGTCTATGAAATGATTACCGCCCTCCGCA
.......190.......200.......210.......220.......230.......240

CCACGCC
.......
```

Computer Output of BLAST Homology Search for Insert Sequence E1:

BLAST Basic Local Alignment Search Tool

Job Title: E1T7

Sequences producing significant alignments: (Click headers to sort columns)		Max score	Total score	Query coverage	E value	Max ident.	
CP000885.1	Clostridium phytofermentans ISDg, complete genome	60.8	60.8	46%	2e-06	71%	
AF169248.2	Opsanus beta acetylglutamate-activated carbamoyl phosphate synthase III mRNA, complete cds	51.8	51.8	11%	0.001	100%	
AJ251660.1	Girardia tigrina mRNA for homeodomain transcription factor (so gene)	48.2	48.2	10%	0.015	100%	
AB290030.1	Phoca sibirica CYP1B1 mRNA for cytochrome P450 1B1, complete cds	44.6	44.6	12%	0.19	93%	
DQ459385.1	Nicotiana tabacum serine/threonine kinase mRNA, partial cds	44.6	44.6	10%	0.19	96%	U
AY445161.1	Anabaena circinalis clone FP170 unknown DNA sequence	44.6	44.6	11%	0.19	96%	
XM_806447.1	Trypanosoma cruzi strain CL Brener	44.6	44.6	13%	0.19	88%	G
AF403384.2	Homo sapiens LGR8 mRNA, complete cds	44.6	44.6	9%	0.19	100%	U E G
AB182645.1	Anguilla japonica eDmc1 mRNA for RecA homolog DMC1, complete cds	44.6	44.6	9%	0.19	100%	
AJ272202.1	Arabidopsis thaliana mRNA for mitochondrial half-ABC transporter (STA1 gene)	44.6	44.6	9%	0.19	100%	U E G
AJ223715.1	Squalus acanthias mRNA for sgk-1 serine-threonine protein kinase	44.6	44.6	9%	0.19	100%	
AC159328.9	Mus musculus 10 BAC RP23-216F23 (Roswell Park Cancer Institute (C57BL/6J Female) Mouse BAC Library) complete sequence	44.6	44.6	11%	0.19	93%	
AF133675.1	Populus tremula x Populus tremuloides retinoblastoma-related protein 1 (RB1) mRNA, complete cds	44.6	44.6	9%	0.19	100%	U
AF133731.2	Rattus norvegicus 11-zinc finger protein (CTCF) mRNA, complete cds	44.6	44.6	9%	0.19	100%	U E G
AC109180.20	Mus musculus chromosome 10, clone RP23-13J14, complete sequence	44.6	44.6	11%	0.19	93%	
EF648567.1	Riftia pachyptila clone TRbwC21 ubiquinol cytochrome reductase mRNA, partial cds	42.8	42.8	9%	0.65	100%	
DQ423779.1	Kryptolebias marmoratus Rhesus glycoprotein (RhCG2) mRNA, complete cds	42.8	42.8	9%	0.65	100%	
AY961924.2	Picea abies dehydrin 1 (Dhn) mRNA, complete cds	42.8	42.8	9%	0.65	100%	
AM712630.1	Ostertagia ostertagi mRNA for activation associated secreted protein (al2 gene)	42.8	42.8	9%	0.65	100%	
CR396591.13	Zebrafish DNA sequence from clone DKEY-43I4 in linkage group 6, complete sequence	42.8	42.8	11%	0.65	92%	
XM_001322268.1	Trichomonas vaginalis G3 hypothetical protein (TVAG_329670) mRNA, complete cds	42.8	42.8	17%	0.65	81%	G
AY243490.1	Stylonychia lemnae RUS macronuclear DNA polymerase catalytic subunit alpha gene, partial cds	42.8	42.8	10%	0.65	96%	
AY243489.1	Stylonychia lemnae SGR1 macronuclear DNA polymerase catalytic subunit alpha gene, partial cds	42.8	42.8	10%	0.65	96%	
AY445150.1	Anabaena circinalis clone FP74 unknown DNA sequence	42.8	42.8	9%	0.65	100%	
AF399843.1	Rattus norvegicus REST/NRSF-interacting lim domain protein (Rilp) mRNA, complete cds	42.8	42.8	9%	0.65	100%	U E G
AC125040.4	Mus musculus BAC clone RP23-335C9 from chromosome 3, complete sequence	42.8	42.8	17%	0.65	81%	
AF258578.2	Homo sapiens PP4519 mRNA, complete cds	42.8	42.8	9%	0.65	100%	E G
AF075583.1	Homo sapiens transforming growth factor alpha precursor (TGFA) gene, exon 1	42.8	42.8	9%	0.65	100%	
AB182999.1	Danio rerio mRNA for RecA homolog Dmc1, complete cds	42.8	42.8	9%	0.65	100%	U G
AF106913.1	Homo sapiens CRL3 protein (CRL3) mRNA, complete cds	42.8	42.8	9%	0.65	100%	U E G
AB032017.1	Homo sapiens mRNA for KPG_003 protein, complete cds	42.8	42.8	9%	0.65	100%	U G
Y12236.1	D.rerio mRNA for Cu/Zn-superoxide dismutase	42.8	42.8	9%	0.65	100%	U E G

DNA Insert Sequence for *C. Piliforme* Suppression Subtractive Hybridization Clone E4:

```
TCGAGCGGCCGCCCGGGCAGGTCTCCAAGGCGGGTCCTTCGCTTTATTTTATTCTTTTTG
1.......10........20........30........40........50........60

TTTTTAATTGTTAAAGATTTGTTTTTTTGTNCGTTTGTTTGCTACCGCCCTCCTCACCAC
........70........80........90.......100.......110.......120

GCCCT
.....
```

Computer Output of BLAST Homology Search for Insert Sequence E4:

BLAST Basic Local Alignment Search Tool

Job Title: E4T7

Sequences producing significant alignments: (Click headers to sort columns)

		Max score	Total score	Query coverage	E value	Max ident.	
AJ640141.1	Homo sapiens mRNA for ceramide kinase-like protein (CERKL gene)	59.0	59.0	64%	4e-06	77%	U G
AF000670.1	Homo sapiens elf-1 related protein (ELFR) mRNA, complete cds	55.4	55.4	59%	4e-05	76%	U E G
AJ272202.1	Arabidopsis thaliana mRNA for mitochondrial half-ABC transporter (STA1 gene)	53.6	53.6	60%	2e-04	76%	U E G
AJ616905.1	Glomeris marginata partial mRNA for hedgehog protein (hh gene)	51.8	51.8	22%	5e-04	100%	
AB286673.1	Lethenteron japonicum LjHox10s gene for LjHox10s homeobox, parital cds	50.0	50.0	21%	0.002	100%	
AB095996.1	Gallus gallus Ghsr1aV mRNA for growth hormone secretagogue receptor type 1a variant, complete cds	48.2	48.2	20%	0.007	100%	U G
AB095995.1	Gallus gallus Ghsr1a mRNA for growth hormone secretagogue receptor type 1a, complete cds	48.2	48.2	20%	0.007	100%	U G
AF074706.1	Bos taurus 11-beta-hydroxysteroid dehydrogenase type 2 mRNA, complete cds	48.2	48.2	20%	0.007	100%	U E G
AF118784.1	Glycine max ribonucleotide reductase large subunit A mRNA, complete cds	48.2	48.2	20%	0.007	100%	U G
AB090165.1	Sus scrofa mRNA for receptor activity-modifying protein, complete cds	48.2	48.2	20%	0.007	100%	U G
AJ010750.1	Rattus norvegicus mRNA for Castration Induced Prostatic Apoptosis Related protein-1 (CIPAR-1)	48.2	48.2	20%	0.007	100%	U E G
AB049620.1	Halocynthia roretzi AsFCN2 mRNA for filcolin 2, complete cds	48.2	48.2	52%	0.007	76%	
DQ222242.2	Lycopersicon esculentum cryptochrome 3 (Cry3) gene, complete cds	46.4	46.4	20%	0.023	100%	
AF075584.1	Homo sapiens transforming growth factor alpha precursor (TGFA) gene, exon 2 and partial cds	46.4	46.4	24%	0.023	93%	G
AF093414.1	Saguinus oedipus estrogen response element binding protein mRNA, complete cds	46.4	46.4	53%	0.023	74%	
AF093139.1	Rattus norvegicus tip associating protein (TAP) mRNA, complete cds	46.4	46.4	25%	0.023	93%	U E G
AF079314.1	Rattus norvegicus nuclear factor kappa B subunit p65 (NFkB) mRNA, partial cds	46.4	46.4	20%	0.023	100%	U E G
AB000814.1	Homo sapiens mRNA for BMAL1f, partial cds	46.4	46.4	54%	0.023	75%	U E G
AB266595.1	Plutella xylostella PxSP1 mRNA for methionine-rich storage protien 1, complete cds	44.6	44.6	21%	0.080	96%	
AB265796.1	Pyrus x bretschneideri PbACS3 mRNA for 1-aminocyclopropane-1-carboxylate synthase, complete cds	44.6	44.6	19%	0.080	100%	
X96789.2	Sporosarcina sp. genes for Sse9I restriction-modification system	44.6	44.6	19%	0.080	100%	
AY273895.1	Brugia malayi transglutaminase mRNA, partial cds	44.6	44.6	19%	0.080	100%	
AB240529.1	Eublepharis macularius ERb mRNA for estrogen receptor beta, complete cds	44.6	44.6	19%	0.080	100%	
AJ238855.1	Rattus norvegicus mRNA for type A/B hnRNP protein p38	44.6	44.6	19%	0.080	100%	U G
AJ238854.1	Rattus norvegicus mRNA for type A/B hnRNP protein p40	44.6	44.6	19%	0.080	100%	U E G
AF039086.1	Pseudomicrothorax dubius articulin 1 mRNA, complete cds	44.6	44.6	19%	0.080	100%	
AB032017.1	Homo sapiens mRNA for KPG_003 protein, complete cds	44.6	44.6	29%	0.080	86%	U G
AJ252088.1	Solanum dulcamara mRNA for gibberellin 20-oxidase (ga20ox1 gene)	44.6	87.3	52%	0.080	100%	
AJ223716.1	Squalus acanthias mRNA for sgk-2 serine-threonine protein kinase	44.6	44.6	19%	0.080	100%	
AB066448.1	Closterium ehrenbergii scdip-1 mRNA for sexual cell division-inducing pheromone, complete cds	44.6	44.6	19%	0.080	100%	
AF026274.1		44.6	44.6	60%	0.080	76%	

DNA Insert Sequence for *C. Piliforme* Suppression Subtractive Hybridization Clone E5:

```
AGGGCGTGGTGCGGAGGGCGGTATTCAAACATTGCACCAGGATTAGTATCAGCCATTTGT
1.......10........20........30........40........50........60

TGCTCAGTTGGTGATAAGCCTTTATCTATTAGGTCGATCACCTGCCCGGGCGGCCGCTCG
........70........80........90.......100.......110.......120

A
.
```

Computer Output of BLAST Homology Search for Insert Sequence E5:

BLAST Basic Local Alignment Search Tool

Job Title: E5T7

Sequences producing significant alignments: (Click headers to sort columns)		Max score	Total score	Query coverage	E value	Max ident.	
AJ251660.1	Girardia tigrina mRNA for homeodomain transcription factor (so gene)	51.8	51.8	23%	5e-04	100%	
AF169248.2	Opsanus beta acetylglutamate-activated carbamoyl phosphate synthase III mRNA, complete cds	48.2	48.2	21%	0.006	100%	
DQ204605.1	Diospyros kaki ISSR marker 807 genomic sequence	46.4	46.4	20%	0.022	100%	
DQ204617.1	Diospyros kaki microsatellite 2 sequence	44.6	44.6	19%	0.077	100%	
AF403384.2	Homo sapiens LGR8 mRNA, complete cds	44.6	44.6	19%	0.077	100%	U E G
AB182645.1	Anguilla japonica eDmc1 mRNA for RecA homolog DMC1, complete cds	44.6	44.6	19%	0.077	100%	
AJ272202.1	Arabidopsis thaliana mRNA for mitochondrial half-ABC transporter (STA1 gene)	44.6	44.6	19%	0.077	100%	U E G
AJ223715.1	Squalus acanthias mRNA for sgk-1 serine-threonine protein kinase	44.6	44.6	19%	0.077	100%	
AF133675.1	Populus tremula x Populus tremuloides retinoblastoma-related protein 1 (RB1) mRNA, complete cds	44.6	44.6	19%	0.077	100%	U
AF133731.2	Rattus norvegicus 11-zinc finger protein (CTCF) mRNA, complete cds	44.6	44.6	22%	0.077	96%	U E G
AB013101.1	Solanum lycopersicum LE-ACO4 mRNA for 1-aminocyclopropane-1-carboxylate oxidase, complete cds	44.6	44.6	33%	0.077	85%	U G
EF648567.1	Riftia pachyptila clone TRbwC21 ubiquinol cytochrome reductase mRNA, partial cds	42.8	42.8	19%	0.27	100%	
CP000820.1	Frankia sp. EAN1pec, complete genome	42.8	42.8	23%	0.27	92%	
DQ423779.1	Kryptolebias marmoratus Rhesus glycoprotein (RhCG2) mRNA, complete cds	42.8	42.8	19%	0.27	100%	
AY961924.2	Picea abies dehydrin 1 (Dhn) mRNA, complete cds	42.8	42.8	19%	0.27	100%	
AM712630.1	Ostertagia ostertagi mRNA for activation associated secreted protein (al2 gene)	42.8	42.8	19%	0.27	100%	
AB290030.1	Phoca sibirica CYP1B1 mRNA for cytochrome P450 1B1, complete cds	42.8	42.8	19%	0.27	100%	
DQ459385.1	Nicotiana tabacum serine/threonine kinase mRNA, partial cds	42.8	42.8	21%	0.27	96%	U
DQ204620.1	Diospyros kaki microsatellite 5 sequence	42.8	42.8	19%	0.27	100%	
DQ204619.1	Diospyros kaki microsatellite 4 sequence	42.8	42.8	19%	0.27	100%	
AY754861.1	Metarhizium anisopliae clone cag5 putative cell wall plasma membrane linker protein-like mRNA, partial sequence	42.8	121	19%	0.27	100%	
AY445150.1	Anabaena circinalis clone FP74 unknown DNA sequence	42.8	42.8	19%	0.27	100%	
AF399843.1	Rattus norvegicus REST/NRSF-interacting lim domain protein (Rilp) mRNA, complete cds	42.8	42.8	19%	0.27	100%	U E G
BT009460.1	Triticum aestivum clone wpi1s.pk008.k5:fis, full insert mRNA sequence	42.8	42.8	25%	0.27	90%	U
AF258578.2	Homo sapiens PP4519 mRNA, complete cds	42.8	42.8	19%	0.27	100%	E G
AF075583.1	Homo sapiens transforming growth factor alpha precursor (TGFA) gene, exon 1	42.8	42.8	19%	0.27	100%	
AB182999.1	Danio rerio mRNA for RecA homolog Dmc1, complete cds	42.8	42.8	19%	0.27	100%	U G
AF106913.1	Homo sapiens CRL3 protein (CRL3) mRNA, complete cds	42.8	42.8	19%	0.27	100%	U E G
AF373712.1	Ovis aries clone 2G8 bone morphogenetic protein receptor-IB (BMPR-IB) mRNA, 5'UTR, partial sequence	42.8	42.8	19%	0.27	100%	U
AB032017.1	Homo sapiens mRNA for KPG_003 protein, complete cds	42.8	42.8	19%	0.27	100%	U G
Y12236.1	D.rerio mRNA for Cu/Zn-superoxide dismutase	42.8	42.8	19%	0.27	100%	U E G
AJ549215.1	Zea mays mRNA for chloroplast SRP receptor cpFtsY precursor (csr1 gene)	42.8	42.8	19%	0.27	100%	U G
AB108670.1	Rattus norvegicus DR-NR#2 mRNA for Down-regulated in nephrectomized rat kidney #2, complete cds	42.8	42.8	19%	0.27	100%	U G

DNA Insert Sequence for *C. Piliforme* Suppression Subtractive Hybridization Clone E6:

```
AGGGCGTGGNGCGGAGGGCGGTAATCTGCAAAAAAAGGATNTTTAACATTATGACAAACT
1.......10........20........30........40........50........60

TGAAGCTATGACTTGNGNATGTTCTGTTGGACTTGNTATGGACTGCTGTACCTGGAGATA
........70........80........90.......100.......110.......120

CAGATGCACATACAATCTCTGCTATAATCGCAGATGAAATGGCTATTGGTANGATAAACA
.......130.......140.......150.......160.......170.......180

ATAAGACGACAGCAGTTAGAATAATACCTGTTATAGGGAAAAATGTTGGCGATATGGTTT
.......190.......200.......210.......220.......230.......240

CTTTTGGAGGATTATTAGGTGAGGCTCCAATAATGGCTGTAAATAAAGCCAAATGCTATG
.......250.......260.......270.......280.......290.......300

ATTTTATCAAGCGTGGNGGAAGAATACCTGCTNCTATTCATAGTTTTAAAAACTAATAGT
.......310.......320.......330.......340.......350.......360

NCATAACCTTATTGATTTAATCTGAATATATTAAAAAATAAGATTACCTGCCCGGGCGGC
.......370.......380.......390.......400.......410.......420

CCGCTCGA
........
```

Computer Output of BLAST Homology Search for Insert Sequence E6:

BLAST Basic Local Alignment Search Tool

Job Title: E6T7

Sequences producing significant alignments: (Click headers to sort columns)		Max score	Total score	Query coverage	E value	Max ident.
CP000382.1	Clostridium novyi NT, complete genome	208	208	80%	1e-50	73%
AE015927.1	Clostridium tetani E88, complete genome	172	172	77%	1e-39	71%
CP000885.1	Clostridium phytofermentans ISDg, complete genome	161	161	71%	2e-36	71%
CP000867.1	Methanococcus maripaludis C6, complete genome	158	158	42%	2e-35	78%
AM180252.1	Lawsonia intracellularis PHE/MN1-00	158	158	71%	2e-35	71%
CP000724.1	Alkaliphilus metalliredigens QYMF, complete genome	156	156	71%	8e-35	71%
CP000743.1	Methanococcus aeolicus Nankai-3, complete genome	154	154	67%	3e-34	71%
CP000609.1	Methanococcus maripaludis C5, complete genome	152	193	49%	9e-34	87%
AE001437.1	Clostridium acetobutylicum ATCC 824, complete genome	149	149	71%	1e-32	70%
CP000745.1	Methanococcus maripaludis C7, complete genome	147	147	44%	4e-32	76%
CP000414.1	Leuconostoc mesenteroides subsp. mesenteroides ATCC 8293, complete genome	145	145	77%	1e-31	69%
BX957223.1	Methanococcus maripaludis S2 complete genome; segment 5/5	143	143	67%	5e-31	70%
DQ372942.1	Methanococcus voltae putative GMP synthase (MVO1745), hypothetical protein (MVO1746), deoxycytidine triphosphate deaminase / dUTP pyrophosphatase (MVO1747), hypothetical protein (MVO1748), STT3 (MVO1749), UDP-N-acetylglucosamine-dolichyl-phosphate n-acetylglucosaminephosphotransferase (MVO1751), and protein translocase subunit SecY (MVO1753) genes, complete cds	132	132	53%	9e-28	72%
L77117.1	Methanocaldococcus jannaschii DSM 2661, complete genome	131	131	57%	3e-27	72%
CP000673.1	Clostridium kluyveri DSM 555, complete genome	129	129	76%	1e-26	69%
BA000016.3	Clostridium perfringens str. 13 DNA, complete genome	129	129	76%	1e-26	68%
CP000246.1	Clostridium perfringens ATCC 13124, complete genome	123	123	76%	4e-25	67%
CP000300.1	Methanococcoides burtonii DSM 6242, complete genome	122	122	47%	2e-24	72%
CP000721.1	Clostridium beijerinckii NCIMB 8052, complete genome	116	116	75%	7e-23	68%
CP000923.1	Thermoanaerobacter sp. X514, complete genome	111	111	37%	3e-21	74%
CP000742.1	Methanococcus vannielii SB, complete genome	111	111	73%	3e-21	67%
CP000233.1	Lactobacillus salivarius UCC118, complete genome	109	109	71%	1e-20	67%
AE008384.1	Methanosarcina mazei strain Goe1, complete genome	105	105	67%	1e-19	67%
CP000254.1	Methanospirillum hungatei JF-1, complete genome	104	104	71%	4e-19	66%
CP000568.1	Clostridium thermocellum ATCC 27405, complete genome	100	100	71%	5e-18	66%
AL596165.1	Listeria innocua Clip11262 complete genome, segment 3/12	95.1	95.1	71%	2e-16	66%
CP000792.1	Campylobacter concisus 13826, complete genome	93.3	93.3	75%	8e-16	66%
CP000705.1	Lactobacillus reuteri F275, complete genome	93.3	93.3	70%	8e-16	66%
AL935259.1	Lactobacillus plantarum strain WCFS1 complete genome; segment 8/11	93.3	93.3	54%	8e-16	68%
AE017262.2	Listeria monocytogenes str. 4b F2365, complete genome	84.2	84.2	71%	4e-13	65%
CP000612.1	Desulfotomaculum reducens MI-1, complete genome	82.4	82.4	71%	1e-12	65%
CR522870.1	Desulfotalea psychrophila LSv54 chromosome	80.6	80.6	71%	5e-12	65%
CP000679.1	Caldicellulosiruptor saccharolyticus DSM 8903, complete genome	77.0	77.0	46%	6e-11	68%
AE005672.2	Streptococcus pneumoniae TIGR4, complete genome	73.4	73.4	71%	7e-10	65%
CP000099.1	Methanosarcina barkeri str. Fusaro, complete genome	71.6	71.6	67%	2e-09	64%
CP000419.1	Streptococcus thermophilus LMD-9, complete genome	69.8	69.8	71%	9e-09	64%
CP000410.1	Streptococcus pneumoniae D39, complete genome	69.8	69.8	71%	9e-09	65%
CP000142.2	Pelobacter carbinolicus DSM 2380, complete genome	69.8	69.8	33%	9e-09	70%
CP000024.1	Streptococcus thermophilus CNRZ1066, complete genome	69.8	69.8	71%	9e-09	64%
AE008403.1	Streptococcus pneumoniae R6 section 19 of 184 of the complete genome	69.8	69.8	71%	9e-09	65%
CP000023.1	Streptococcus thermophilus LMG 18311, complete genome	69.8	69.8	71%	9e-09	64%

DNA Insert Sequence for *C. Piliforme* Suppression Subtractive Hybridization Clone F2:

```
AGGGCGTGGTGCGGAGGGCGGTGAGGATTGTGATTGTGTGCTGTGACCGGCGGCAGCATC
1.......10........20........30........40........50........60

CGAGTGCTGATATTTATTAATTCAGCATATGAATATTTGACAACATGTTTGTATGGTTAC
........70........80........90.......100.......110.......120

AGCATACATGTAGAGGACCTGCCCGGGCGGCCGCTCGA
.......130.......140.......150........
```

Computer Output of BLAST Homology Search for Insert Sequence F2:

BLAST Basic Local Alignment Search Tool

Job Title: F2T7

Sequences producing significant alignments: (Click headers to sort columns)

		Max score	Total score	Query coverage	E value	Max ident.	
AB266321.1	Musa acuminata AAA Group MA-EIL4 mRNA for ethylene signal transcription factor, complete cds	50.0	50.0	17%	0.003	100%	
AY327034.1	Ixodes ricinus glutathione S-transferase mRNA, partial cds	50.0	50.0	19%	0.003	96%	
DQ355438.1	Gecarcinus lateralis NO-insensitive guanylyl cyclase III (GCIII) mRNA, complete cds	48.2	48.2	16%	0.009	100%	
AM422096.1	Danio rerio partial mRNA for retinol dehydrogenase 10 (rdh10 gene)	44.6	44.6	17%	0.11	96%	UG
AB266318.1	Musa acuminata AAA Group MA-EIL1 mRNA for ethylene signal transcription factor, complete cds	44.6	44.6	15%	0.11	100%	
AC165353.4	Mus musculus BAC clone RP23-167C2 from chromosome 3, complete sequence	44.6	44.6	27%	0.11	81%	
X97991.1	M.musculus mRNA for calcitonin	44.6	44.6	15%	0.11	100%	UEG
AJ310908.1	Fucus vesiculosus mRNA for ALA dehydratase (hemB gene)	44.6	44.6	15%	0.11	100%	
AB040991.1	Oryctolagus cuniculus mRNA for prostaglandin D synthase, complete cds	44.6	44.6	15%	0.11	100%	UG
AJ276466.1	Klebsiella pneumoniae contig region pSL004	44.6	44.6	17%	0.11	96%	
AB104414.1	Cucumis melo GeAAT-2 mRNA for alcohol acyltransferase, complete cds	44.6	44.6	15%	0.11	100%	
AB075227.1	Cucumis melo GeAAT-1 mRNA for alcohol acetyltransferase, complete cds	44.6	44.6	15%	0.11	100%	
AF033850.1	Homo sapiens phospholipase D2 (PLD2) mRNA, complete cds	44.6	44.6	15%	0.11	100%	UEG
AC161251.3	Mus musculus BAC clone RP24-174C13 from chromosome 3, complete sequence	44.6	44.6	27%	0.11	81%	
AF093139.1	Rattus norvegicus tip associating protein (TAP) mRNA, complete cds	44.6	44.6	15%	0.11	100%	UEG
AJ293391.1	Homo sapiens mRNA differentially expressed in malignant melanoma, clone MM J9	44.6	44.6	17%	0.11	96%	U
AJ293390.1	Homo sapiens mRNA, differentially expressed in malignant melanoma, clone MM A2	44.6	44.6	17%	0.11	96%	UE
AB017520.1	Bombyx mori mRNA for Bacteriophage T7 lysozyme-like protein 2 (BTL-LP2), complete cds	44.6	44.6	15%	0.11	100%	UG
AB019563.1	Homo sapiens mRNA expressed only in placental villi, clone SMAP42	44.6	44.6	18%	0.11	93%	
EU022152.1	Montipora capitata clone DCMU1L5 unknown mRNA	42.8	42.8	16%	0.38	96%	
D89732.1	Cucumis sativus mRNA for 1-aminocyclopropane-1-carboxylate synthase, complete cds, CS-ACS2	42.8	83.7	14%	0.38	100%	
AB286673.1	Lethenteron japonicum LjHox10s gene for LjHox10s homeobox, parital cds	42.8	42.8	14%	0.38	100%	
AB266595.1	Plutella xylostella PxSP1 mRNA for methionine-rich storage protien 1, complete cds	42.8	42.8	14%	0.38	100%	
AB265796.1	Pyrus x bretschneideri PbACS3 mRNA for 1-aminocyclopropane-1-carboxylate synthase, complete cds	42.8	42.8	14%	0.38	100%	
CT029336.1	Poplar cDNA sequences	42.8	42.8	16%	0.38	96%	
CT029125.1	Poplar cDNA sequences	42.8	42.8	16%	0.38	96%	
CT028739.1	Poplar cDNA sequences	42.8	42.8	16%	0.38	96%	
CT028316.1	Poplar cDNA sequences	42.8	42.8	16%	0.38	96%	
X96789.2	Sporosarcina sp. genes for Sse9I restriction-modification system	42.8	42.8	14%	0.38	100%	
DQ222242.2	Lycopersicon esculentum cryptochrome 3 (Cry3) gene, complete cds	42.8	42.8	14%	0.38	100%	
AB257139.1	Tubifex tubifex vasa mRNA for RNA helicase, complete cds	42.8	42.8	14%	0.38	100%	
AY273895.1	Brugia malayi transglutaminase mRNA, partial cds	42.8	42.8	16%	0.38	96%	
AC136513.2	Mus musculus BAC clone RP23-477N9 from chromosome 5,	42.8	42.8	27%	0.38	82%	

DNA Insert Sequence for *C. Piliforme* Suppression Subtractive Hybridization Clone K4:

```
GAGCGGCCGCCCGGGCAGGTAATCCCGTTATCCACCCTAGGGACCCTAAGGTCATATGCA
1.......10........20........30........40........50........60

ATAACAAATAATATAATAATATGGGTCACTAGCTCAGTTGGTAGAGCACCTGGACTTTTA
........70........80........90.......100.......110.......120

ATCCAGGTGTCCCGACCGCCCTCCGCACCACGCCCT
.......130.......140.......150......
```

Computer Output of BLAST Homology Search for Insert Sequence K4:

BLAST Basic Local Alignment Search Tool

Job Title: K4T7

Sequences producing significant alignments: (Click headers to sort columns)		Max score	Total score	Query coverage	E value	Max ident.
AP008971.1	Finegoldia magna ATCC 29328 DNA, complete genome	73.4	317	40%	2e-10	91%
AB109771.1	Finegoldia magna rrnC operon, complete sequence	73.4	114	36%	2e-10	89%
AE001437.1	Clostridium acetobutylicum ATCC 824, complete genome	71.6	509	42%	8e-10	86%
CP000885.1	Clostridium phytofermentans ISDg, complete genome	69.8	294	40%	3e-09	86%
CP000721.1	Clostridium beijerinckii NCIMB 8052, complete genome	69.8	499	39%	3e-09	88%
AM180355.1	Clostridium difficile 630 complete genome	68.0	393	39%	9e-09	91%
CP000612.1	Desulfotomaculum reducens MI-1, complete genome	66.2	416	38%	3e-08	91%
CP000448.1	Syntrophomonas wolfei subsp. wolfei str. Goettingen, complete genome	66.2	107	40%	3e-08	84%
CP000728.1	Clostridium botulinum F str. Langeland, complete genome	64.4	394	35%	1e-07	89%
CP000727.1	Clostridium botulinum A str. Hall, complete genome	64.4	400	40%	1e-07	89%
CP000726.1	Clostridium botulinum A str. ATCC 19397, complete genome	64.4	400	40%	1e-07	89%
CP000673.1	Clostridium kluyveri DSM 555, complete genome	64.4	180	35%	1e-07	88%
AM412317.1	Clostridium botulinum A str. ATCC 3502 complete genome	64.4	446	40%	1e-07	89%
CP000568.1	Clostridium thermocellum ATCC 27405, complete genome	64.4	178	35%	1e-07	87%
AP008230.1	Desulfitobacterium hafniense Y51 DNA, complete genome	64.4	175	42%	1e-07	89%
AE015927.1	Clostridium tetani E88, complete genome	64.4	178	35%	1e-07	89%
CP000141.1	Carboxydothermus hydrogenoformans Z-2901, complete genome	62.6	164	32%	4e-07	91%
CP000930.1	Heliobacterium modesticaldum Ice1, complete genome	60.8	303	28%	1e-06	91%
CP000853.1	Alkaliphilus oremlandii OhILAs, complete genome	60.8	243	30%	1e-06	89%
CP000724.1	Alkaliphilus metalliredigens QYMF, complete genome	60.8	303	30%	1e-06	89%
AM494475.1	Orientia tsutsugamushi Boryong complete genome	60.8	60.8	28%	1e-06	91%
CP000382.1	Clostridium novyi NT, complete genome	60.8	269	40%	1e-06	87%
CP000263.1	Buchnera aphidicola str. Cc (Cinara cedri), complete genome	60.8	101	41%	1e-06	84%
CP000312.1	Clostridium perfringens SM101, complete genome	60.8	588	48%	1e 06	88%
EU084746.1	Bacillus subtilis strain PY79 tRNA-Asn, tRNA-Ser, tRNA-Glu, tRNA-Gln, tRNA-Lys, and tRNA-Leu genes, complete sequence; and YddN (yddN) gene, partial cds	59.0	59.0	34%	5e-06	85%
AP009389.1	Pelotomaculum thermopropionicum SI DNA, complete genome	59.0	157	32%	5e-06	87%
CP000246.1	Clostridium perfringens ATCC 13124, complete genome	59.0	449	36%	5e-06	88%
CP000127.1	Nitrosococcus oceani ATCC 19707, complete genome	59.0	105	32%	5e-06	92%
AE016827.1	Mannheimia succiniciproducens MBEL55E, complete genome	59.0	216	34%	5e-06	89%
CP000232.1	Moorella thermoacetica ATCC 39073, complete genome	59.0	112	41%	5e-06	86%
AJ970604.1	Candidatus Phytoplasma solani tRNA-Val gene, tRNA-Thr gene, tRNA-Lys gene and, tRNA-Leu gene, clone SDR0033	59.0	59.0	26%	5e-06	92%
Z99106.2	Bacillus subtilis complete genome (section 3 of 21): from 415769 to 611680	59.0	59.0	34%	5e-06	85%
BA000016.3	Clostridium perfringens str. 13 DNA, complete genome	59.0	624	36%	5e-06	88%
AB001488.1	Bacillus subtilis genome sequence, 148 kb sequence of the region between 35 and 47 degree	59.0	59.0	34%	5e-06	85%
L13170.1	Bacillus subtilis DNA fragment with the sup-2 mutation	59.0	59.0	34%	5e-06	85%
CP000381.1	Neisseria meningitidis 053442, complete genome	57.2	381	33%	2e-05	100%
CP000868.1	Burkholderia multivorans ATCC 17616 chromosome 1, complete sequence	57.2	103	27%	2e-05	91%
DQ832717.1	Phytophthora sojae mitochondrion, complete genome	57.2	57.2	30%	2e-05	87%
CP000614.1	Burkholderia vietnamiensis G4 chromosome 1, complete sequence	57.2	103	27%	2e-05	91%
CP000521.1	Acinetobacter baumannii ATCC 17978, complete genome	57.2	330	35%	2e-05	91%
AL157959.1	Neisseria meningitidis serogroup A strain Z2491 complete genome	57.2	328	33%	2e-05	100%
AM421808.1	Neisseria meningitidis serogroup C FAM18 complete genome	57.2	381	33%	2e-05	100%
CP000510.1	Psychromonas ingrahamii 37, complete genome	57.2	717	41%	2e-05	100%
CP000360.1	Acidobacteria bacterium Ellin345, complete genome	57.2	57.2	25%	2e-05	95%

DNA Insert Sequence for *C. Piliforme* Suppression Subtractive Hybridization Clone K5:

```
TGTGCGTGAAGACGACAGAACGGAAGGCCCTATAGTGAGTCGTATTACAACGCCCTCCGC
1.......10........20........30........40........50........60

ACCACGCCCTGCNCAAATNCAAAAGNNNGNCNAAAACCCCGCCCAGGNC
........70........80........90.......100.........
```

Computer Output of BLAST Homology Search for Insert Sequence K5:

BLAST Basic Local Alignment Search Tool

Job Title: K5T7

Sequences producing significant alignments: (Click headers to sort columns)		Max score	Total score	Query coverage	E value	Max ident.
U76715.1	Cloning vector pBRkanf4 kanamycin acetyl transferase and beta galactosidase alpha complement (lacZ) genes, complete cds	46.4	46.4	22%	0.019	100%
AB294212.1	Escherichia coli O157:H7 ompW gene for outer membrane protein W, complete cds, strain: MP37	44.6	44.6	22%	0.067	100%
AB294211.1	Escherichia coli O157:H7 ompW gene for outer membrane protein W, complete cds, strain: F2	44.6	44.6	22%	0.067	100%
CU679849.1	Synthetic construct Homo sapiens gateway clone IMAGE:100023353 5' read NTS mRNA	44.6	44.6	26%	0.067	93%
AM940001.1	Cloning vector pIMC	44.6	44.6	26%	0.067	93%
AM940000.1	Cloning vector pIMK	44.6	44.6	26%	0.067	93%
AM931402.1	Musa textilis partial nbs gene for truncated NBS-LRR disease resistance protein, clone N431_TT	44.6	44.6	22%	0.067	100%
EU292740.1	Cloning vector pFOSKAN, complete sequence	44.6	44.6	22%	0.067	100%
EU292739.1	Cloning vector pFOSAMP, complete sequence	44.6	44.6	22%	0.067	100%
AC215487.1	Solanum lycopersicum Tomato chromosome 2, C02SLm0076E07, complete sequence	44.6	44.6	22%	0.067	100%
EU257522.1	Cloning vector pNC-GFP, complete sequence	44.6	44.6	22%	0.067	100%
EF488748.1	Cloning vector pOK12, complete sequence	44.6	44.6	22%	0.067	100%
EF488745.1	Cloning vector pCR2.1-gentR, complete sequence	44.6	44.6	22%	0.067	100%
EF488744.1	Cloning vector pCR2.1-kanR, complete sequence	44.6	44.6	22%	0.067	100%
AB305024.1	Vaccinium ciliatum DNA, microsatellite marker VM32	44.6	44.6	22%	0.067	100%
EU250578.1	Broad host range reporter vector pMJ445, complete sequence	44.6	81.9	22%	0.067	100%
AM884385.1	Cloning vector pGHGWY	44.6	44.6	22%	0.067	100%
AM884384.1	Cloning vector pGHGWG	44.6	44.6	22%	0.067	100%
AM884383.1	Cloning vector pGHGWC	44.6	44.6	22%	0.067	100%
EU251692.1	Cloning vector pAW34, complete sequence	44.6	44.6	22%	0.067	100%
EU251691.1	Cloning vector pAW33, complete sequence	44.6	44.6	22%	0.067	100%
EU251690.1	Cloning vector pAW32, complete sequence	44.6	44.6	22%	0.067	100%
EU233623.1	Cloning vector pEASY-T1, complete sequence	44.6	44.6	22%	0.067	100%
EU161577.1	Cloning vector pSB156, complete sequence	44.6	44.6	22%	0.067	100%
EU146228.1	Transposon delivery vector pAW068, complete sequence	44.6	128	22%	0.067	100%
AM884388.1	Cloning vector pGBGWY	44.6	44.6	22%	0.067	100%
AM884387.1	Cloning vector pGBGWG	44.6	44.6	22%	0.067	100%
AM884386.1	Cloning vector pGBGWC	44.6	44.6	22%	0.067	100%
AM884382.1	Cloning vector pGKGWC	44.6	44.6	22%	0.067	100%
AM884381.1	Cloning vector pGKGWG	44.6	44.6	22%	0.067	100%
AM884380.1	Cloning vector pGKGWY	44.6	44.6	22%	0.067	100%
AM884379.1	Cloning vector pGKPGWY	44.6	44.6	22%	0.067	100%
AM884378.1	Cloning vector pGKPGWG	44.6	44.6	22%	0.067	100%
AM884377.1	Cloning vector pGKPGWC	44.6	44.6	22%	0.067	100%
AM884376.1	Cloning vector pGHPGWY	44.6	44.6	22%	0.067	100%
AM884375.1	Cloning vector pGHPGWG	44.6	44.6	22%	0.067	100%
AM884374.1	Cloning vector pGHPGWC	44.6	44.6	22%	0.067	100%
AM884373.1	Cloning vector pGBPGWY	44.6	44.6	22%	0.067	100%
AM884372.1	Cloning vector pGBPGWG	44.6	44.6	22%	0.067	100%
AM884371.1	Cloning vector pGBPGWC	44.6	44.6	22%	0.067	100%
EU126551.1	Cloning vector pTriplEx2, complete sequence	44.6	44.6	22%	0.067	100%
EU140754.1	Cloning vector pIndigoBAC-5, complete sequence	44.6	44.6	22%	0.067	100%
EU140753.1	Cloning vector pEPIFOS-5, complete sequence	44.6	44.6	22%	0.067	100%
EU140752.1	Cloning vector pCC2FOS, complete sequence	44.6	44.6	22%	0.067	100%

DNA Insert Sequence for *C. Piliforme* Suppression Subtractive Hybridization Clone K7:

```
GNGNCATTACACNNCACGATGTNAGACCTGNNCTTCGCCTCGGNCGAGCACATCATGCGC
1.......10........20........30........40........50........60

AACGTGAACGGCGGCTTCATGCTGCGCTACCTGCATGCGAACGGNGCCTCGNTGTTCTTC
........70........80........90.......100.......110.......120

ATCGNGGNACTATCTGCACATCTTCCGAGGCACTCTACTACGGCAGCTNACAAGGCAGCC
.......130.......140.......150.......160.......170.......180

TGCGCAGAGGTCACCTGNATCGNGGGGATGCGTCATCTATCTNGCGATGATGGCNACCGG
.......190.......200.......210.......220.......230.......240

CTTNATGGGCTACGNGCTGCCGNGGGGCCAGATGTNCTTGTGGGGCNCCNCCGGGATCAC
.......250.......260.......270.......280.......290.......300

CGGCCTNTTCGGCGCGATCCCGGGCATCGGCCATTCNATCCAGACCTGGCTGCTCGGCGG
.......310.......320.......330.......340.......350.......360

CCCGGCGGTGGACAATGCCACGCTCAACCGGTTCTTCTCGCTGCACTACCTGCTGACCTT
.......370.......380.......390.......400.......410.......420

CGTGATCGCGGACGTCGAGGNCATGCACATNGTGGGCCTTCCACTCGACGGNCAACAACA
.......430.......440.......450.......460.......470.......480

ACCCGACCGGCGTCNAAGTGCGCCNNACCNCNAAGGCNGAAGCNCATAANGACACGGGCT
.......490.......500.......510.......520.......530.......540

CCCNTTNTGGCCNTANTNCATCATCAAGGACCNCGTTNNCCCTGGCCGAAACCTGCCGGG
.......550.......560.......570.......580.......590.......600

GGNTCTGGACCATCGGAGCGTTCNTCCCGANTACCNAGGNCACCCGGGCANCTNNNNNGT
.......610.......620.......630.......640.......650.......660
```

Computer Output of BLAST Homology Search for Insert Sequence K7:

BLAST Basic Local Alignment Search Tool

Job Title: K7T7

Sequences producing significant alignments: (Click headers to sort columns)

		Max score	Total score	Query coverage	E value	Max ident.
CP000143.1	Rhodobacter sphaeroides 2.4.1 chromosome 1, complete sequence	796	796	91%	0.0	85%
X56157.1	R. sphaeroides fbc operon for cytochrome bc1 complex reductase (EC 1.10.2.2)	796	796	91%	0.0	85%
CP000577.1	Rhodobacter sphaeroides ATCC 17029 chromosome 1, complete sequence	792	792	91%	0.0	84%
CP000661.1	Rhodobacter sphaeroides ATCC 17025, complete genome	625	625	91%	1e-175	79%
CP000489.1	Paracoccus denitrificans PD1222 chromosome 1, complete sequence	556	556	91%	4e-155	76%
X05799.1	P. denitrificans bc1 gene for cytochrome bc1 complex (EC 1.10.2.2)	556	556	91%	4e-155	76%
M17522.1	P.denitrificans bc1 operon genes encoding three subunits (FeS, b and c1) of the cytochrome bc1 complex, complete cds	556	556	91%	4e-155	76%
X03476.1	Rhodopseudomonas sphaeroides fbc operon (fbcF, fbcB, fbcC genes)	524	524	90%	2e-145	75%
X05630.1	Rhodopseudomonas capsulata petABC operon	511	511	91%	2e-141	75%
CP000830.1	Dinoroseobacter shibae DFL 12, complete genome	488	488	88%	2e-134	75%
CP000031.1	Silicibacter pomeroyi DSS-3, complete genome	443	443	77%	6e-121	75%
CP000377.1	Silicibacter sp. TM1040, complete genome	426	426	74%	5e-116	75%
CP000264.1	Jannaschia sp. CCS1, complete genome	378	378	87%	2e-101	71%
CP000362.1	Roseobacter denitrificans OCh 114, complete genome	370	370	75%	3e-99	73%
CP000699.1	Sphingomonas wittichii RW1, complete genome	336	377	63%	7e-89	87%
CP000927.1	Caulobacter sp. K31, complete genome	313	313	63%	8e-82	74%
AE005673.1	Caulobacter crescentus CB15, complete genome	306	306	63%	1e-79	74%
CP000248.1	Novosphingobium aromaticivorans DSM 12444, complete genome	304	304	62%	4e-79	74%
AP007255.1	Magnetospirillum magneticum AMB-1 DNA, complete genome	298	298	54%	2e-77	75%
AF466752.1	Rhizobium leguminosarum bv. viciae strain UPM791 fbc operon, partial sequence	291	291	63%	3e-75	73%
CP000283.1	Rhodopseudomonas palustris BisB5, complete genome	286	286	64%	1e-73	72%
CP000943.1	Methylobacterium sp. 4-46, complete genome	284	284	61%	4e-73	73%
BA000012.4	Mesorhizobium loti MAFF303099 DNA, complete genome	282	282	63%	1e-72	73%
AL591788.1	Sinorhizobium meliloti 1021 complete chromosome; segment 7/12	280	280	61%	5e-72	73%
AE007869.2	Agrobacterium tumefaciens str. C58 circular chromosome, complete sequence	277	277	62%	6e-71	72%
CP000390.1	Mesorhizobium sp. BNC1, complete genome	269	269	54%	8e-69	74%
CP000250.1	Rhodopseudomonas palustris HaA2, complete genome	266	266	63%	1e-67	72%
CP000158.1	Hyphomonas neptunium ATCC 15444, complete genome	262	262	63%	1e-66	71%
CP000738.1	Sinorhizobium medicae WSM419, complete genome	260	260	62%	4e-66	72%
AF109172.1	Rhizobium galegae ubiquinol-cytochrome c reductase iron-sulfur subunit (fbcF), ubiquinol-cytochrome c reductase cytochrome b subunit (fbcB), cytochrome c1 (fbcC), and adenine phosphoribosyltransferase (aprt) genes, complete cds	260	260	63%	4e-66	72%
BX572596.1	Rhodopseudomonas palustris CGA009 complete genome; segment 4/16	257	257	63%	5e-65	71%
CP000115.1	Nitrobacter winogradskyi Nb-255, complete genome	255	255	63%	2e-64	72%
CP000319.1	Nitrobacter hamburgensis X14, complete genome	253	253	66%	7e-64	70%
AP009384.1	Azorhizobium caulinodans ORS 571 DNA, complete genome	248	248	63%	3e-62	71%
CP000133.1	Rhizobium etli CFN 42, complete genome	248	248	60%	3e-62	71%
CP000781.1	Xanthobacter autotrophicus Py2, complete genome	246	246	61%	1e-61	71%
CP000157.1	Erythrobacter litoralis HTCC2594, complete genome	244	244	64%	3e-61	71%
AM236080.1	Rhizobium leguminosarum bv. viciae chromosome complete genome, strain 3841	242	242	60%	1e-60	71%
CP000908.1	Methylobacterium extorquens PA1, complete genome	239	239	61%	1e-59	71%

VITA

David Wesley Goad

Candidate for the Degree of

Doctor of Philosophy

Thesis: METHODS FOR DETECTION AND IDENTIFICATION OF PATHOGENIC BACTERIA

Major Field: Veterinary Biomedical Science

Biographical:

Education:
Bachelor of Science in Animal Science, Kansas State University, Manhattan, KS in 1986.
Master of Science in Animal Science, Kansas State University, Manhattan, KS in 1990.
Completed the requirements for the Doctor of Philosophy in Veterinary Biomedical Sciences at Oklahoma State University, Stillwater, Oklahoma in July, 2008.

Experience:
Senior Scientist and Molecular Biologist, ICx Technologies, Stillwater, OK, 2003-Present.
Research Associate, Physiological Sciences, Oklahoma State University, Stillwater, OK, 1999-2003.
Graduate Research Assistant, Infectious Diseases and Physiology, Oklahoma State University, Stillwater, OK, 1997-1999.
Research Technician, Molecular and Cancer Biology, Department of Zoology, Oklahoma State University, Stillwater, OK, 1994-1997.
Research Technician, Molecular Genetics and Physiology, Department of Physiology, Kansas State University, Manhattan, KS, 1991-1994.
Research Technician, Department of Plant Pathology, Kansas State University, Manhattan, KS, 1989-1991.

Name: David Wesley Goad Date of Degree: July, 2008

Institution: Oklahoma State University Location: Stillwater, Oklahoma

Title of Study: METHODS FOR DETECTION AND IDENTIFICATION OF PATHOGENIC BACTERIA

Pages in Study: 197 Candidate for the Degree of Doctor of Philosophy

Major Field: Veterinary Biomedical Sciences

Scope and Method of Study:

1. Identification of unique genomic sequences associated with low versus high cytotoxicity isolates of *Clostridium piliforme*.;
2. Develop an amplified fluorescent antigen displacement assay directed toward methicillin-resistant *Staphylococcus aureus* low affinity penicillin binding protein PBP2a.;
3. Develop a label-free multiplex assay for specific detection of enteric pathogens *Salmonella typhimurium* and *E. coli* O157:H7 using optical microring resonators.

Findings and Conclusions:

1. Markers specific for high cytotoxicity *C. piliforme* isolate were not identified. However, 16 possible and 1 confirmed *C. piliforme*-specific marker were identified.;
2. Amplified fluorescent peptide displacement assay component was developed, intended as part of a flow-through detection platform. Some detection of antigen (labeled peptide) was detected in assay when applied to Amplifying Fluorescent Polymer (AFP), but results were not strongly positive, possibly due to poor performing peptide antigen-derived antibody.
3. Label-free detection of whole bacterial cells was clearly demonstrated with concentrations as low as 10e5 CFU/ml. Whole cell detection on microring arrays was performed in a sequential binding assay to demonstrate multiplex capability with good success.

ADVISER'S APPROVAL: Jerry R. Malayer